The Okanagan subterrane:

a ‘Subduction Initiation Rule’ ophiolite in the Canadian Cordillera

by

Gerri L. McEwen
Bachelor of Science, University College of the Cariboo, 1994
Bachelor of Science (Honours), University of Victoria, 2014

A Thesis Submitted in Partial Fulfillment of the
Requirements for the Degree of

MASTER OF SCIENCE

in the School of Earth and Ocean Sciences

We acknowledge and respect the lək^{w}əŋən peoples on whose traditional territory the university stands and the Songhees, Esquimalt and W̱SÁNEĆ peoples whose historical relationships with the land continue to this day.

The Okanagan subterrane:
a ‘Subduction Initiation Rule’ ophiolite in the Canadian Cordillera

by

Gerri L. McEwen
Bachelor of Science, University College of the Cariboo, 1994
Bachelor of Science (Honours), University of Victoria, 2014

Supervisory Committee

Dr. Stephen T. Johnston, Co-Supervisor
School of Earth and Ocean Sciences

Dr. Dante Canil, Co-Supervisor
School of Earth and Ocean Sciences

Dr. Lucinda Leonard, Member
School of Earth and Ocean Sciences

Abstract

The Okanagan subterrane in south-central British Columbia is commonly referred to as the basement to Quesnellia, a composite arc terrane in the Canadian Cordillera. Distinct geochemical, lithologic, and structural characteristics allow for interpretation of the Okanagan subterrane as a forearc ophiolite formed over a long-lived west-dipping subduction zone initiating in western Panthalassa. The forearc ophiolite model has significant impacts on existing Cordilleran models which focus on a North American origin for this terrane. The Okanagan subterrane is comprised of harzburgites, gabbros, basaltic lavas, and ocean basin sediments. The age of the subterrane spans the Middle Devonian through the Early Permian. New stratigraphic, structural, and whole rock geochemical data are presented together with a synthesis of pre-existing data from regional studies to better constrain the origins and evolution of the Okanagan subterrane. The results indicate a transition from quiet shallow ocean basin deposition to the initiation of subduction and construction of a new forearc crustal sequence and mantle wedge. The earliest crustal sequences were formed from the eruption of basalts geochemically similar to those produced at oceanic spreading centres in the Late Devonian to earliest Mississippian. A chemostratigraphic magmatic progression through the Early and Middle Mississippian resulted in lavas becoming increasingly island arc-like in composition. Uplift and erosion dominated through the Pennsylvanian and Permian, punctuated by periods of carbonate deposition and capped by a regional Permo-Triassic unconformity and a Mesozoic volcanic arc. The Okanagan subterrane was affected by two main compressional deformation events, both interpreted as products of ophiolite obduction. The first, in the Permo-Triassic, resulted in tight to isoclinal folding, uplift, and erosion yielding the Permo-Triassic unconformity and the obduction of the Okanagan subterrane onto an extinct island arc within the lower plate. The second, in the Middle Jurassic, resulted in a southwest-verging fold and thrust belt

which likely records the subsequent accretion to pericratonic terranes of western Laurentia. Comparing this ophiolite to other supra-subduction zone ophiolites worldwide allows for an interpretation of the Okanagan subterrane as a forearc ophiolite constructed during Late Devonian intra-oceanic subduction initiation.

Table of Contents

List of Figures

List of Tables

Acknowledgements

Tremendous thanks to Dr. Stephen T. Johnston for providing this opportunity and for his unwavering patience during this endeavour. He went above and beyond in helping me finish this project. I will be forever grateful to him for his guidance and support. I would also like to thank Dr. Dante Canil for his input during the finishing stages of this thesis.

Vancouver Island University (VIU) was instrumental in this process by providing financial support in the form of a VIU Inquiry Grant to cover field work expenses and geochemical analyses plus the facilities for rock sample cutting, storage, and petrographic analysis. My colleagues at VIU, Sandra Johnstone, Dr. Jerome Lesemann, Dr. Tim Stokes, and Dr. Rhy McMillan each deserve a special shout-out for their continued encouragement and support throughout this process.

Thanks go out to David Nelles, Senior Laboratory Instructor (retired) for the UVic School of Earth and Ocean Sciences, who provided invaluable support during the initial stages of my graduate journey.

Mitch Mihalynuk and Larry Diakow of the British Columbia Geological Survey were instrumental in teaching me about the realities of geological field surveys during our intensive summer program in the BC Interior; long days, strenuous traverses, days with no outcrop, days with lots of outcrop, and days with lots of the same outcrop station after station. These two were also responsible for kickstarting my experience with digital field mapping through total immersion.

Finally, I would like to thank my field assistant Martha Henderson for her help and never-ending enthusiasm.

Dedication

This thesis would not be possible without the love and support of my family, and it is to them my thesis is dedicated. They've stood by me through thick and thin and shown resounding patience with me throughout this process. I've been able to recruit them to act as field assistants, editors, and sounding boards.

Introduction

Ophiolites are obducted remnants of oceanic lithosphere emplaced during collisional orogenesis (Whattam and Stern 2011). The Cordilleran Orogen of western North America is commonly cited as an accretionary orogen that developed due to long-lived subduction beneath the western margin of the Laurentian continent (e.g. Monger et al. 1982, Monger and Price 2002), in part based on the identification and interpretation of ophiolitic terranes along the length of the orogen. Among these, one of the least studied is the Devonian to Permian Okanagan subterrane. The Okanagan subterrane is encapsulated within and basement to the southern extent of Quesnellia, a composite arc terrane situated in central British Columbia, Canada (Figure 1). Although an ophiolitic interpretation has become widely accepted (e.g. Fyles 1990, Dostal et al. 2001, Massey 2006a, Massey and Dostal 2013), the Okanagan subterrane records a protracted 90 million year history and much remains poorly understood. Such unknowns include: the type of ophiolite (lower plate, forearc, or backarc), the polarity of subduction and obduction, and the relationship to the North American craton. Supra-subduction zone ophiolites, those formed on the upper plate at a subduction zone, are considered to be the most common and well-preserved in the geologic record (Miyashiro 1975, Pearce et al. 1984, Pearce 2003, Stern 2004). Distinct signatures of supra-subduction zone ophiolites reflect development over a subducting plate. Subduction initiation rule ophiolites, a subset of forearc supra-subduction zone ophiolites, and perhaps the most common type (Moores 1982, Pearce et al. 1984, Whattam and Stern 2011, Stern et al. 2012), record the complete history of a volcanic arc, from subduction initiation to obduction (Shervais 2001). Volcanic rocks within these ophiolites exhibit a characteristic chemostratigraphic progression believed to reflect evolution of a single mantle source as the nascent subduction zone develops (Pearce et al 1984; Shervais 2001; Whattam and Stern 2011). This chemostratigraphy is designated the

'subduction initiation rule' (Whattam and Stern 2011). The 'subduction initiation rule' states that: "magmatic sequences preserved in ophiolite volcanic sections record a stratigraphic progression (from bottom to top) from less to more high field strength element (HFSE)-depleted and large ion lithophile element (LILE)-enriched compositions and (a) generally comprise a lower, usually mid-ocean ridge basalt (MORB)-like unit and an upper island arc basalt (IAB)-like unit, sometimes along with boninites, both of which (b) form in a proto-forearc setting during subduction initiation" (Whattam and Stern 2011). In the earliest stage of subduction initiation, denser lithosphere subsides into the asthenosphere (Figure 2). Asthenosphere upwells into the resulting gap and decompressively melts spreading laterally over the descending lithosphere (Stern and Bloomer 1992, Stern 2004, Whattam and Stern 2011). Increased pressures and temperatures induce dehydration and densification of the sinking plate (Stern 2004). As the rate of subsidence increases, the newly-formed trench rolls back causing extension of the upper plate (Stern 2004; Shervais 2001; Stern and Bloomer 1992). Dehydration fluids released from the downgoing plate flux into the mantle triggering extensive asthenospheric melting and the eruption of forearc basalts with MORB-like geochemistry (Pearce et al. 1984, Stern and Bloomer 1992, Stern 2004, Stern and Gerya 2018). These MORB-like lavas are typically tholeiitic and nearly indistinguishable from typical MORB in a mid-ocean ridge setting but do display minor enrichment in LILE and depletions in HFSE (Whattam and Stern 2011; Shervais 2001). Additional rock types emplaced at this stage include layered and isotropic gabbros and sheeted dikes (Shervais 2001). Layered gabbros are often foliated or boudinaged possibly due to emplacement during proto-forearc extension. As the proto-forearc continues to extend and develop, continued fluid flux from the sinking slab and depletion of the melt source creates a rapid transition to lavas with a tholeiitic IAB-like signature, followed in some cases by a subsequent stage of boninite eruption (Pearce et al. 1984, Stern and Bloomer 1992, Shervais 2001, Stern 2004, Whattam and Stern 2011, Stern and Gerya 2018). These volcanic rocks erupt through

and overlie the initial proto-forearc layers. Plutonic equivalents lack the foliation of their earlier counterparts and form as sills and dikes of olivine and pyroxene gabbros, pyroxenites, wehrlite, dunite, and harzburgite (Shervais 2001). Comparison of the Okanagan subterrane ophiolite against these parameters can help to address some of the aforementioned unknowns (the type of ophiolite, the polarity of subduction and obduction, and the relationship to the North American craton) and may have important implications for models of Cordilleran evolution, as well as for our understanding of the processes responsible for ocean basin closure and ophiolite formation.

To contribute to our understanding of the tectonic history of the Okanagan subterrane, a program of data compilation, stratigraphic and structural mapping and geochemical characterization of Paleozoic rock units was undertaken in the Thompson-Nicola, Okanagan-Similkameen, and Kootenay-Boundary regions of southern British Columbia. Historically, the tectonic setting of the Okanagan subterrane had been interpreted based on both large-scale mapping and focused studies of localized regions (e.g. Okulitch 1973, Barnes and Ross 1975, Ross 1981, Milford 1984, Fyles 1990, Ray et al. 1992, 1996, Ray and Dawson 1994, Dostal et al. 2001, Massey 2006a, Höy 2018). New stratigraphic, structural, and whole rock geochemical data are presented to help constrain the origins and evolution of the Okanagan subterrane. These data, together with a synthesis of constraints provided by regional studies, provide the basis for interpretation of the Okanagan subterrane as a subduction initiation rule ophiolite.

In this thesis, the geological setting and current models for Quesnellia are summarized followed by a review of available geological constraints on the Okanagan subterrane. The methods employed and the results of the study are presented next, ending with a discussion of the implications of the study and a proposed tectonic model explaining the evolution of the Okanagan subterrane.

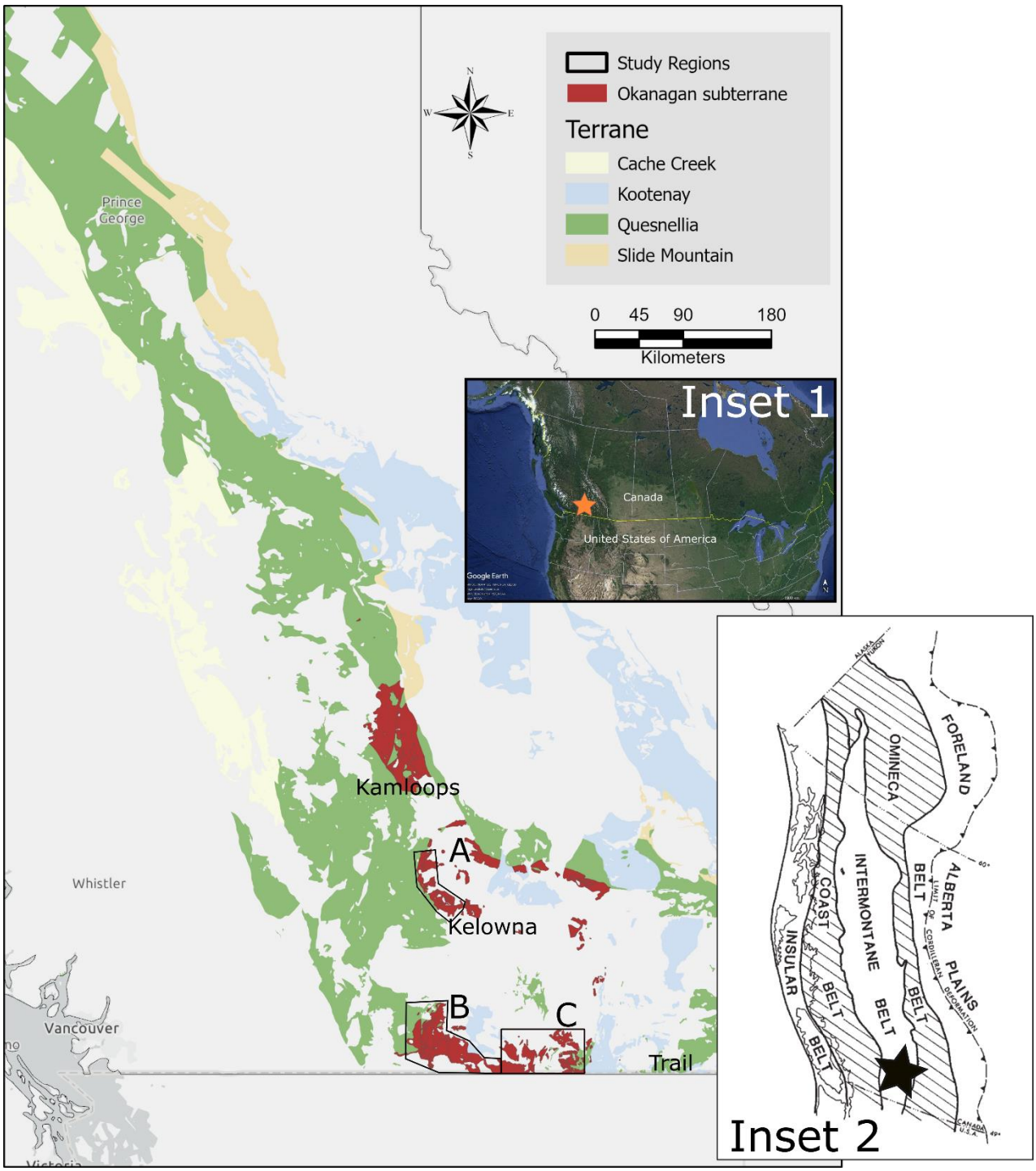

Figure 1. Geologic map of accreted terranes of Central British Columbia (modified after Cui et al. (2017)) showing the location of the Okanagan subterrane within southern Quesnellia and simplified boundaries for the study regions which encompass them: A) Thompson-Nicola region (TNR), B) Okanagan-Similkameen region (OSR); and C) Kootenay Boundary region (KBR). Inset 1 map is from Google Earth [accessed December 15, 2023] showing the location of the study area within North America. Inset 2 is from Monger and Price (2000) showing the location of the study area relative to the geomorphological belts that make up the Canadian Cordillera.

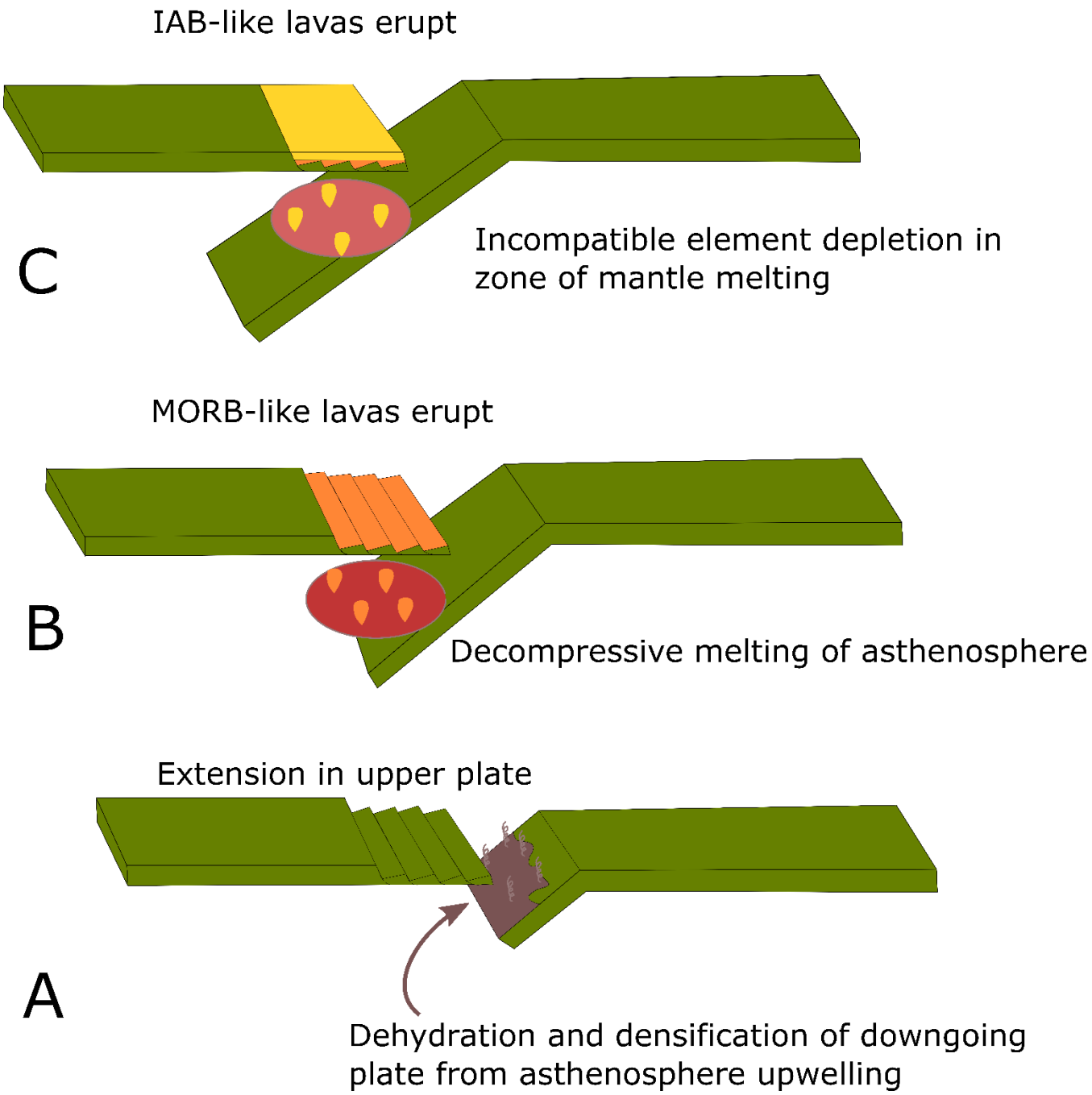

Figure 2. Schematic illustration of subduction initiation modified after Stern and Bloomer (1992), Stern (2004), and Whattam and Stern (2011). A) Denser lithosphere subsides into the asthenosphere. Asthenosphere upwells into the resulting gap and decompressively melts spreading laterally over the descending lithosphere. As the rate of subsidence increases, the newly-formed trench rolls back causing extension of the upper plate. B) Dehydration fluids released from the downgoing plate flux into the mantle triggering extensive asthenospheric melting and the eruption of forearc basalts with MORB-like geochemistry. C) As the proto-forearc continues to extend and develop, continued fluid flux from the sinking slab and depletion of the melt source creates a rapid transition to lavas with a tholeiitic island arc basalt (IAB) signature, followed in some cases by a subsequent stage of boninite eruption. These volcanic rocks erupt through and overlie the initial proto-forearc layers.

Chapter One: Geological Setting

1.1. Geological Setting

Quesnellia is a major tectonostratigraphic component of the allochthonous Intermontane superterrane of the Canadian Cordillera. The oceanic Slide Mountain and Cache Creek terranes are situated along the eastern and western flanks of Quesnellia, respectively (Figure 1). The Slide Mountain terrane largely separates Quesnellia from pericratonic crust of Laurentian affinity to the east. In southern British Columbia, Paleozoic assemblages within Quesnellia underlie and are separated from Mesozoic arc assemblages by a Permo-Triassic unconformity (e.g. Read and Okulitch 1977).

Traditional models for Cordilleran evolution (e.g. Roback et al. 1994, Monger and Price 2002, Nelson et al. 2006, Colpron et al. 2007) depict Quesnellia as a marginal arc complex that formed over an east-dipping subduction zone. Rollback of the subducting slab is inferred to have rifted Quesnellia from Laurentia in the Paleozoic opening of the Slide Mountain Ocean as a back-arc basin. The maximum width achieved by back-arc spreading is not well constrained. Paleomagnetic data combined with paleontological evidence, detrital zircon populations, and isotopic compositions have led some researchers to postulate Quesnellia may have been as far as 4000 km west of the North American continent in the early Permian (e.g. Belasky et al. 2002, Nelson et al. 2006, Colpron et al. 2007) or earliest Triassic (e.g. Johnston and Borel 2007). Alternatively, stratigraphic correlations have been used to argue that Quesnellia remained on or only a short distance from the Laurentian margin throughout its development (e.g. Unterschutz et al. 2002).

In models involving a Slide Mountain Ocean, collapse of the back-arc is linked to obduction of the Slide Mountain ophiolite and accretion of its associated arc terrane onto the Laurentian margin. Some

researchers suggest repatriation of the arc terrane with Laurentia was complete by middle to late Permian (Nelson et al. 2006, Ruks et al. 2006, Colpron et al. 2007), whereas others suggest a timeframe of early Triassic (Piercey et al. 2012) to Jurassic (Monger and Price 2002, Johnston and Borel 2007).

1.1.1. The Okanagan subterrane

The Okanagan subterrane exists as a disrupted assemblage encompassed within the southern regions of Quesnellia (Figure 3). Units comprising the Okanagan subterrane have undergone a variety of changes in naming convention, proposed associations, correlations, and aerial distributions in the literature (Okulitch 1973, Barnes and Ross 1975, Monger 1977, Smith 1979, Ross 1981, Milford 1984, Church 1986, Fyles 1990, Dostal et al. 2001, Massey 2006a, 2006b, Massey and Dostal 2013, Mortensen et al. 2017). Within some areas, much of the distinction between units is based on relative abundance of the various lithologies and metamorphic grade. Following the nomenclature and aerial distribution used in Mortensen et al. (2017), the Okanagan subterrane is made up of Permian and older rocks of the Chapperon, Kobau, and Anarchist groups, the Knob Hill Complex, the Attwood, and Oregon Claims, formations, and the Old Tom, Shoemaker, Blind Creek, Barslow, and Independence-Bradshaw assemblages. For this study, rocks belonging to the Harper Ranch Group are included with the Okanagan subterrane based on relative age and stratigraphic relationships with the Chapperon Group and Triassic overlap assemblages although some consider the Harper Ranch Group to be part of a distinct subterrane (e.g. Beatty et al. 2006). Unconformably overlying the Okanagan subterrane are Mesozoic volcanic arc facies of the Brooklyn Formation in the east and Nicola Group in the west. The Late Carboniferous to Permian Blind Creek Formation is believed to be a block of limestone eroded from the Old Tom or Shoemaker assemblage and emplaced by gravity sliding in the Eocene (Barnes and Ross 1975, Milford 1984, Mortensen et al. 2011). Apart from the Blind Creek Formation, therefore, each unit of the Okanagan subterrane are discussed in greater detail below.

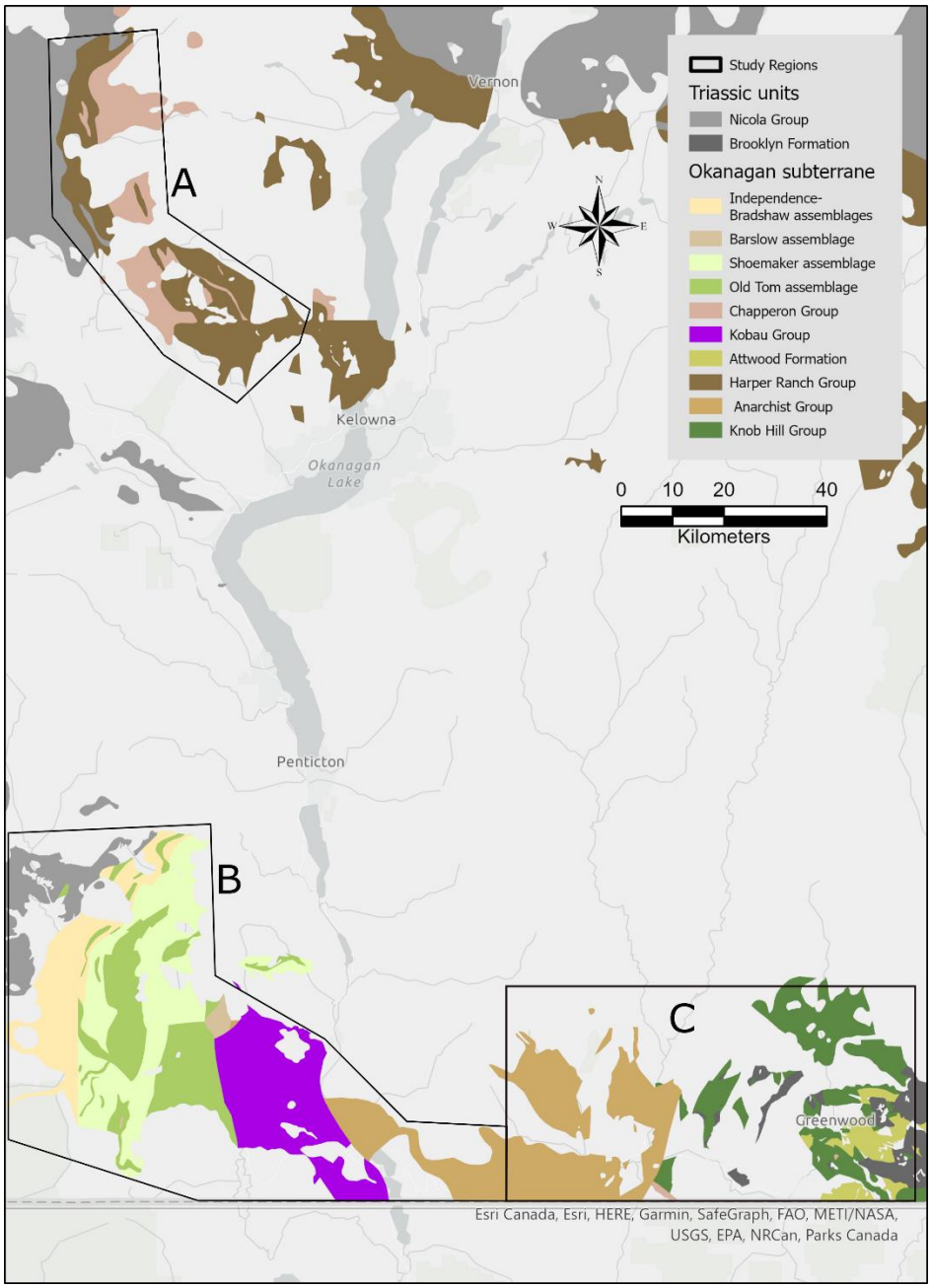

Figure 3. Geologic units of the Okanagan subterrane within Southern Quesnellia. Regional boundaries A, B, and C as in Figure 1. Modified after Cui et al. (2017).

Table 1. Unit names, lithologies, and age constraints for units of the Okanagan subterrane listed by study region. Data from Okulitch (1973, 1979), Read and Okulitch (1977), Milford (1984), Mäder et al. (1988), Fyles (1990), Daughtry et al. (2000), Beatty et al. (2006), Massey and Dostal (2013), Massey et al. (2013), Mortensen et al. (2017), Höy (2018). Terms: DZ MDA = detrital zircon maximum depositional age, U-Pb Zircon = U-Pb geochronologic age in zircon, Fossil = fossil age, Stratigraphic position = stratigraphic constraints based on the age of overlying or underlying strata, n.a. = not applicable.

Region	Unit name	Major lithologies	Lower Age Constraints	Type	Upper Age Constraints	Type
Thompson-Nicola region	Harper Ranch Group	Siliceous argillite, tuff, siltstone, slate, and minor greenstone	Permian	Fossil	Pre-Late Triassic	Stratigraphic position
	Chapperon Group	Chert, greenstone, quartzite, siliceous argillite, phyllite, schist, gneiss, and serpentinized ultramafic rocks	none	n.a.	Pre-Permian	Stratigraphic position
Okanagan-Similkameen region	Oregon Claims Formation	Fine-grained siliciclastic rocks with interlayered mafic volcanics	296 Ma	DZ MDA	Pre-Late Triassic	Stratigraphic position
	Independence-Bradshaw assemblages	Fine-grained siliciclastic rocks with interlayered mafic volcanics	Middle Devonian	Fossil	301 Ma	DZ MDA
	Shoemaker assemblage	Chert and minor greenstone, greywacke, sandstone, and limestone	Middle Devonian	Fossil	Pennsylvanian to Permian	Fossil
	Old Tom assemblage	Greenstone and minor chert, greywacke, sandstone, and limestone	Devonian to Mississippian	Fossil	none	n.a.
	Barslow assemblage	Siliciclastic rocks and conglomerate with interlayered greenstone, plus minor chert and limestone	342 Ma	DZ MDA	312 Ma	DZ MDA
	Kobau Group	Quartzite, phyllite, schist, gneiss, greenstone, and marble	none	n.a.	none	n.a.
Kootenay-Boundary region	Anarchist Group	Phyllite, schist, recrystallized chert, and meta-argillite with minor greenstone, limestone, mafic tuff, and serpentinized dunite and harzburgite	365 Ma	U-Pb zircon	299	DZ MDA
	Knob Hill Complex	Mafic volcanic rocks, gabbro, sheeted diabase dikes, serpentinites, and chert, with lesser argillite and fossiliferous limestone	390 Ma	U-Pb zircon	Pennsylvanian to Permian	Fossils
	Attwood Formation	Chert conglomerate, argillite, phyllite, slate and fossiliferous limestone with minor mafic volcanic rocks	Carboniferous and Permian	Fossils	327 Ma	DZ MDA

1.1.1.1. Thompson-Nicola Region

Two units make up the Okanagan subterrane in the Thompson-Nicola region: the Chapperon and Harper Ranch Groups (Figure 4). The Chapperon Group is a variably metamorphosed assemblage of chert, greenstone, quartzite, siliceous argillite, phyllite, schist, gneiss, and serpentinized ultramafic rocks of pre-Permian age (Read and Okulitch 1977, Okulitch 1979, Daughtry et al. 2000). Fine to coarse-grained Permian-aged fossiliferous siliciclastics of the Harper Ranch Group lie with slight angular unconformity between the Chapperon Group and Mesozoic strata of the Nicola Group. The Late Devonian to Middle Permian Harper Ranch Group has been interpreted as an assemblage of volcanic arc facies with an apron of massive to laminated mudstones with limestone lenses, and fine to very coarse-grained reworked volcanic sandstones intercalated with tuffaceous layers (Smith 1979, Ross 1981, Acton et al. 2000, Beatty et al. 2006). The Harper Ranch Group has been studied in greatest detail at its type locality, approximately 50 km north of our Thompson-Nicola region study area. At the type locality, chert pebble conglomerates overlie latest Famennian shallow-water bioclastic limestones, together forming the base of the Harper Ranch stratigraphic sequence (Beatty et al. 2006). The conglomerates are, in turn, overlain by deep-water turbidites which contain minor interbeds of reworked fine-grained volcaniclastic sandstones with Early Mississippian conodonts (Beatty et al. 2006). Volcaniclastics increase in abundance within the stratigraphic sequence of the Harper Ranch Group until they are largely replaced by thick carbonate deposition through the Late Mississippian to Early Pennsylvanian (Beatty et al. 2006). Early to Middle Permian limestones which contain Tethyan fossil assemblages unconformably cap the sequence (Smith 1979, Ross 1981, Orchard and Forster 1988, Crasquin-Soleau and Orchard 1994, Beatty et al. 2006). The Late Triassic Nicola Group is a volcanic arc sequence locally represented in this region by fine- to coarse-grained, locally calcareous sedimentary rocks and limestones of Carnian to Norian age (Mortimer 1987, Ray et al. 1996, Massey 2011).

The geometry and distribution of units in the Thompson-Nicola region is a product of a series of folding and faulting events spanning from the Permo-Triassic to the Eocene. Chapperon Group rocks form the core of an arcuate north-plunging antiform (Ross 1981) that post-dates Permo-Triassic tight to isoclinal interfolding with the Harper Ranch Group (Read and Okulitch 1977, Ross 1981, Daughtry et al. 2000). Serpentinized ultramafic rocks occur as pods throughout the Chapperon Group but outcrop in proximity and parallel to the westernmost contact with the Harper Ranch Group (Read and Okulitch 1977). A moderately-dipping basal conglomerate of the Nicola Group overlies the Chapperon and Harper Ranch groups along a Permo-Triassic angular unconformity and contains variably-oriented, foliated clasts of these underlying units (Read and Okulitch 1977, Ross 1981, Daughtry et al. 2000).

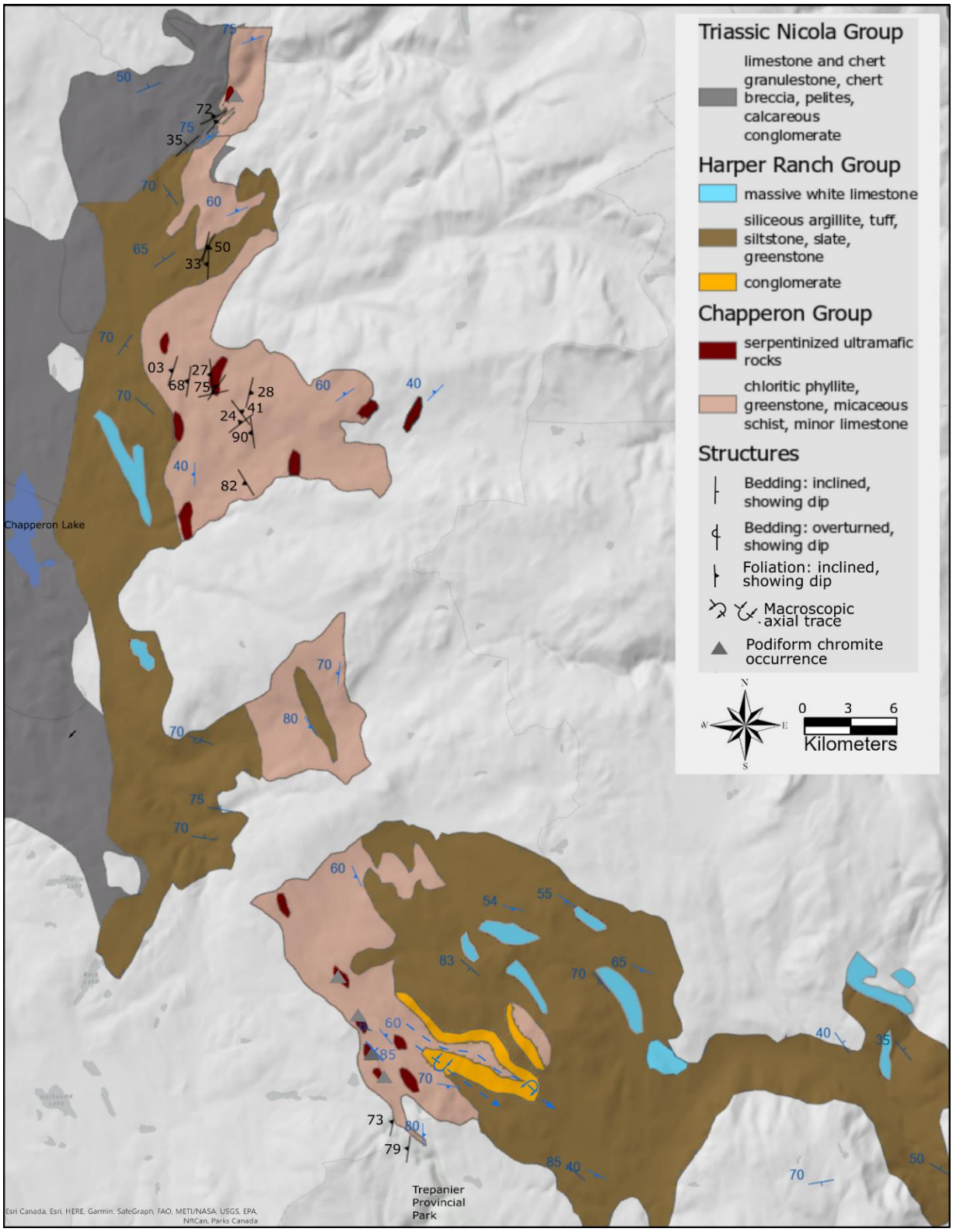

Figure 4. Geologic map of the Okanagan subterrane in the Thompson-Nicola Region (study area A) modified from Read and Okulitch (1977) and Cui et al. (2017). Black structural symbols are from this study. Blue symbols are data from Read and Okulitch (1977).

1.1.1.2. Okanagan-Similkameen Region

A paucity of age constraints makes relative stratigraphic interpretations difficult in the Okanagan-Similkameen region. Fossil and detrital zircon ages span Middle Devonian to Early Permian in a number of units (Mortensen et al. 2017). From east to west, this region is composed of the Kobau Group, the Barslow, Shoemaker, Old Tom, and Independence-Bradshaw assemblages, and the Oregon Claims Formation (Figure 5). The latter two units are in unconformable or fault contact with Late Triassic rocks of the Nicola Group to the west. A fault-bounded metamorphic assemblage of quartzite, phyllite, schist, gneiss, greenstone, and marble make up the Kobau Group (Okulitch 1973, Milford 1984, Mäder et al. 1988, Mortensen et al. 2017). Biostratigraphy is not possible given the degree of strain and metamorphic recrystallization and the Mississippian age of this unit is based solely on lithologic and structural correlations to other Okanagan subterrane units (Okulitch 1973, Mortensen et al. 2017). The remaining units consist of a collection of greenstone, siliciclastic rocks, limestone, and chert; the relative abundance of lithologies defines the unit to which they have been assigned (Mortensen et al. 2017). Fine- to coarse-grained siliciclastic rocks and conglomerate with interlayered greenstone, plus minor chert and limestone characterizes the Barslow assemblage (Mortensen et al. 2017). Conodonts and brachiopods within this unit indicate an earliest Mississippian to Pennsylvanian age. Detrital zircons in sandstones 6 km and 8 km east of Keremeos yield maximum depositional ages of 312 Ma and 342 Ma, respectively (Mortensen et al. 2017). The Shoemaker assemblage is dominated by chert whereas greenstone is the primary lithology in the Old Tom assemblage (Read and Okulitch 1977, Milford 1984, Mortensen et al. 2017). In both, greywacke, sandstone, and limestone are present in minor abundance. Fossil ages in chert and limestone of the Old Tom and Shoemaker assemblages span Middle Devonian to Pennsylvanian or Early Permian (Mortensen et al. 2017). As with the Barslow assemblage, fine-grained siliciclastic rocks with interlayered mafic volcanics characterize the

Independence-Bradshaw assemblages and the Oregon Claims Formation. Detrital zircons indicate maximum depositional ages ranging from Latest Devonian to as young as 296 Ma while fossil ages in crinoidal limestone indicate that parts of the Independence-Bradshaw assemblages are as old as Middle Devonian (Mortensen et al. 2017). In either unconformable or fault contact along the western boundary of the Okanagan-Similkameen region are fine-grained calcareous siliciclastic turbidites of the Nicola Group (Milford 1984, Ray et al. 1996). The Permo-Triassic unconformity is locally characterized by conglomerate and breccia containing pebble to cobble-sized clasts of chert and limestone derived from underlying Okanagan subterrane strata.

As in the Thompson-Nicola region, Paleozoic assemblages in the Okanagan-Similkameen region form an arcuate NE-plunging west-verging antiform (Read and Okulitch 1977). Units were tight to isoclinally folded in the Permo-Triassic then multiply-refolded during younger deformation events to yield the observed map pattern (Figure 5; Read and Okulitch 1977, Ross 1981). Complicating stratigraphic and structural interpretations, a bioclastic limestone in the Old Tom or Shoemaker assemblage contains clasts with Late Silurian to Early Devonian corals in a matrix with Carnian- to Norian-aged fossils (Read and Okulitch 1977, Pohler et al. 1989). The Late Triassic age of the matrix led Milford (1984) to assign a Late Triassic age to the entirety of the Old Tom and Shoemaker assemblages. These limestone entities are now understood to represent either klippes or unconformably-deposited erosional remnants of the Nicola Group (Read and Okulitch 1977, Mortensen et al. 2017). An unusual assemblage of Middle to Late Ordovician conodonts are found in limestone 16 km north of Keremeos in a region mapped as the Shoemaker assemblage (Pohler et al. 1989). These particular conodont species being found together is un-documented in the literature and is interpreted as evidence of transportation or reworking (Pohler et al. 1989). Nearby cherts yield Late Devonian to Mississippian fossil ages thus the Ordovician limestone has been interpreted as an olistolith or a faulted fragment

structurally imbricated with strata of the Shoemaker assemblage (Milford 1984, Mortensen et al. 2017). Intact pre-middle Devonian strata have yet to be identified in the Okanagan subterrane (Mortensen et al. 2017); therefore, the source of the Ordovician to early Devonian fossils is enigmatic.

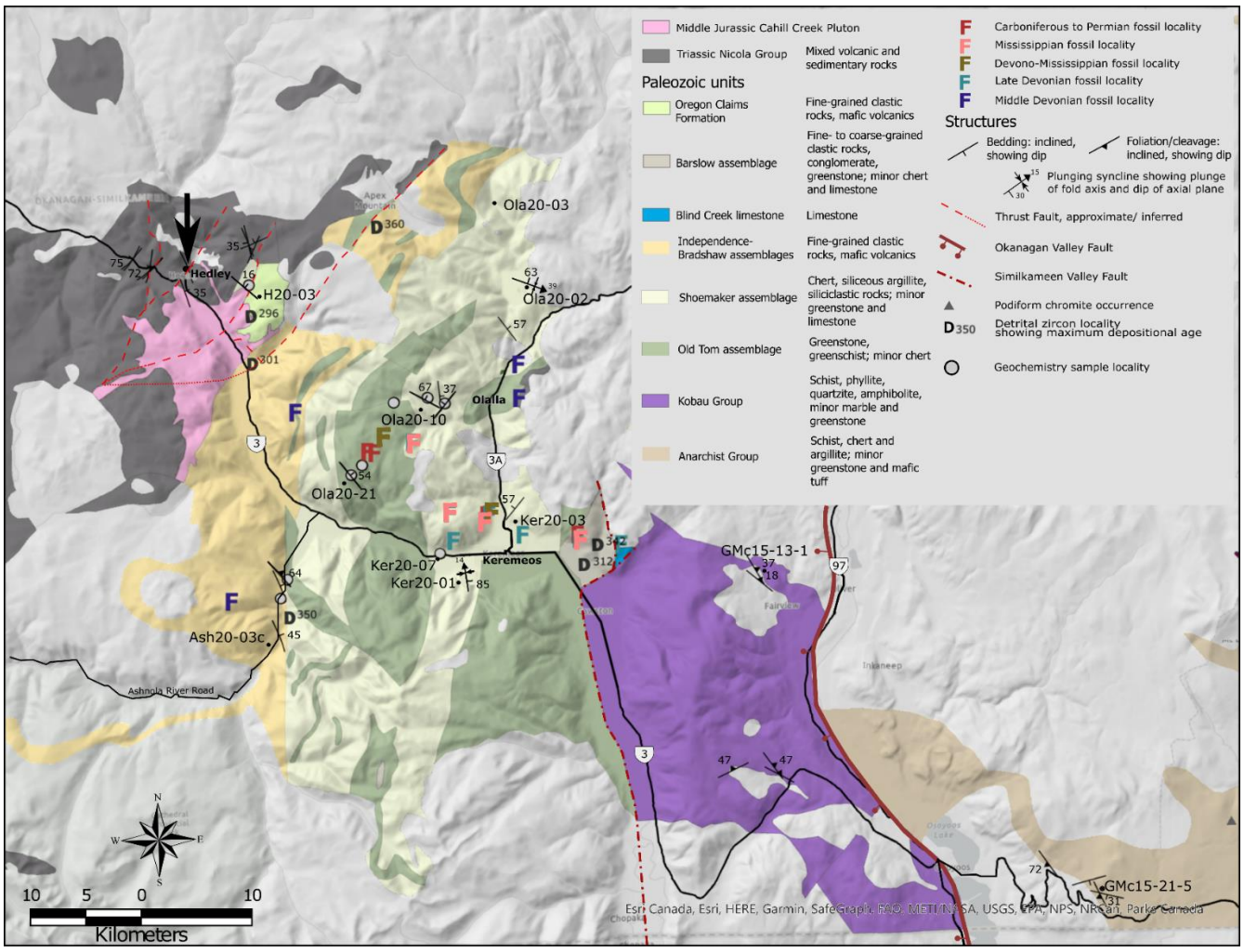

Figure 5. Geologic map of the Okanagan subterrane within the Okanagan-Similkameen region (study region B) modified from Milford (1984) and Cui et al. (2017) Structural symbols and geochemistry sample locations are data collected in this study. Detrital zircon maximum depositional ages are from Mortensen et al. (2017) as are fossil ages. West-dipping faults in the Hedley region are approximated based on mapping by Ray et al. (1996) and Dawson et al. (1990). From west to east, these are the Chuchuwayha, Bradshaw, Cahill Creek, and Winters Creek faults all of which cut the Cahill Creek pluton which yields a U-Pb zircon age of 163 Ma (Mortensen 2014). Milford (1984) infers a curvilinear north-trending fault tracing the western margin of the Old Tom assemblage. Tempelman-Kluit (1989) infers the steeply-dipping fault separating the Kobau Group from other units in the Okanagan Similkameen region. The arrow above the town of Hedley indicates the approximate location of duplex thrusts shown in Figure 23.

1.1.1.3. Kootenay-Boundary Region

Within the study area for the Kootenay-Boundary region, the Okanagan subterrane is represented by the Knob Hill Complex, the Anarchist Group, and the Attwood Formation (Figure 6). Paleozoic strata are unconformably overlain by conglomerate, sandstone, siltstone, limestone, greenstone, and pyroclastic breccia of the Middle Triassic Brooklyn Formation (Fyles 1990, Massey 2006b). Apart from serpentinites, conglomerate clasts are derived from all lithologies of the underlying Paleozoic units (Fyles 1990). The Pennsylvanian(?) or Permian to Early Triassic Mount Roberts Formation lies outside the study area, 65 km east of Greenwood, and has been interpreted as the easternmost and youngest exposures of the Harper Ranch Group (Roback and Walker 1995). Clastic sediments in the Mount Roberts Formation are consistent with derivation from strata within the Okanagan subterrane with a Pennsylvanian or Permian to Middle Triassic age range that bridges the time gap between the youngest Okanagan subterrane and oldest Triassic arc strata. Middle to Late Devonian detrital zircon peaks in the Mount Roberts Formation (Roback and Walker 1995) coincide well with those in the Okanagan subterrane (Mortensen et al. 2017) consistent with the genetic relationship inferred based on age and clastic composition. Thus, for the purposes of this study, the Mount Roberts Formation is considered an overlap assemblage.

The Knob Hill Complex consists of mafic volcanic rocks, gabbro, sheeted diabase dikes, serpentinites, and chert, with lesser argillite and fossiliferous limestone (Fyles 1990, Massey and Dostal 2013, Mortensen et al. 2017). Serpentinites are closely associated with a series of north to northeast-dipping thrust faults west of Greenwood (Fyles 1990, Höy 2018). Gabbro from the Knob Hill Complex along the Lind Creek Fault and north of Rock Creek yielded U-Pb zircon ages between 380 and 390 Ma (Massey et al. 2013). Radiolaria in chert of upper sequences are as young as earliest Permian with a younging trend toward the north or northeast (Fyles 1990, Massey 2006a). The Anarchist Group is

comprised of phyllite, schist, recrystallized chert, and meta-argillite with minor greenstone, limestone, mafic tuff, and serpentinized dunite and harzburgite (MINFILE 1985, Fyles 1990, Massey and Dostal 2013, Mortensen et al. 2017, Höy 2018). Serpentinites hosting podiform chromitite deposits present as NW trending, steeply-dipping lenses up to 1000 meters long by 100 meters wide with well-developed foliation paralleling internal shearing and sharp contacts with the host rock (MINFILE 1985). A quartz-muscovite schist, interpreted as a metatuff, within the Anarchist Group yielded a U-Pb zircon age of 365 Ma (Mortensen et al. 2017). Detrital zircons indicate maximum depositional ages as young as 299 Ma (Mortensen et al. 2017).

The Attwood Formation is composed of chert conglomerate, argillite, phyllite, slate and fossiliferous limestone with minor mafic volcanic rocks (Church 1986, Fyles 1990, Massey 2006b, Massey and Dostal 2013, Mortensen et al. 2017). Carboniferous or Permian macrofossils characterize the Attwood Formation and detrital zircon populations indicate maximum depositional ages as young as 327 Ma (Church 1986, Massey 2006b, Mortensen et al. 2017).

In the southeastern portion of the Kootenay-Boundary region, the Okanagan subterrane is imbricated, forming five north-dipping thrust sheets (Figure 6; Fyles 1990). From north to south, the major faults involved are the Lind Creek, Mount Attwood, Mount Wright, and Number 7 faults. The Lind Creek fault separates a hanging wall of primarily Knob Hill Complex from a footwall comprised of rocks from the Attwood Formation (Massey 2006a). Along the Mount Attwood and Mount Wright faults, the Attwood Formation dominates the hanging wall and the Anarchist Group forms the footwall. Lastly, the Anarchist Group has been thrust over Brooklyn and Attwood Formation rocks along the Number 7 fault. Tight to isoclinal folding has deformed strata within most thrust sheets (Fyles 1990) suggesting folding pre-dates or is coeval with thrusting. Involvement of the Brooklyn Formation in all thrust sheets indicates post-middle Triassic thrust imbrication. Undeformed stitching plutons of the Middle Jurassic

Nelson plutonic suite intrude the thrust sheets and provide a minimum age constraint on imbrication (Fyles 1990, Massey 2006b).

Overall patterns observed within the Okanagan subterrane include: 1) deeper crustal components such as gabbro and serpentinites are exposed in the Kootenay-Boundary region; 2) chert, while ubiquitous across the Okanagan subterrane, is more heavily concentrated in the Okanagan-Similkameen region; 3) available age constraints from fossils, detrital zircons and U-Pb zircon indicate that the Okanagan subterrane spans the Middle Devonian to Middle Permian; and 4) strata in all regions have been subjected to multiple phases of Permo-Triassic and younger folding and thrust imbrication.

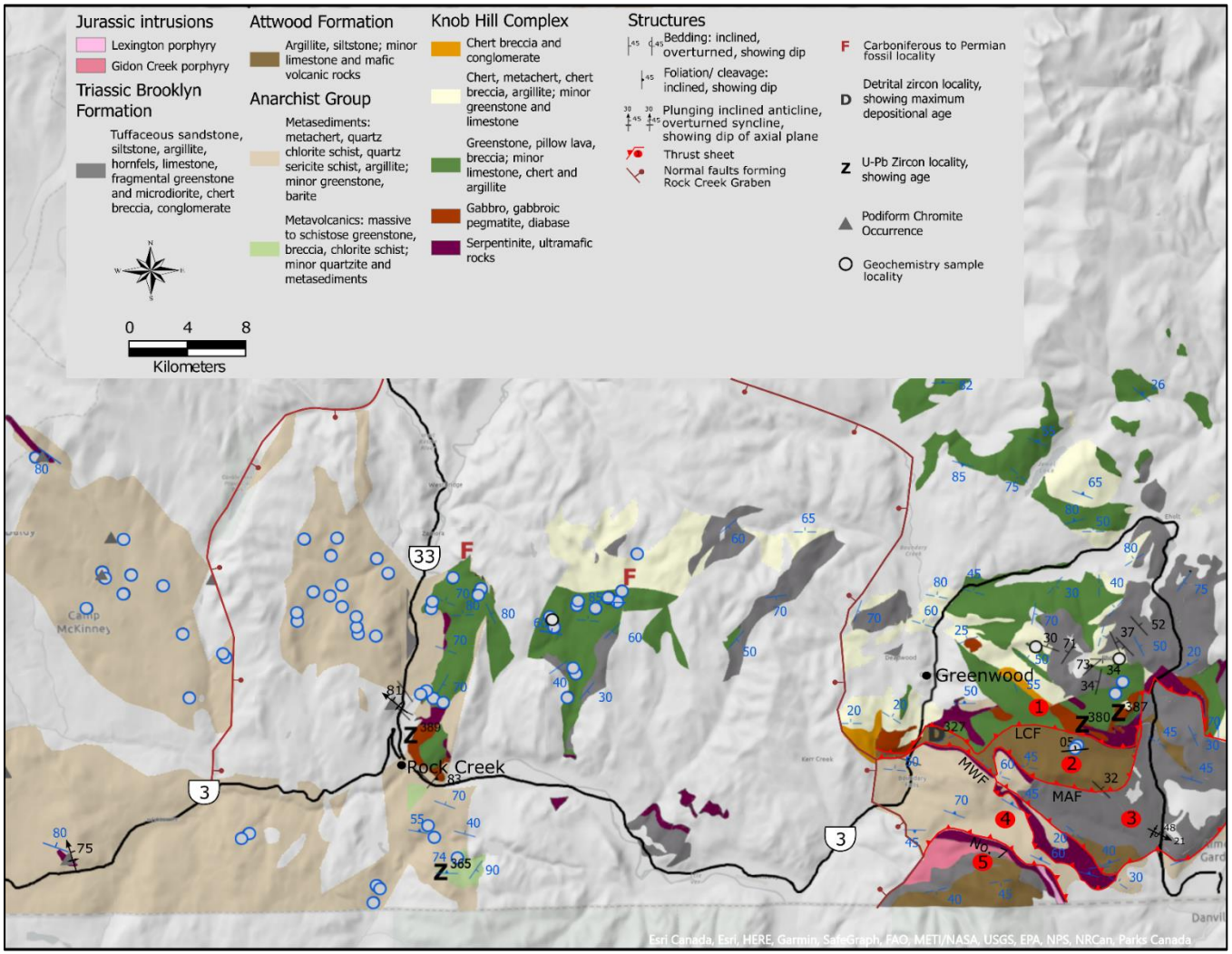

Figure 6. Geological map of the Okanagan subterrane within the Kootenay-Boundary region (study region C) modified from Cui et al. (2017) and Höy (2018). Black structural symbols are data collected from this study. Blue symbols are from Höy (2018). Geochemistry sample locations with black outlines are from this study and those with blue outlines are from Massey and Dostal (2013). Fossil, detrital zircon, and U-Pb zircon data are from Mortensen et al. (2011, 2017), Massey (2006), and Massey et al. (2013). Five northward-dipping thrust sheets south of Greenwood described in detail by Fyles (1990) are labelled 1 through 5. The splay faults of these thrust sheets include the Lind Creek fault (LCF), the Mount Attwood fault (MAF), the Mount Wright fault (MWF), and the Number 7 fault (No. 7). The 200 Ma Lexington porphyry is truncated and sheared by the Number 7 fault (Fyles 1990). Sheared margins are also found within the 172 Ma Gidon Creek porphyry (Massey et al. 2010).

Chapter Two: Results

2.1. Field Observations and Petrography

Detailed and regional mapping built on previous studies and resulted in a collection of stratigraphic and structural data and whole rock geochemistry to be used together to characterize the Okanagan subterrane. A presentation of field and petrographic observations is followed by structural and stratigraphic observations and the presentation of geochemical data. Rocks within the Okanagan subterrane have been regionally deformed and metamorphosed typically to lower greenschist facies but locally as high as amphibolite grade and are locally weakly to pervasively pyritiferous.

2.1.1. Ultramafic Rocks and Gabbro

Ultramafic rocks are encountered in both the Thompson-Nicola and Kootenay-Boundary regions. Commonly serpentinized, these rocks are strongly magnetic with well-defined, steeply-dipping to subvertical foliation. In the Thompson-Nicola region, serpentinites outcrop in lenticular zones paralleling foliation and weather orange and green. A blocky, bluff-forming outcrop at the northernmost extent of the Chapperon Group, 27 km NE of Chapperon Lake consists of medium grey weathering serpentinite pervasively cut by pink veins thought to consist of the manganese silicate rhodonite. Ultramafic rocks also occur as lenticular bodies in the Kootenay-Boundary region cropping out largely along thrust faults south and east of Greenwood but also as chromitite-bearing, NW-striking, subvertical lenses north and west of Rock Creek (MINFILE 1985, Fyles 1990, Dostal et al. 2001, Massey and Dostal 2013). They present as either dark green- to black-weathering serpentinite (Figure 7) or orange- to buff-weathering listvenite, a carbonatized serpentinite. North of Rock Creek 4 km from the junction

of Highway 3 and Highway 33, a 30 m roadside outcrop of black-weathering serpentinite anastomoses between disrupted panels of orange-weathering listvenite (Figure 8).

Figure 7. A serpentinite outcrop 13 km SE of Greenwood in the Kootenay Boundary region. Serpentinite outcrops in this area vary from competent to heavily fractured, forming knobby hills. The rocks are aphanitic, strongly magnetic and foliated.

Figure 8. Photo looking westward at a roadside outcrop, GMc15-20-3, north of Rock Creek in the Kootenay Boundary region where aphanitic greenstone dips northward beneath serpentinite anastomosing between disrupted panels of listvenite.

Gabbroic rocks are a minor component in the Old Tom assemblage of the Okanagan-Similkameen region where they present as thick sills intruding greenstone. Gabbros are most prevalent in the Kootenay-Boundary region where they are spatially associated with serpentinites, form bluffs and high-standing outcrops, and range from patchy and pegmatitic to fine-grained microgabbro. Fyles (1990) noted that, locally, grain size was gradational from coarse- through to fine-grained gabbro into aphanitic greenstone, and that gabbro can be found intruding greenstone. Gabbros are composed primarily of plagioclase and relict clinopyroxenes which have been extensively replaced by hornblende (Dostal et al. 2001, Massey and Dostal 2013) likely resulting in this unit's original designation by Church (1986) as 'Old Diorite'.

2.1.2. Podiform Chromitite

Podiform chromitite occurrences are found within the Anarchist Group approximately 25 km northwest and west of Rock Creek within steeply-dipping, NW-SE trending lenses of serpentinite (Figure 6). A 9 km-long, discontinuous series of occurrences is also found along trend in the Chapperon Group 6 km north of Trepanier Provincial Park (Figure 4). Deposits consist of fine- to coarse-grained stringers, nodules, crystal aggregates and pods primarily hosted within serpentinized dunite or harzburgite lenses up to 1000 meters long x 100 meters wide. The Chrome-Vanadium deposit within the Chapperon Group, for example, occurs as crystal aggregates and lenses hosted in NW-trending, fault-bounded, serpentinized harzburgite. The Anarchist Chrome deposit, 24 km SW of Rock Creek, consists of massive, coarsely crystalline angular pods hosted in fine-grained grey carbonate, believed to be listvenite. In the Bridon deposit, 30km NW of Rock Creek, fine-to medium-grained chromitite lenses are boudinaged in the NW-SE direction parallel to subvertical foliation and shearing within serpentinized dunite and metasediments of the Anarchist Group. Some of the chromitite lenses in this deposit are openly folded. The characteristics of each occurrence are summarized in Table 1.

Table 2. Summary of podiform chromite occurrences compiled from MINFILE (1985).

Name	MINFILE #	Location	OS Unit	Host Rock	Orientation	Dimensions of serpentinite body (L x W in meters)	Structural features
Chrome-Vanadium	082LSW056	11U 294620 E, 5543371 N	Chapperon Group	Serpentinized harzburgite	330/85	9000 x 500	Sheared, fractured
Anarchist Chrome	082ESW024	11U 338780 E, 5432331 N	Anarchist Group	Listvenite	~300/80	15 x 5^	Chromite grains are fractured but not sheared
Rock Creek	082ESW149	11U 353232 E, 5438604 N	Anarchist Group	Serpentinized peridotite	n/a*	500 x 50	Sheared, fractured, fault bounded
Jolly Creek Chrome	082ESW159	11U 345519 E, 5444437 N	Anarchist Group	Serpentinized peridotite	n/a*	600 x 100	n/a*
Elk	082ESW228	11U 34178 E, 5446477 N	Anarchist Group	Serpentinized peridotite	n/a*	n/a*	n/a*
Bridon	082ESW025	11U 338408 E, 5450203 N	Anarchist Group	Serpentinized dunite	330/90	1000 x 75	Sheared parallel to regional foliation, boudinaged, openly folded
KET20	082ESW232	11U 336029 E, 5436213 N	Anarchist Group	Serpentinite	n/a*	n/a*	n/a
BEV 97	082ESW285	11U 340767 E, 5444881 N	Anarchist Group	Serpentinite	n/a*	n/a*	Brecciated

** Information not available*
^ Dimensions for the listvenite body is not available, reported dimensions are for the chromitite pod

2.1.3. Metavolcanic Rocks

Metavolcanic rocks, ubiquitous throughout the Okanagan subterrane, are represented by aphanitic greenstone with locally prevalent greenschist, tuff, pillow lava, and breccia. Phenocrysts, if present, consist of fine-grained plagioclase and pyroxene with minor hornblende. Greenstones range from dark green with red-weathering surfaces to sage green with smooth, green-weathering surfaces depending on the degree of silicification and epidotization. Locally, these rocks contain screens or interbeds of varicolored chert and mudstone (Figure 9). Calcite or chlorite occur as amygdules and, along with quartz and epidote, as fracture fill. Metavolcanic rocks exist primarily as flows but also as diabase dikes intruding flows. In the Okanagan-Similkameen region, diabase dikes of the Old Tom assemblage NW of Keremeos are heavily epidotized and are found intruding through and containing screens of grey to white chert. In the Kootenay-Boundary region, 12 km ESE of Greenwood, diabase is observed both intruding and as inclusions within gabbro of the Knob Hill Complex (Massey 2006a).

Figure 9. Screens of chert within greenstone in an outcrop along Ashnola River Road 19 km west of Keremeos (Okanagan Similkameen region).

2.1.4. Chert

Chert rocks are most abundant in the Old Tom and Shoemaker assemblages of the Okanagan-Similkameen region and the Knob Hill Complex of the Kootenay-Boundary region. In the Okanagan-Similkameen, cherts are massive, thickly-bedded, ribboned, or conglomeratic (Figure 10) They are found in a variety of colors including black, grey, green, and red, and are locally pyritiferous. Mottled cherts are veruginous and locally contain thin clayey layers. Chalcedony or microcrystalline quartz fills fractures. Microscopic circular zones of coarser quartz likely represent recrystallized radiolarians

(Figure 11). Black chert weathers light to dark grey with light grey mottled surfaces. Grey chert ranges from light to dark grey. Both black and grey chert are locally ribboned or medium- to thickly-bedded with thin interbeds of siliceous siltstone or shale. Red cherts have burgundy or orange-red mottling on fresh and weathered surfaces and are locally gradationally interbedded with white and grey chert or thin laminae of argillite. Green cherts range from sage-green to green-grey and are locally mixed or interbedded with siliceous greenstone or thin laminae of light green mudstone. Hosted primarily within chert rocks in the Okanagan-Similkameen region are several rhodonite occurrences. Rhodonite is pink and brown with black and brown weathered surfaces and occurs as thin beds or veins. Chert rocks encountered in the Kootenay-Boundary region are brecciated, conglomeratic or bedded and white, grey or green in color. Chert granulestones and pebble conglomerates 8 km NE of Greenwood and 3 km north of Rock Creek, respectively, are clast-supported with sub-rounded clasts of white, dark grey and green chert to 10 mm in diameter.

Figure 10. A) Bedded and B) ribboned chert from the Shoemaker Formation in the Okanagan-Similkameen Region.

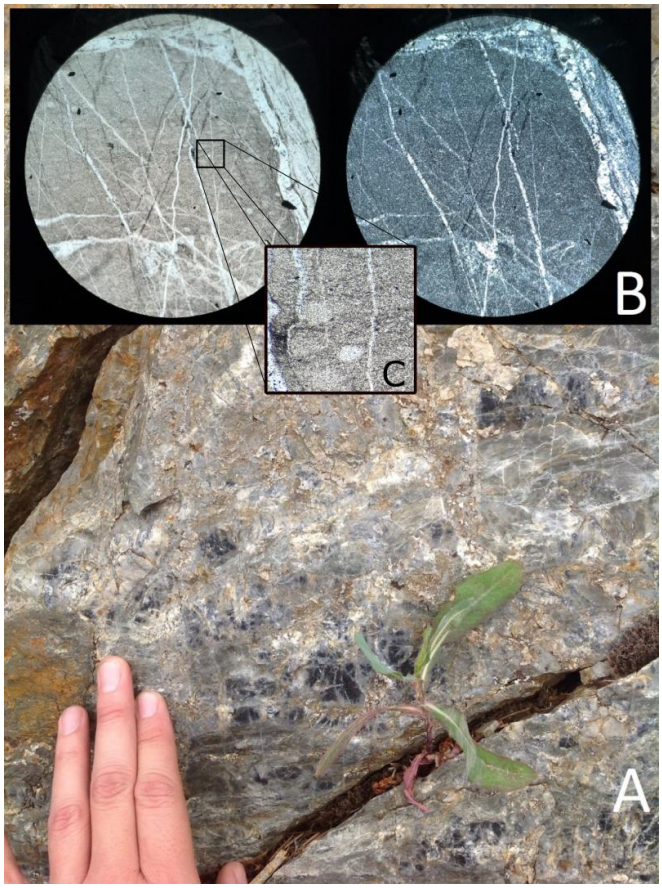

Figure 11. A) Photo of an outcrop of massive, variegated grey and black chert, 4 km north of Keremeos (Okanagan-Similkameen Region). B) Photomicrographs of chert from this outcrop. The image on the left is in plane-polarized light showing circular zones possibly representing recrystallized radiolarians. The image on the right shows the same region under crossed-polarized light. Coarser quartz and chalcedony fill fractures. C) A zoomed-in view of the circular 'radiolarian' zones. These areas are also filled with coarser quartz crystals than the surrounding chert. Viewed at 100x magnification (field of view = 0.2 mm).

2.1.5. Shale and Sandstone

Shale and sandstone are minor components in most Okanagan subterrane units but prevalent within the Independence-Bradshaw and Barslow assemblages and Oregon Claims Formations of the Okanagan-Similkameen region and in the Attwood Formation of the Kootenay-Boundary region. Black shale 20 km NW of Keremeos, in the Independence-Bradshaw assemblages, weathers dark grey with rusting on joint surfaces. Calcite veins, where present, are commonly folded or boudinaged. In the Old Tom assemblage, black and dark-red shales are interleaved with greenstone 15 km NW of Keremeos (Figure

12). Red-brown weathering tuffaceous sandstones 20 km west of Keremeos in the Independence-Bradshaw assemblages are well-sorted, fine-grained, and micaceous with grey-brown fresh surfaces. Microscopic analysis reveals angular to sub-angular clasts extensively replaced by silica (Figure 13).

Figure 12. Red shale interleaved with red-weathering greenstone at an outcrop 15 km north of Keremeos (Okanagan Similkameen region) in the Old Tom assemblage.

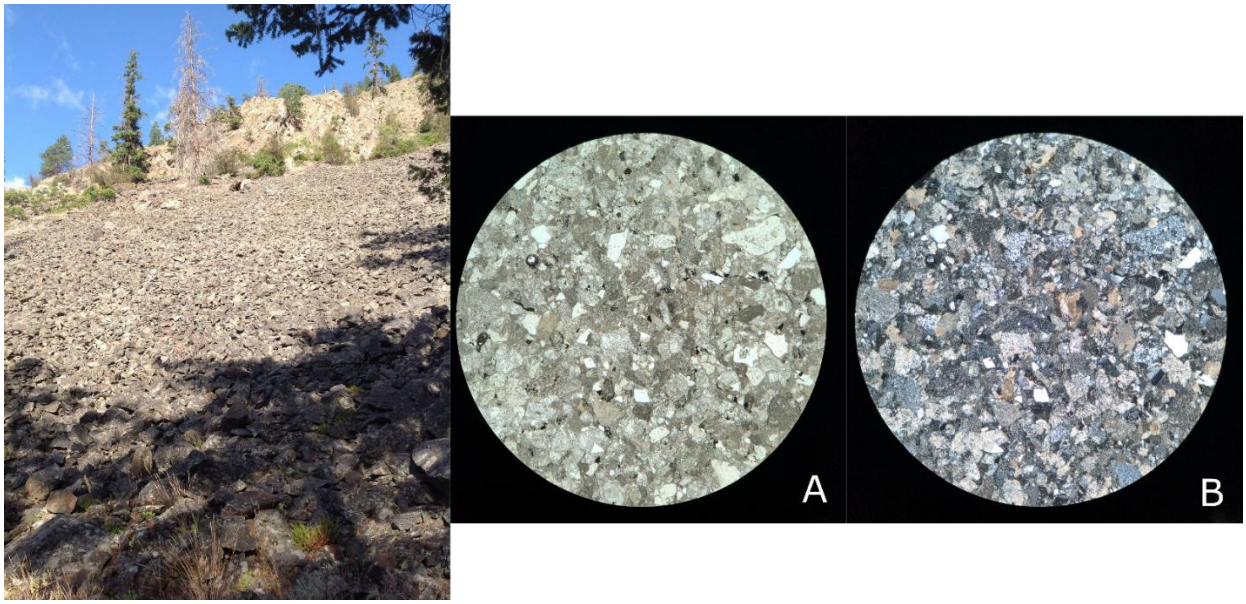

Figure 13. Tuffaceous sandstone of the Okanagan-Similkameen region at site Ash20-07. Photomicrograph of a sample from this locality under A) plane-polarized and B) cross-polarized light viewed at 100x magnification (field of view = 0.2 mm).

2.1.6. Carbonate rocks

Carbonate rocks are ubiquitous throughout the Okanagan subterrane albeit in minor abundance relative to other lithologies. These range from black marl or dark grey micrite to white coarse-grained marble (Figure 14 A). In the Thompson-Nicola region, grey- and white-banded coarsely crystalline marble 16 km NE of Trepanier Provincial Park is interbedded with minor sandstone and is intruded by a series of microgabbro sills of unknown age. In the Okanagan-Similkameen region, outcrops within the Shoemaker assemblage along Olalla Creek 15 km north of Keremeos have white to red marble cut by steeply-dipping epidote-rich diabase dikes. The red marble is due to a dense fracture network filled with red, hematite-stained quartz and calcite (Figure 14 B). Middle Devonian limestone in the Independence-Bradshaw, Old Tom and Shoemaker assemblages contains a mix of conodont, crinoid and brachiopod fossils and are interlayered with chert, argillite, sandstone, chert pebble conglomerate and greenstone. Limestone 14 km SE of Greenwood within the Attwood Formation of the Kootenay-Boundary region are dark grey with white to light brown weathered surfaces and white marbling and dark grey stringers throughout.

Figure 14. A) Grey marble from the Thompson-Nicola region 40 km NW of Kelowna. B) Hematite-stained marble from the Okanagan-Similkameen region 16 km NW of Keremeos.

2.1.7. Phyllite, Schist and Gneiss

Phyllites encountered in the Anarchist Group are siliceous and grey or chloritic imparting a dark brown-green to mint-green color. Muscovite biotite schists encountered in this study are fine- to coarse-grained and occasionally crenulated with orange to red weathering and folded quartz veins. Gneissic rocks in both the Chapperon and Kobau groups have well-developed banding and light to dark grey weathered and fresh surfaces.

2.2. Structural Geology

The Okanagan subterrane was subjected to multiple phases of deformation between the latest Permian and Late Jurassic. The study areas can be divided into six structural domains (Figure 15): Thompson-Nicola region – North (TNR-N), Thompson-Nicola region – South (TNR-S), Okanagan-Similkameen region – North (OSR-N), Okanagan-Similkameen region – South (OSR-S), Okanagan-Similkameen region – East (OSR-E), and the Kootenay-Boundary region as a single structural domain (KBR). Detailed observations of mesoscopic structures attributable to each deformation event are outlined below and summarized in Table 2.

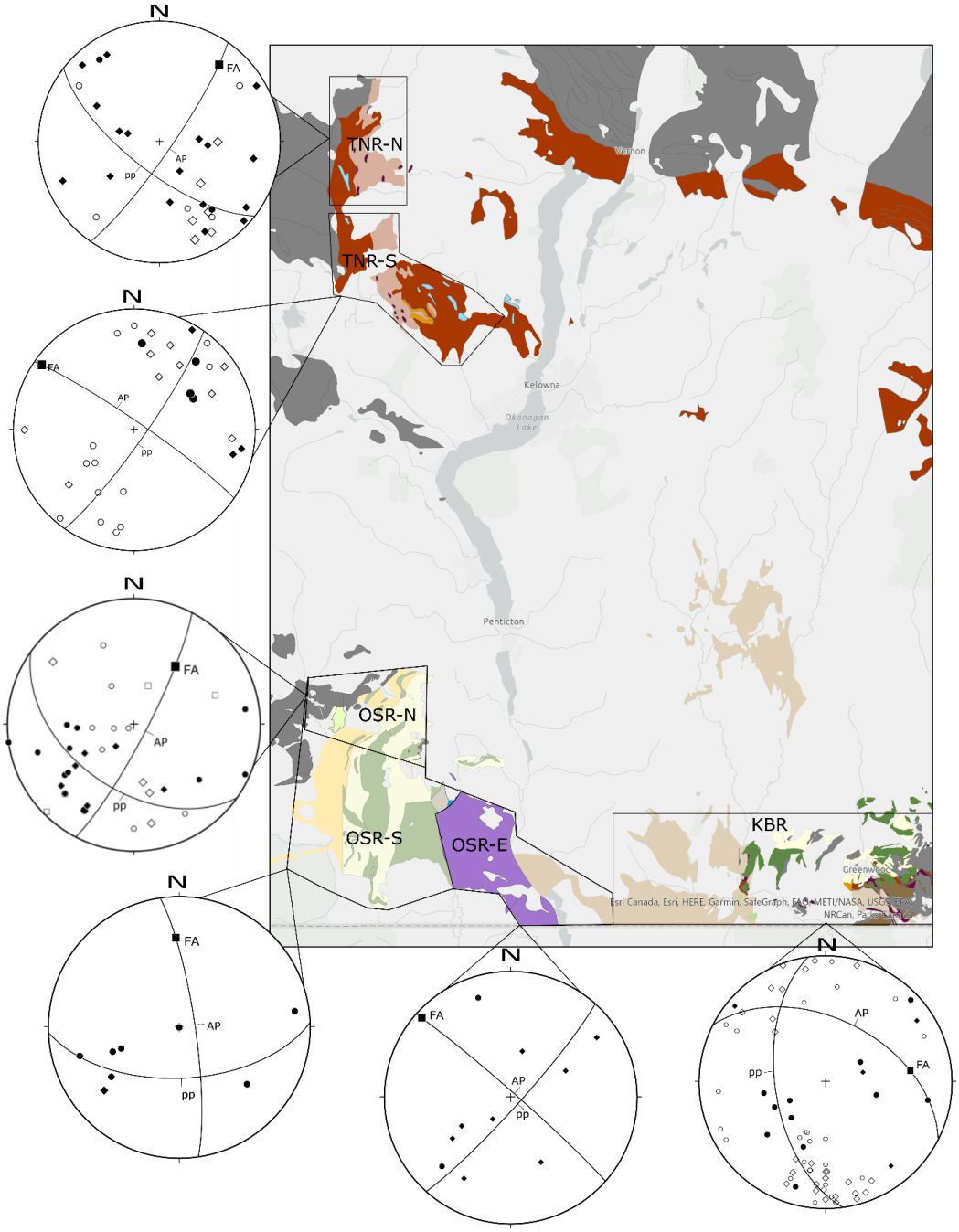

Figure 15. Graphic illustration depicting the distribution and characteristics of F2 folds within six structural domains of the Okanagan subterrane: Thompson Nicola Region-north (TNR-N), Thompson Nicola Region-south (TNR-S), Okanagan Similkameen region-north (OSR-N), Okanagan Similkameen region-south (OSR-S), Okanagan Similkameen region-east (OSR-E), and Kootenay Boundary region-east (KBR-E). Unit colors and descriptions are the same as shown in Figures 4, 5, and 6. All stereonet plots of poles to bedding (circles), poles to S1 foliation (diamonds), and F2 hinge lines (squares) were drawn and analyzed using Stereonet v.11 (Allmendinger et al. 2012, Cardozo and Allmendinger 2013). Filled symbols represent data from this study. Open symbols represent data from Read and Okulitch (1977) in the Thompson-Nicola and Okanagan-Similkameen regions and Höy (2018) in the Kootenay-Boundary region. No S2 axial planar cleavage was observed to constrain the F2 axial plane therefore the axial planes of F2 folds shown here (AP) were determined using the axial plane finder function within the program. F2 Fold axes (FA) and profile planes (pp) were determined using the Bingham analysis of the cylindrical best fit to the data.

Table 3. Characteristics of F1 and F2 Folds within the Okanagan subterrane and overlying Nicola and Brooklyn Groups

Study area		Thompson-Nicola Region		Okanagan-Similkameen Region			Kootenay-Boundary Region	Timing of Deformation
Structural Domain		TNR-N	TNR-S	OSR-N	OSR-S	OSR-E	KBR	
D1	Tightness	Near isoclinal~*	Near isoclinal~*	Isoclinal*	Isoclinal*	Tight to Isoclinal^	Tight to isoclinal #	Early Permian through Early Triassic
	Vergence	Upright~*	Upright~*	Inclined to Overturned to SE or SW*	Inclined to Overturned to SE or SW*	Recumbent^	Upright to Inclined to SW~	
	Fold Axis Trend (plunge)	NE (gentle)~*	NW (moderate)*	NE (moderate)*	NE (moderate)*	N (gentle to moderate)@	NW (moderate)~	
D2	Tightness	Open~	Open~	Open~	Open~	Open to Tight~^&	Open to Tight~	Middle Jurassic
	Vergence (direction)	Upright (NW)~	Upright (SW)~	Upright (NW)~	Upright (W)~	Upright (SW)^	Upright (SE) to Overturned (SW)~	
	Fold Axis Trend (plunge)	NE (gentle)~	NW (gentle)~	NE (moderate)~	N (moderate)~	NW to SE (gentle)~^	E to NE (gentle)~	

n.a.: information not available
** Read and Okulitch (1977)*
^ Okulitch (1979)
 # Fyles (1990)
@ Ross (1981)
& Mäder et. al. 1988
~ this study

F1 folds within the Thompson-Nicola and Kootenay-Boundary domains are upright to inclined with variably-trending axes and a bedding-parallel S1 foliation such as that observed within phyllites of the Chapperon Group in the TNR-N domain (Figure 16). Rare mesoscopic hinges of isoclinal minor F1 folds in the OSR-N domain plunge moderately NE. The axial planes of these folds dip moderately to steeply toward the northeast and northwest. F1 folds within the OSR-E domain are recumbent with shallowly to moderately north-plunging hinge lines (Figure 17). D1 structures in the study regions are restricted to earliest Permian and older rocks and are truncated by the regional Permo-Triassic unconformity (Read and Okulitch 1977) constraining the age of D1 to post-earliest Permian but pre-middle Triassic. Clastic sediments in the Mount Roberts Formation are consistent with derivation from strata within the Okanagan subterrane with an age range that bridges the time gap between the youngest Okanagan subterrane and oldest Triassic arc strata. D1 structures do not appear to be represented within the Mount Roberts Formation (Simony 1979) thus constraining the timing of D1 in this region as

pre-latest Pennsylvanian or earliest Permian. Carbonate platform deposition continued into the Middle Permian in the Harper Ranch Group type section north of Kamloops (Figure 1) and was affected by D1 folding (Smith 1979, Beatty et al. 2006) suggesting a D1 event that initiated by the latest Pennsylvanian or earliest Permian east of Greenwood and continued at least through the Middle Permian younging northwestward beyond Kamloops.

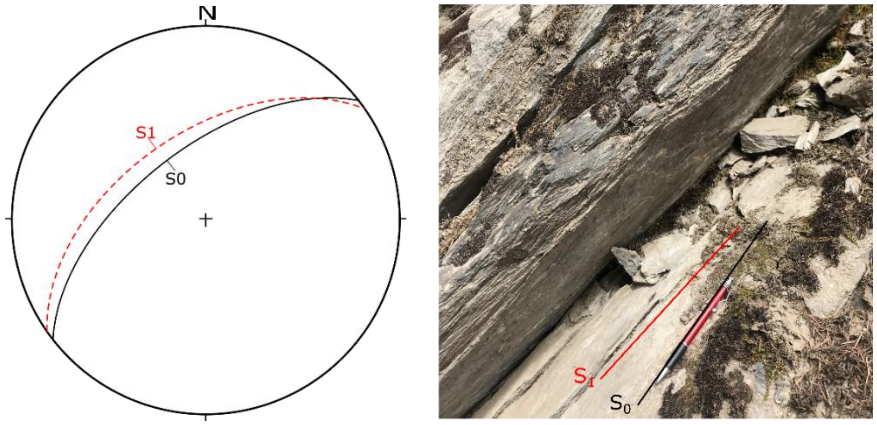

Figure 16. F1 folds in Chapperon Group phyllite 29 km NE of Chapperon Lake in the Thompson-Nicola region – North domain (TNR-N) with the pen positioned parallel to the intersection of NW-dipping bedding (S_0) and S_1 foliation with the rock face.

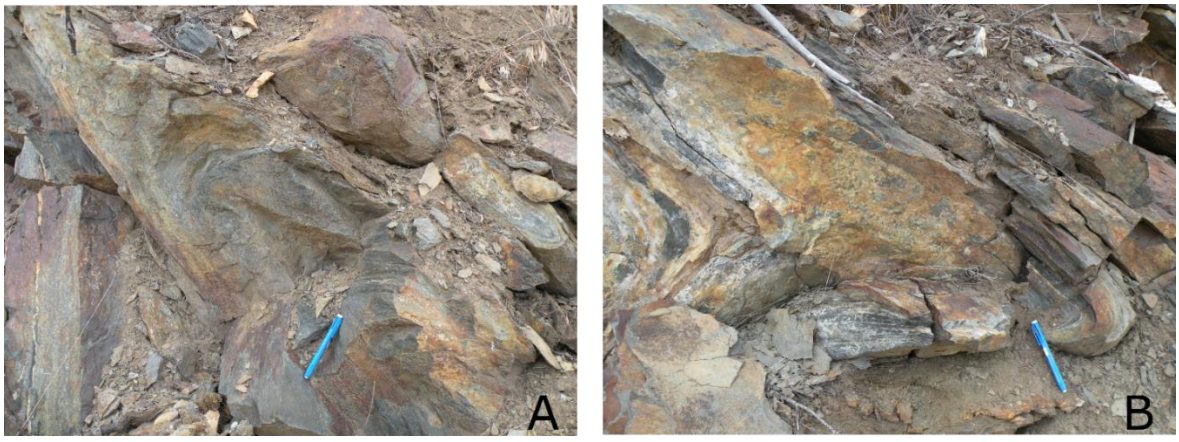

Figure 17. Photos of overturned (A) to recumbent (B) F1 folds in Anarchist Group phyllite 62 km SE of Keremeos at station GMc15-21-5 in the Okanagan-Similkameen region – East domain (OSR-E). The hinge lines plunge shallowly to moderately to the North.

In the OSR-N domain, the Nicola Group is cut by a series of northeasterly-trending, steeply west-dipping listric faults (Figure 5). From west to east, these are the Chuchuwayha, Bradshaw, Cahill Creek, and Winters Creek faults. The earliest successions of the Nicola Group here are fault-bounded, shallow to deep marine sedimentary facies suggesting that the faults were rifts which post-date D1 but formed prior to or during the Late Carnian to Early Norian deposition of these packages during an extensional deformation phase, E1. Overlying Late Triassic boulder conglomerate, clastic sediments and tuffs are widespread across the area constraining the end of E1 rifting in the OSR-N domain to pre-middle Norian. In the KBR domain, Middle Triassic Brooklyn Formation strata are cut by a series of north- to NE-dipping thrust faults (Figure 6). From north to south these include the Lind Creek Fault, the Mount Attwood Fault, the Mount Wright Fault, and the No. 7 Fault. Chert and limestone pebble conglomerates form the base of the Brooklyn Formation. Siltstone, shale, and limestone comprise upper sequences and indicate deposition in a progressively deepening basin. The lithologic similarities between Brooklyn and Nicola Group strata suggest the faults in the KBR domain may have also originally been E1 rift-related extensional faults which formed prior to and controlled deposition of the Brooklyn Group thereby constraining E1 rifting in this region to pre-Ladinian time.

A subsequent phase of compressional deformation, D2, resulted in primary folding of the overlying Nicola Group and Brooklyn Formation, secondary folding of Okanagan subterrane strata, and late stage thrust faulting. Stereonet plots of D2-related folds (F2) are depicted relative to their structural domains in Figure 15. F2 folds are open and upright with axes ranging from NW- to E-trending. Re-folding of S1 cleavage planes in phyllite of the Chapperon Group defines the close to open gently-inclined F2 folds in the TNR-N domain (Figure 18). Conglomerate exposures of the Harper Ranch Group outline an overturned, SE-plunging antiform/synform pair which exposes rocks of the Chapperon Group in the core of the antiform and preserves Harper Ranch Group rocks in the core of the synform. In the OSR-N

domain, F2 folds are gently NW-verging, and moderately NE-plunging. These folds in grey-green chert of the Shoemaker assemblage at station Ola20-02, 23 km north of Keremeos, however, are overturned, south-verging and east-plunging (Figure 19). A synform in black chert at station Ker20-01 in the OSR-S domain is upright with a slightly west-verging orientation and a gently north-plunging axis (Figure 20). F2 folds in the OSR-E domain are open to tight and upright with northwest-plunging axes. Parasitic F2 folds are observed re-folding phyllitic cleavage within the Anarchist Group 62 km southeast of Keremeos at station GMc15-21-5 (Figure 21). In the KBR domain, F2 folds are overturned and south-verging with gently east-plunging axes as observed at Gre20-12 in a 50 m outcrop of bedded limestone of the Brooklyn Formation (Figure 22). Further west, mesoscopic F2 folds near serpentinite outcrops north and west of Rock Creek are inclined, verging to the SW with NW-plunging axes. Serpentinite exposures in all three domains which host podiform chromitite trend NW-SE, dip steeply, and are often fault-bounded with contacts and foliation that parallel their regional D2 axial planes (MINFILE, 1985; Figures 4 and 6). D2 folds within the Mount Roberts Formation are overturned to the east with NNE-SSW trending axes. The Mount Roberts Formation overlies a Devonian intra-oceanic island arc, the Trail Gneiss Complex, along a folded mylonitic contact. The axial plane of folds in the mylonite parallels S2 in the Mount Roberts Formation and shallows eastward toward sub-horizontal within the Trail Gneiss Complex over a distance of approximately 8 km (Simony 1979).

Figure 18. F2 re-folding of S1 cleavage planes in Chapperon Group phyllite of the TNR-N structural domain.

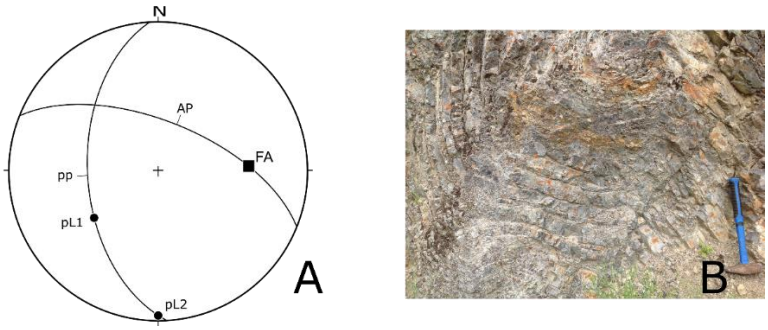

Figure 19. A) Stereonet plot of mesoscopic F2 folds within grey-green chert at Ola20-02 within the Shoemaker Formation of the OSR-N structural domain. FA= F2 fold axis, AP = F2 axial plane, pp = F2 profile plane, pL1 and pL2 = poles to limbs 1 & 2, respectively. B) Photo taken looking NE at the outcrop of folded chert at Ola20-02.

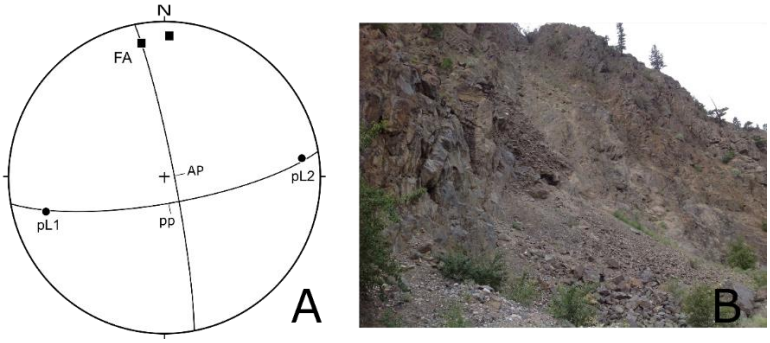

Figure 20. A) Stereonet plot of a mesoscopic F2 synform at Ker20-01 within black chert of the Shoemaker Formation in the OSR-S structural domain. FA= F2 fold axis, AP = F2 axial plane, pp = F2 profile plane, pL1 and pL2 = poles to limbs 1 & 2, respectively. B) Photo taken looking south toward the outcrop at Ker20-01 depicting the steeply east-dipping western limb of the fold.

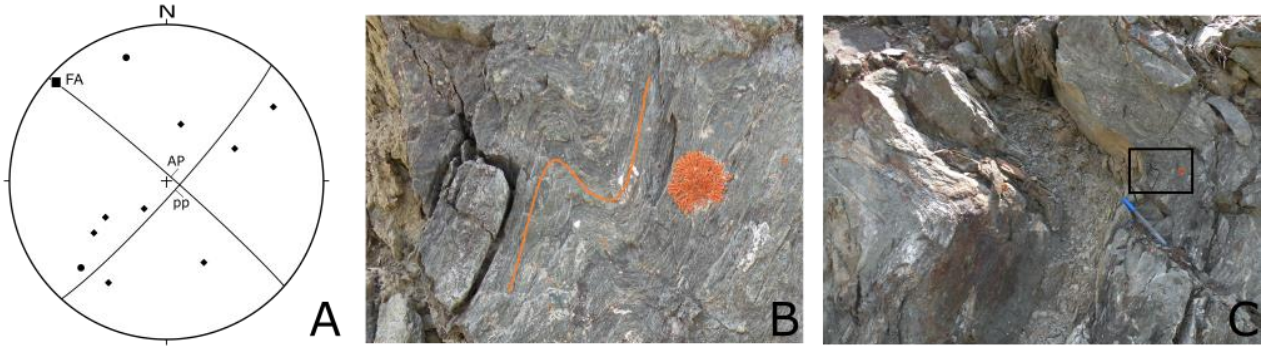

Figure 21. A) Stereonet plot of bedding (circles) and S1 foliation (diamonds) from the OSR-E structural domain of the Okanagan subterrane. FA = F2 fold axis, AP = F2 axial plane, pp = F2 profile plane. No S2 axial planar cleavage was observed. B) Parasitic F2 folds (example highlighted in orange) in phyllite of the Kobau Group 7km SE of Keremeos. C) Recumbent F1 fold in the same phyllite. Black rectangle highlights the location of F2 folds shown in B.

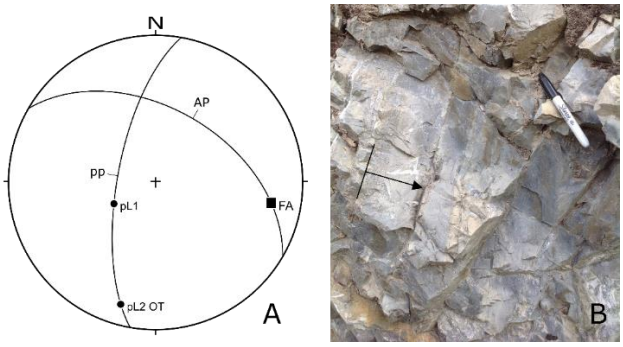

Figure 22. A) Stereonet plot of an overturned F2 fold within a 50m continuous roadside outcrop of bedded limestone of the Brooklyn Formation at station Gre20-12 in the KBR structural domain. FA= fold axis, AP = axial plane, pp = profile plane, pL1 = pole to limb 1, pL2 OT = pole to overturned limb 2. B) East-facing photo of steeply-dipping overturned limb of this fold. The arrow indicates graded bedding fines southward from left to right. The upright limb is to the south.

The trace of the E1 faults in the OSR-N domains parallels the northeast trend of the regional F2 fold axis suggesting the original rift-related extensional faults were reactivated during D2 as imbricate thrusts. A duplex thrust fault system is exposed in a cliff face north of the town of Hedley, 37 km NW of Keremeos in the OSR-N domain (Figure 23). Bounding faults include the Chuchuwayha fault to the west and the Bradshaw fault at its base to the east. The faults cut up-section to the southeast through hanging wall and footwall strata defining hanging wall and footwall ramps that connect through bedding parallel flats and indicate a transport direction toward the southeast (Figures 23 and 24). The thrust faults cut but do not offset the 163 Ma Cahill Creek pluton suggesting that thrust faulting in the west terminates in the earliest Late Jurassic shortly after pluton emplacement. In the KBR domain, truncation and shearing of the 200 Ma Lexington porphyry by the Number 7 fault (Fyles 1990), sheared margins within the 172 Ma Gidon Creek porphyry (Massey et al. 2010) less than 3 km to the west and the lack of shearing in plutons considered part of the Middle Jurassic Nelson Suite in the hanging wall of the Mount Attwood fault constrain thrust faulting in the KBR domain to have occurred between early and late Middle Jurassic. The above age constraints suggest northwestward younging of a D2 event which includes both folding and east-directed thrust faulting spanning the Middle Jurassic.

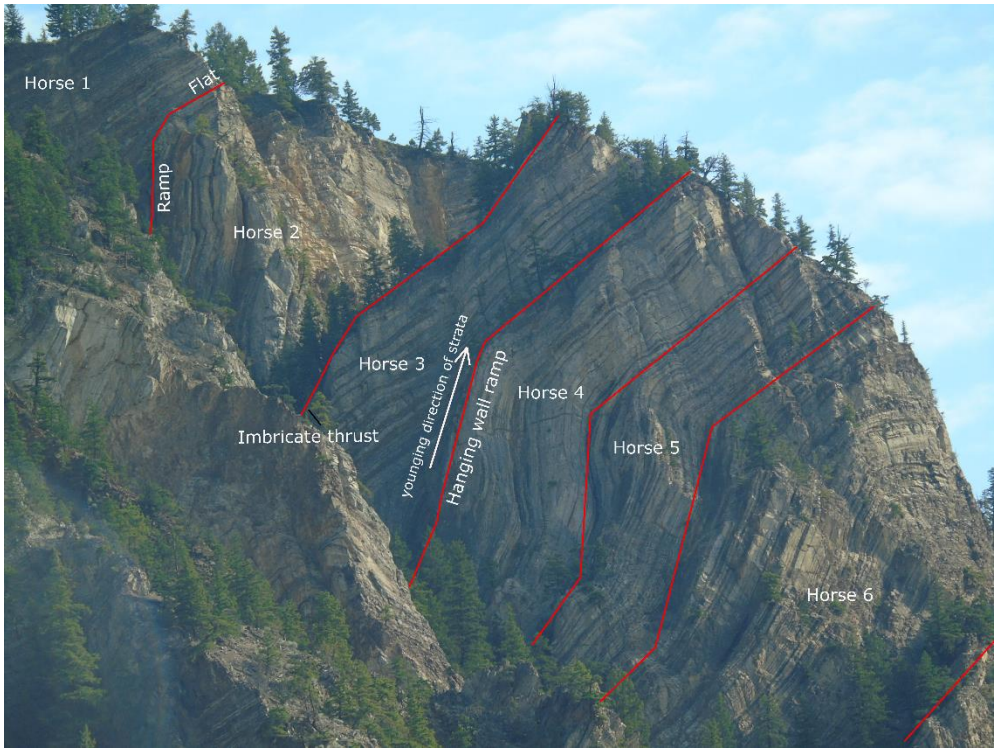

Figure 23. Thrust duplex visible in the steep east face of a hill flanking the northern border of the Hedley townsite of the OSR-N domain (location indicated with an arrow in Figure 5). Imbricate thrusts are indicated in red. Hanging wall ramps cut upsection toward younger strata. Combined with a steeply dipping western ramp limb and SE-dipping axial plane of the fault bend folds within the duplex, these indicators suggest transport direction is to the SE.

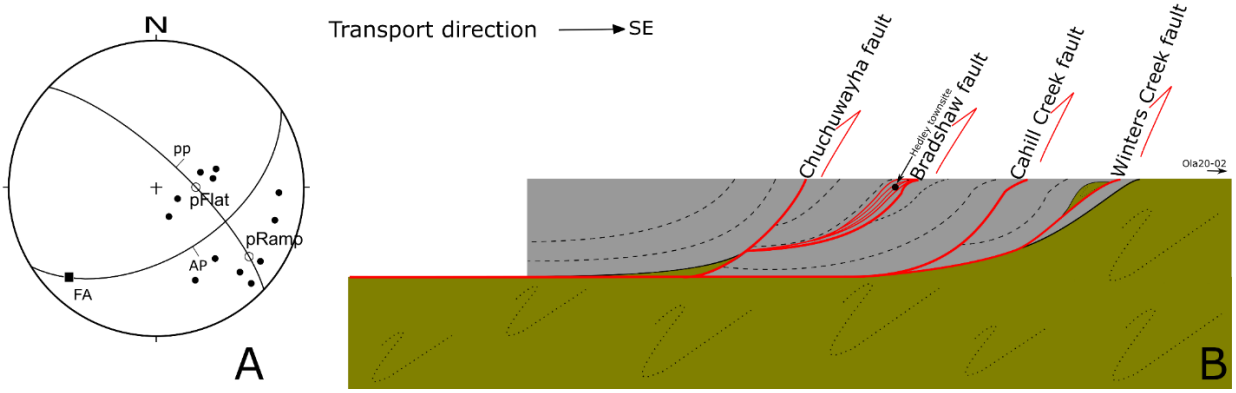

Figure 24. A) Stereonet plot of bedding within Nicola Group of the southern portion of the OSR-N domain as a proxy for fault bend folds observed in the cliff face above the Hedley townsite. Open circles labelled pRamp and pFlat = mean poles to ramp and flat, respectively; pp= F2 profile plane, AP= F2 axial plane, FA= F2 fold axis. Fault-bend fold have a SE-dipping axial plane indicative of transportation direction of layers in this thrust system is to the southeast. B) Cartoon illustrating reactivated E1 extension faults to produce the fold geometry in the duplex at the Hedley townsite and Okanagan subterrane units of the OSR-N domain. Olive green unit represents the Okanagan subterrane. Grey strata represent the Nicola Group. Illustration demonstrates the approximate location of the Hedley townsite duplex and relative direction of SE-verging folds at site Ola20-02.

North to south, D2 folds in structural domains alternate between NW- and S-verging (Figure 15). The variability can be explained by post-Jurassic D3 folding about a vertical fold axis. These D3 folds have a near-vertical, east-west striking axial plane and resulted in bending an originally linear, northwest-southeast trending D2 fold and thrust belt. An Eocene-aged extensional event, E2, resulted in up to 90 km of east-west extension from west-directed gravity sliding of the upper crustal block along the Okanagan Valley fault (Figure 5; Tempelman-Kluit and Parkinson 1986, Brown et al. 2012). Palinspastic reconstruction removing this extensional component places the Kobau Group over the Anarchist Group and juxtaposes it with the KBR domain along the longitude of Greenwood.

2.3. Stratigraphy

The aforementioned deformation events have complexly folded and disarticulated much of the Okanagan subterrane, therefore stratigraphic correlations are difficult to discern particularly in the Kootenay-Boundary region. However, observations made during this study combined with compiled data from previous workers allow generalized sequence stratigraphy to be determined. These sequences are constrained where possible by biostratigraphy, U-Pb and detrital zircon ages and are graphically displayed by structural domain in Figure 25. The stratigraphic columns labelled ‘Harper Ranch Group north of TNR-N’ and ‘Mount Roberts Formation’ are adapted from those presented in Beatty et al. (2006) and Roback and Walker (1995), respectively.

Within the Thompson-Nicola region, there is a paucity of biochronologic or geochronologic age constraints, thus relative ages form the basis for this stratigraphic interpretation. Massive white limestone is confined to and intercalated with fine-grained siliciclastics and greenstone of the Harper Ranch Group. A bed of calcareous conglomerate containing fossils of probable Permian age in the Harper Ranch Group 8 km NNE of Trepanier Provincial Park (Figure 4) lies with slight angular

unconformity above metapelites of the Chapperon Group implying a pre-Permian age for the Chapperon Group. A pre-Permian, possibly Mississippian age has been inferred for the Chapperon Group based in part on correlations with units of similar composition and metamorphic grade. Metapelites of the Chapperon Group are phyllitic nearest the western contact with the Harper Ranch Group and gneissic in the center of the mapped extent of the Chapperon Group. Serpentinite pods are confined to the Chapperon Group constraining their time of emplacement to pre-Permian deposition of the Harper Ranch Group.

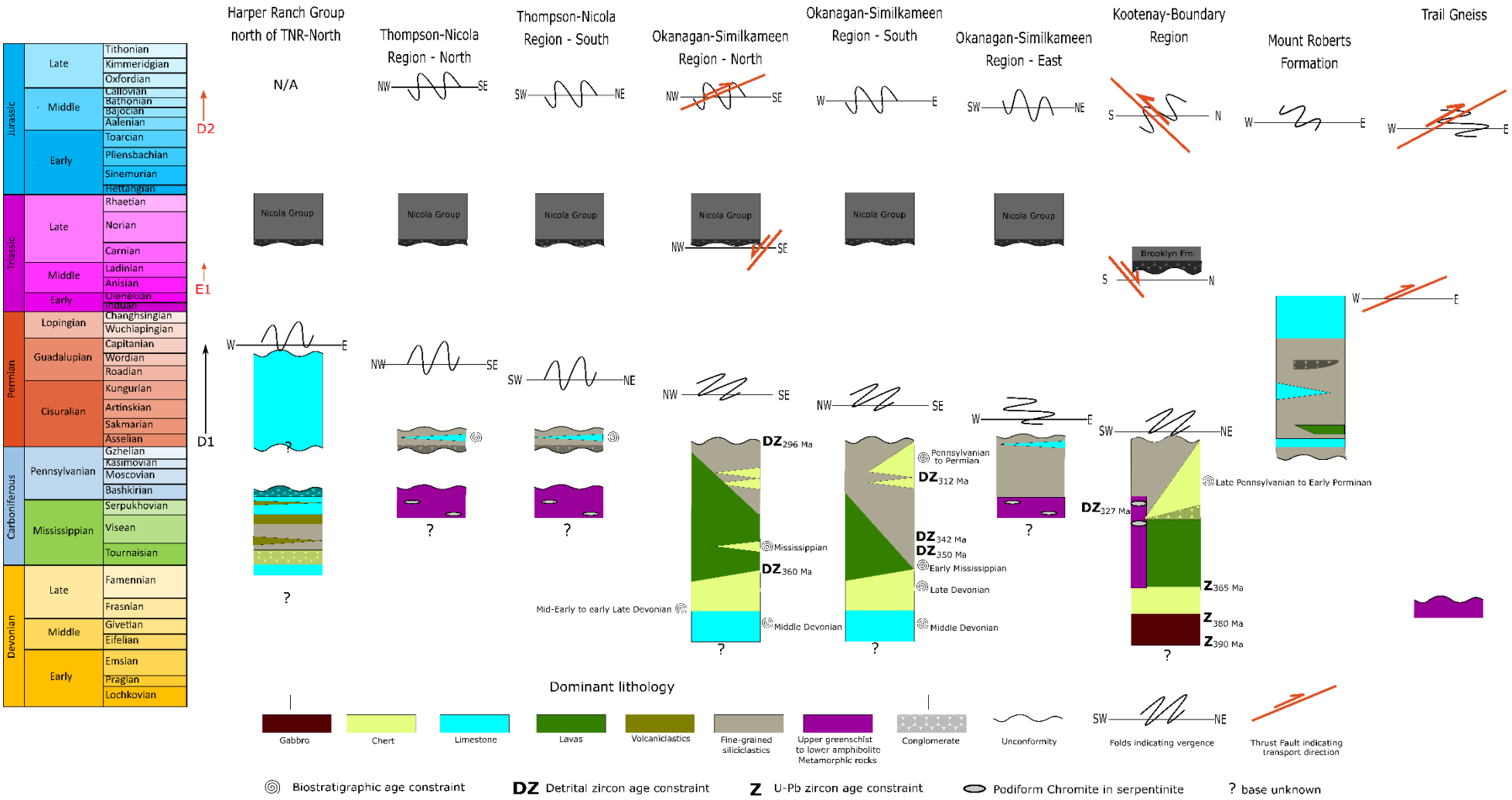

Figure 25. Generalized stratigraphic and structural timeline of the Okanagan subterrane study regions and potential correlative units. (Data compiled from Jones 1959, Okulitch 1973, Read and Okulitch 1977, Simony 1979, Milford 1984, Fyles 1990, Roback and Walker 1995, Massey 2006, Beatty et al. 2006, Mortensen et al. 2011, 2017, Massey and Dostal 2013, Massey et al. 2013; this study).

The oldest rocks of the Okanagan-Similkameen region are Middle Devonian crinoidal limestones stratigraphically interleaved with black and green pyritiferous chert, argillite, sandstone, and minor chert pebble conglomerate and greenstone of the Old Tom, Shoemaker, and Independence-Bradshaw assemblages. These are superseded by greenstones interleaved with middle to late Famennian thinly laminated red cherts, early Mississippian non-pyritiferous grey ribbon chert, crinoidal limestone, and brachiopod-bearing argillite of the Shoemaker assemblage, and Late Mississippian to earliest Permian siliciclastics and minor green and grey chert and limestone of the Shoemaker, Independence-Bradshaw and Barslow assemblages and Oregon Claims Formation. The youngest age recorded in the Okanagan-Similkameen region, 296 Ma, is from detrital zircons in a siliciclastic unit within the Oregon Claims Formation. In the OSR-E domain, the Kobau Group has been assigned a Mississippian age based solely on lithologic and structural correlations with other units. Within the Kobau Group, quartzite with minor phyllite, schist, and marble passes stratigraphically upwards into massive and foliated phyllitic quartzite, chloritic phyllite and schist with minor greenstone and gneiss.

In the Kootenay-Boundary region, the oldest rocks include 390 – 380 Ma gabbro and associated greenstone and serpentinite of the Knob Hill Complex. These are overlain by massive and pillowed greenstone with minor limestone, chert, and argillite. The youngest stratigraphic units in the region consist of Pennsylvanian to Permian-aged chert breccia, chert, and argillite with minor greenstone and limestone of the upper stratigraphic units of the Knob Hill Complex and Late Mississippian to Permian argillite with minor limestone and greenstone of the Attwood Formation. Stratigraphic analysis is not possible in the Anarchist Group with the data available from previous workers but predominant lithologies include phyllitic to schistose metapelites, recrystallized chert and limestone, plus chloritic greenstones, and serpentinites of latest Devonian to earliest Permian age. Minor amphibolitic greenstone is reported by Okultich (1973).

2.4. Whole Rock Geochemistry

2.6.1. Methods

Whole rock geochemistry is commonly used for classifying and postulating tectonic environments of formation for igneous rocks. Chert also has geochemical signatures indicative of depositional environment based on affiliations of certain oxides and rare earth elements to the characteristics of input sources influencing the water column (Murray 1994). The lithogeochemical dataset from this study includes 14 metavolcanic rocks and 18 chert samples from the Okanagan-Similkameen and Kootenay-Boundary regions. Grab samples were initially prepared by cutting on Vancouver Island University's Highland Park power-feed slab saw, cooled by HP Cool Cut™ Pure Low Viscosity mineral oil. Weathered surfaces were removed to obtain at least a 20 g slab with minimal fractures or inhomogeneities. Initial processing at Bureau Veritas in Vancouver, British Columbia included crushing so that more than 70% of the particles could pass through a 2 mm mesh followed by pulverization to less than 75 µm. Lithium borate fusion was used to dissolve the pulp. Major oxides and minor elements were measured by Inductively Coupled Plasma Emission Spectroscopy (ICP-ES). Trace elements were measured by Inductively Coupled Plasma Mass Spectrometry (ICP-MS). The standards analyzed recorded concentrations of major element oxides to within 3% and trace elements to within 5% of expected values. Appendices B and C present the raw data from these analyses and the method detection limit for each element. The datasets were plotted on a variety of classification and tectonic discrimination diagrams. For comparison, discriminant function calculations were performed as outlined in Agrawal et al. (2008), Verma and Agrawal (2011), and Verma and Verma (2013). Cherts were normalized against average North American Shale Composite as presented in Gromet et al. (1984) and plotted on discrimination diagrams as described in Murray (1994).

2.6.2. Results

2.6.2.1. Metavolcanic Rocks

Previous workers in the Okanagan subterrane have focused on analyses of mafic metavolcanic rocks and gabbro, particularly in the Kootenay-Boundary region. The literature search yielded partial datasets of major oxides, trace elements, and rare earth elements on 69 metavolcanic rocks and 4 gabbros from the Kootenay-Boundary region in Massey and Dostal (2013) and Dostal et al. (2001) and 15 metavolcanic rocks in the Okanagan-Similkameen region from Milford (1984) and Ray et al. (1996). The compiled data are presented in Appendix D. Classifications from the Okanagan-Similkameen region were graphically estimated from published plots in Mortensen et al. (2017). Following the magma type classification defined in Le Bas et al. (1986), including the fourteen samples collected in this study, seventy-nine metavolcanic rocks are basic to ultrabasic in composition, with SiO_2 ranging from 42.26 wt.% to 51.96 wt.%. Thirteen samples are of intermediate composition with SiO_2 ranging from 52.08 wt.% to 59.02 wt.%. The metavolcanic rocks of the Okanagan subterrane span the range of classifications from within plate basalt (WPB; Ti/V > 50) to island arc basalt (IAB; Ti/V < 20) on a standard Ti-V diagram (Figure 26; Shervais 1982). Nearly two-thirds of points occupy the IAB domain with 15 of these plotting in the Low-Ti IAB field (Ti/V < 10). These plots show that: the Anarchist Group and Old Tom and Shoemaker assemblages yield approximately equal proportions of IAB, MORB, and WPB samples; three of the four samples from the Independence-Bradshaw assemblages are of MORB-like composition (Ti/V = 20-50), and samples from the Attwood Formation, Barslow assemblage, and Oregon Claims Formation plot almost exclusively as IAB; the Kobau Group largely yields Ti/V > 20 with minor representation in the IAB field; and two-thirds of the Knob Hill Complex is represented in the IAB field with the remaining one-third split between the MORB and WPB fields. The distribution of tectonic environments derived from these analyses is graphically displayed in Figure 27.

As a test of the classifications obtained from Ti-V diagrams, linear discriminant analysis (LDA) calculations using log-transformed ratios of immobile trace elements were performed as presented in Agrawal et al. (2008), Verma and Agrawal (2011), and Verma and Verma (2013). The LDA classifications show a strong (83%) agreement with those obtained from Ti/V ratios on samples with complete geochemical datasets.

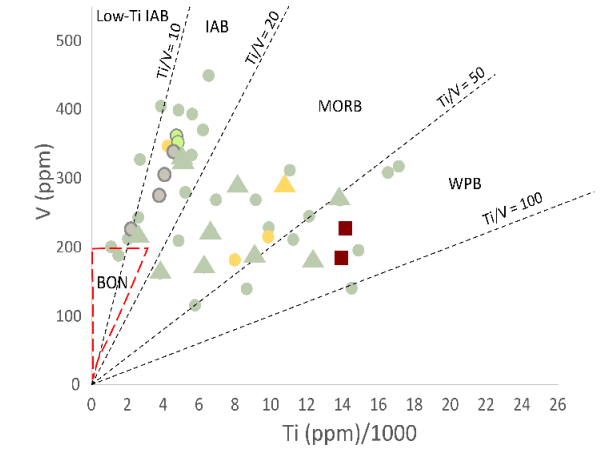

A Okanagan-Similkameen Region (OSR-N and OSR-S)

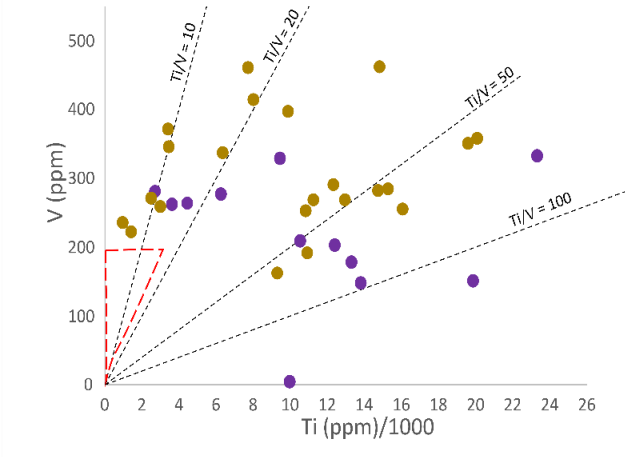

B Okanagan-Similkameen Region East (OSR-E)

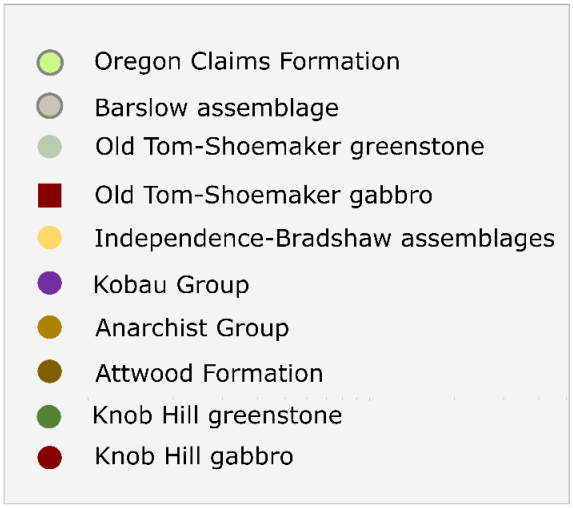

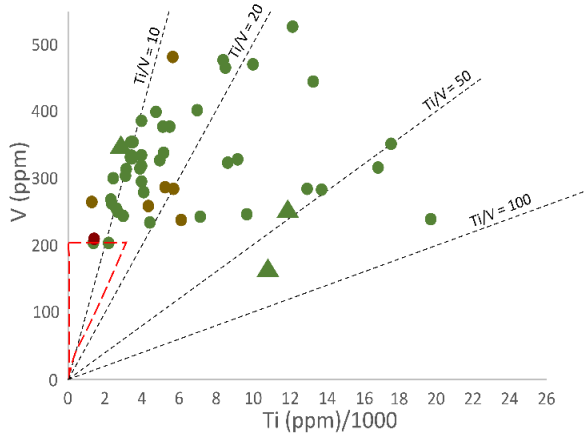

C Kootenay-Boundary Region (KBR)

Figure 26. Standard Ti/V tectonic discrimination diagrams (Shervais 1982) of mafic and intermediate metavolcanic rocks of various Okanagan subterrane units separated by structural domain. Field labels include: BON = boninite (area outlined by dashed red lines; Ti ≤ 2500 ppm, V ≤ 200 ppm); Low-Ti IAB = low titanium island arc basalts (Ti/V < 10); IAB = island arc basalts (Ti/V < 20); MORB = mid-ocean ridge basalt (20 ≤ Ti/V ≤ 50); and WPB = within plate basalt (50 ≤ Ti/V ≤ 100). Triangle symbols are data from this study (n= 13). Circles are data are from Massey and Dostal (2013), Dostal et al. (2001), Mortensen et al. (2017), and Ray et al. (1996).

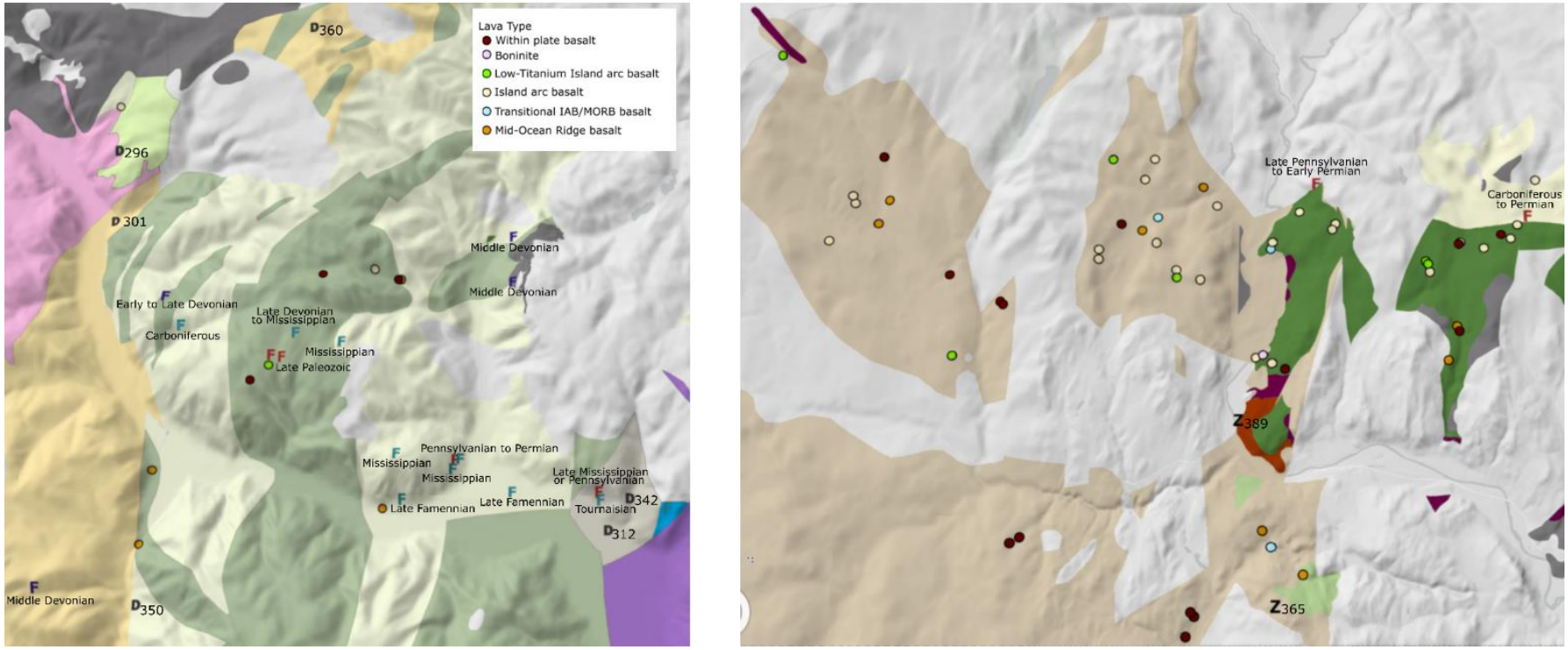

Figure 27. Distribution maps of the geochemistry of lavas in the A) Okanagan Similkameen region and B) Kootenay Boundary Region. Geochemical data in the OSR is from this study and data in the KBR is from Massey and Dostal (2013). Transitional IAB/MORB basalts are those with Ti/V ~ 20. Symbols and geology as in Figures 5 and 6.

2.4.2.1.1. MORB-like and IAB-like Metavolcanic Rocks

MORB-like lavas are spatially associated with late Devonian- to early Mississippian-aged strata. For example, in the Okanagan-Similkameen region MORB-like lavas were sampled approximately 1 km west of a middle late Famennian fossil locality 5.5 km west of Keremeos and 3.5 km north of middle Tournaisian clastic sediments 20 km west of Keremeos (Figure 27). In the Kootenay-Boundary region, three MORB-like samples lie within a 4 km radius of a 365 Ma metatuff 8 km south of Rock Creek (Figure 27). Samples with IAB-like geochemistry are spatially associated with earliest Middle Mississippian to earliest Permian strata, e.g. in the Okanagan-Similkameen Oregon Claims Formation and Barslow assemblage, and in the Kootenay-Boundary region 10-18 km north and northeast of Rock Creek (Figure 27). A plot of Ti/V ratios versus relative age inferred from proximity to available age and structural constraints provides a near-linear trend with a negative slope demonstrating decreasing Ti/V in progressively younger lavas (Figure 28). Twenty-three samples had sufficient trace element data to determine magmatic affinity. Of the thirteen samples with MORB- or IAB-like tectonic affinity, 85% are tholeiitic (Figure 29; Ross and Bédard 2009).

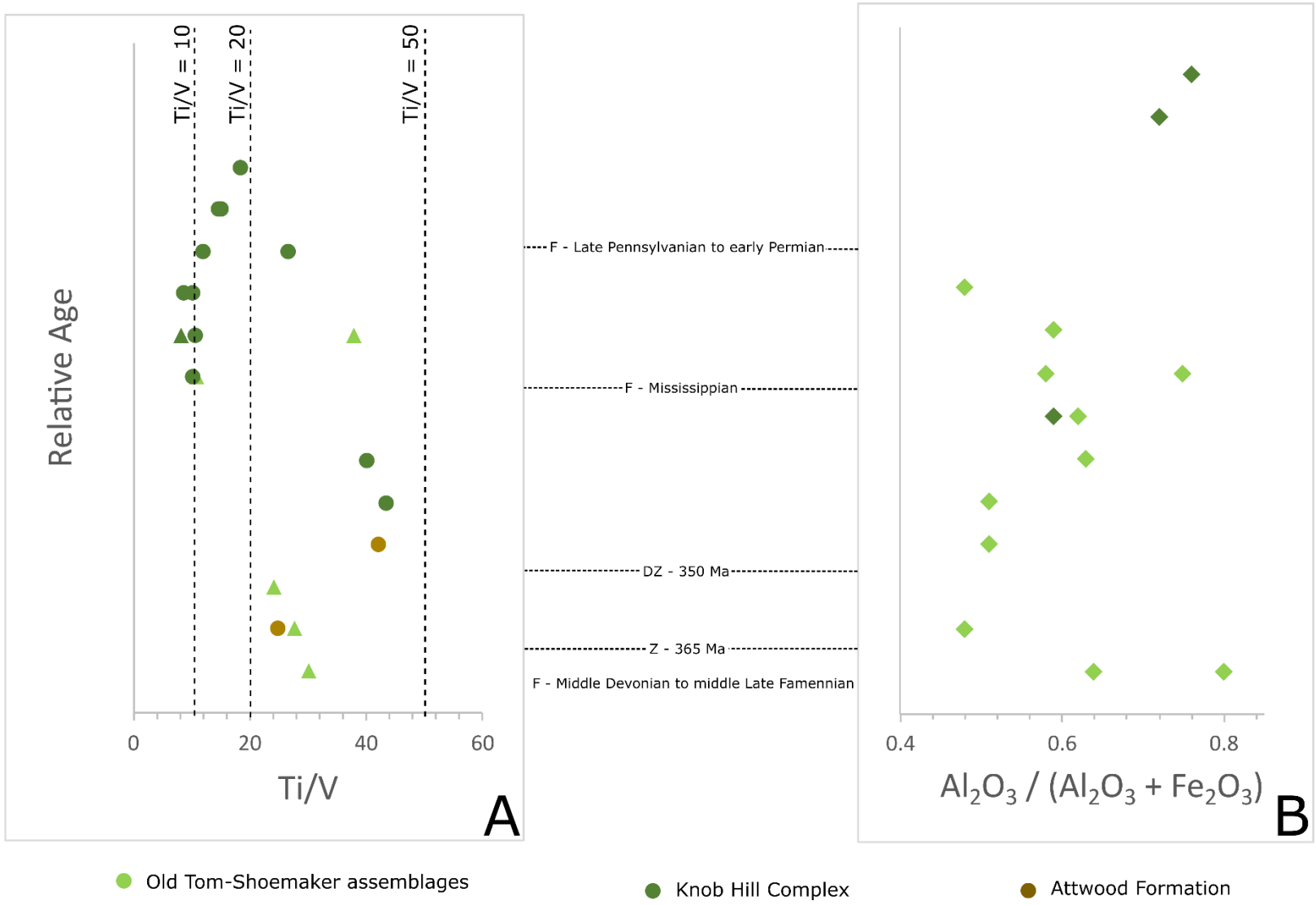

Figure 28. A) A plot of Ti/V ratio versus relative age for lavas of the Okanagan subterrane demonstrating a progressive decrease in Ti/V ratios consistent with evolution from MORB-like to IAB-like geochemistry with decreasing age. Relative age was predicted for samples based on proximity to fossil, detrital zircon, and U-Pb locales and in conjunction with structural data. The vertical lines indicate the major field delineators for tectonic affinity from the Ti/V plot in Figure 26. Data are from Massey and Dostal (2013) (circles) and this study (triangles). B) A plot of chert geochemistry demonstrating a general increase in aluminum with decreasing age representing an increase in terrigenous input. A correlation is observed whereby cherts with lower aluminum are found proximal to lavas with higher Ti/V ratios and aluminous input increases as lavas evolve toward lower Ti/V ratios (data from this study). Abbreviations: F = fossil age constraint, Z = U-Pb zircon age constraint, DZ = detrital zircon maximum depositional age constraint.

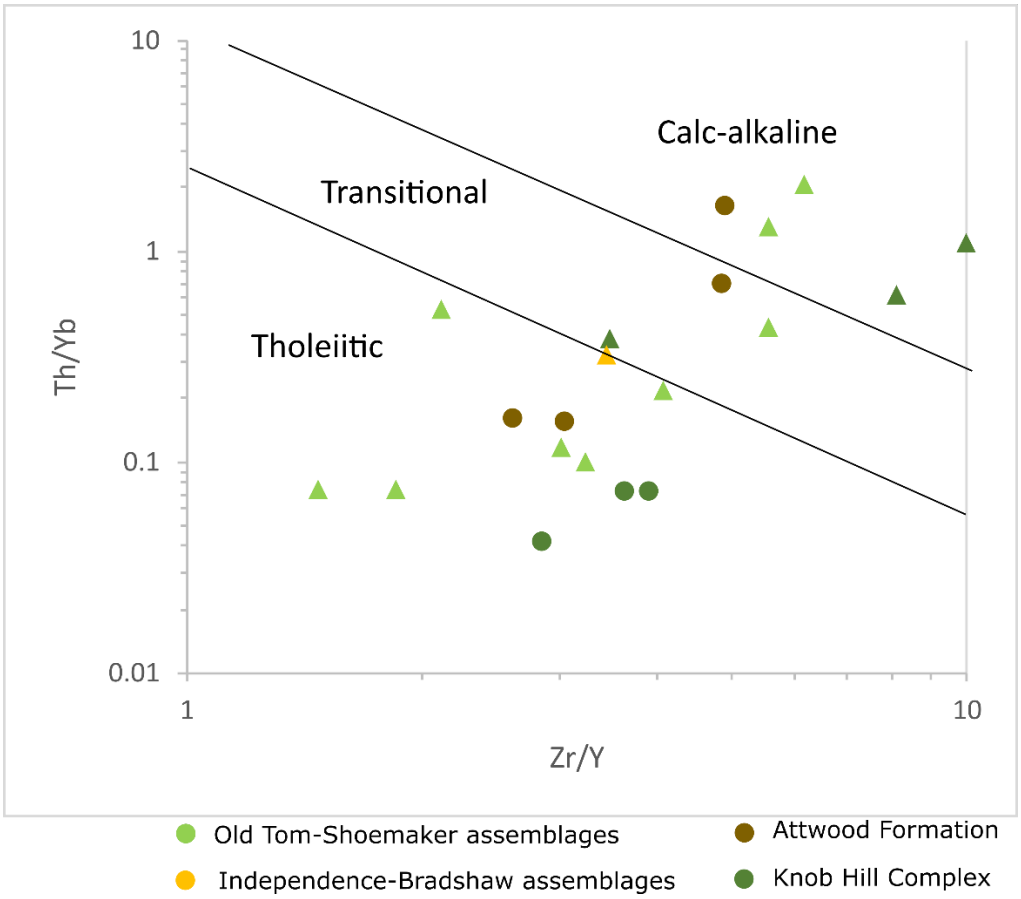

Figure 29. Magmatic affinity of lavas by trace element data as in Ross and Bédard. Data are from Dostal et al. (2001) (circles) and this study (triangles).

Based on their Ti-V classifications, MORB-like and IAB-like samples with available data were next plotted on a series of diagrams to detect trends in trace element abundances. A Zr-Zr/Y discriminant plot (Figure 30 A; Pearce and Norry 1979), demonstrates a linear progressive depletion in zirconium which characterizes the evolution from MORB-like to IAB-like lavas. On a Cr-Y plot (Figure 30 B; Pearce et al. 1984), projection up to the partial melting trendline of samples which follow a MORB vector indicates that the MORB-like magmas could have been generated from ~15-20% partial melting of a primitive mantle. IAB-like samples follow the IAB vector, and a single sample lies left of the boninite vector. Projection of the IAB and boninite vectors up to the left-shifted partial melting

trendline indicates IAB-like magmas were likely derived from similar degrees of partial melting but of a depleted mantle. On chondrite-normalized REE diagrams (Figure 31; Sun and McDonough 1989), five volcanic rocks with MORB-like chemistry were plotted and exhibit flat REE patterns and total REE concentrations 10 to 30 times higher than chondrite values. A positive slope, and lower overall REE concentrations 2-10 times greater than chondrite values are characteristic of three of the four IAB-like samples plotted. The fourth sample, H20-03b, is calc-alkaline and despite plotting firmly in the IAB field of the Ti-V diagram, exhibits elevated HREE and a negative slope similar to samples with enriched-MORB (E-MORB) geochemistry.

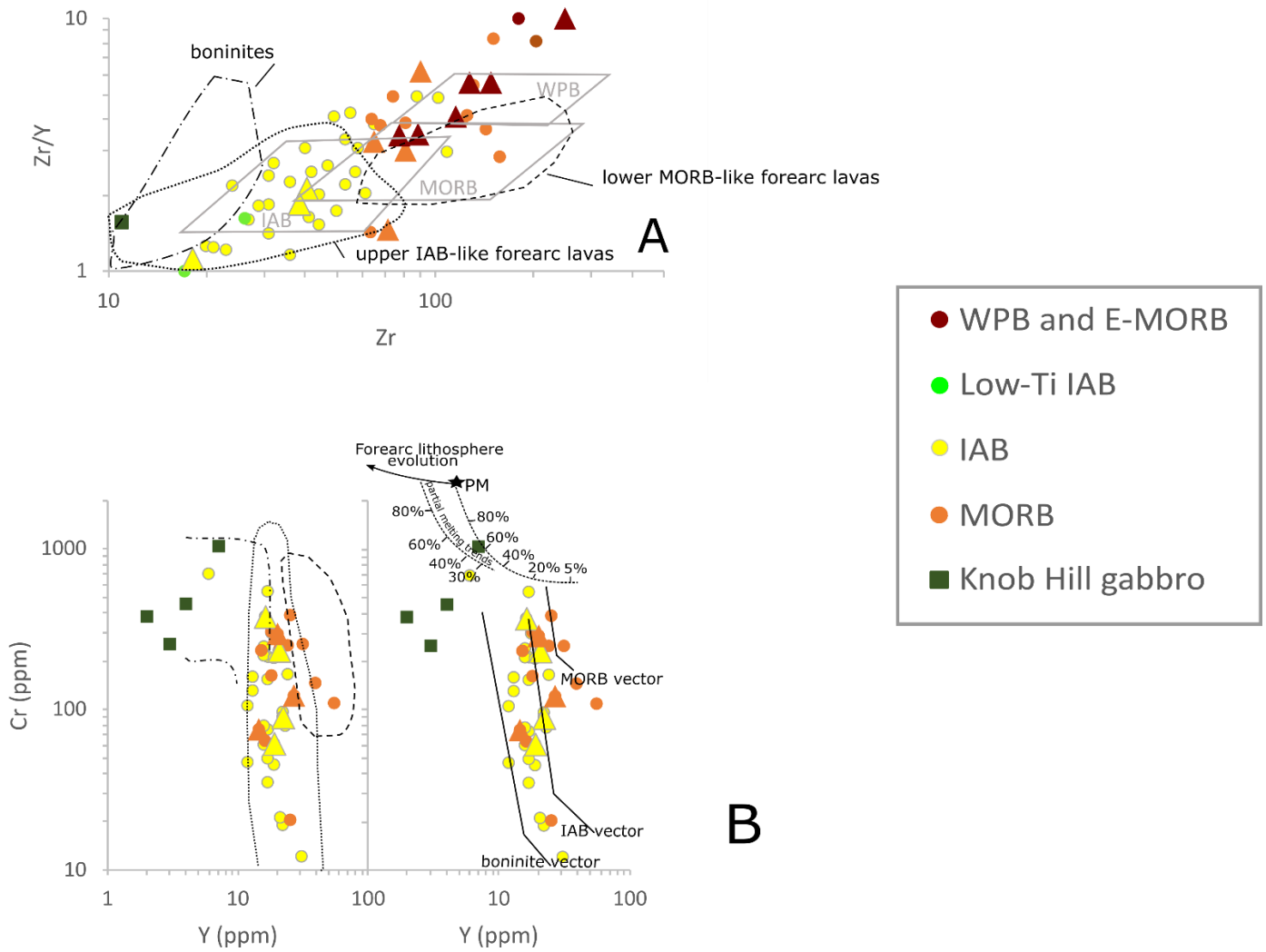

Figure 30. A) Zr-Zr/Y log-log tectonic discrimination plot (Pearce and Norry 1979 in Whattam and Stern 2011) demonstrates the progressive depletion Zr from MORB-like to IAB-like and boninitic lavas. Knob Hill gabbros plot mostly off the chart in the low end of the boninite field with Zr values between 2 and 11 ppm. B) Cr/Y discrimination plots of Okanagan subterrane (Whattam and Stern 2011 modified after Pearce et al. 1984). Cr is highly compatible during mantle melting and fractional crystallization yet is not preferentially added to the mantle wedge during subduction therefore can be used as an index of fractional crystallization (Pearce et al 1984; p81). Petrogenetic pathways are shown for MORB, IAB and boninite lavas of SSZ ophiolites as well as the partial melting trend for primitive mantle (PM) composition. MORB vector represents magma derivation from ~15% partial melting of primitive upper mantle. IAB and boninite vectors represent derivation from a common mantle source becoming increasingly depleted toward a harzburgitic composition. Triangle data points are from this study. Circle data points are from Massey and Dostal (2013), Mortensen et al. (2017), Ray et al. (1996), and Dostal et al. (2001).

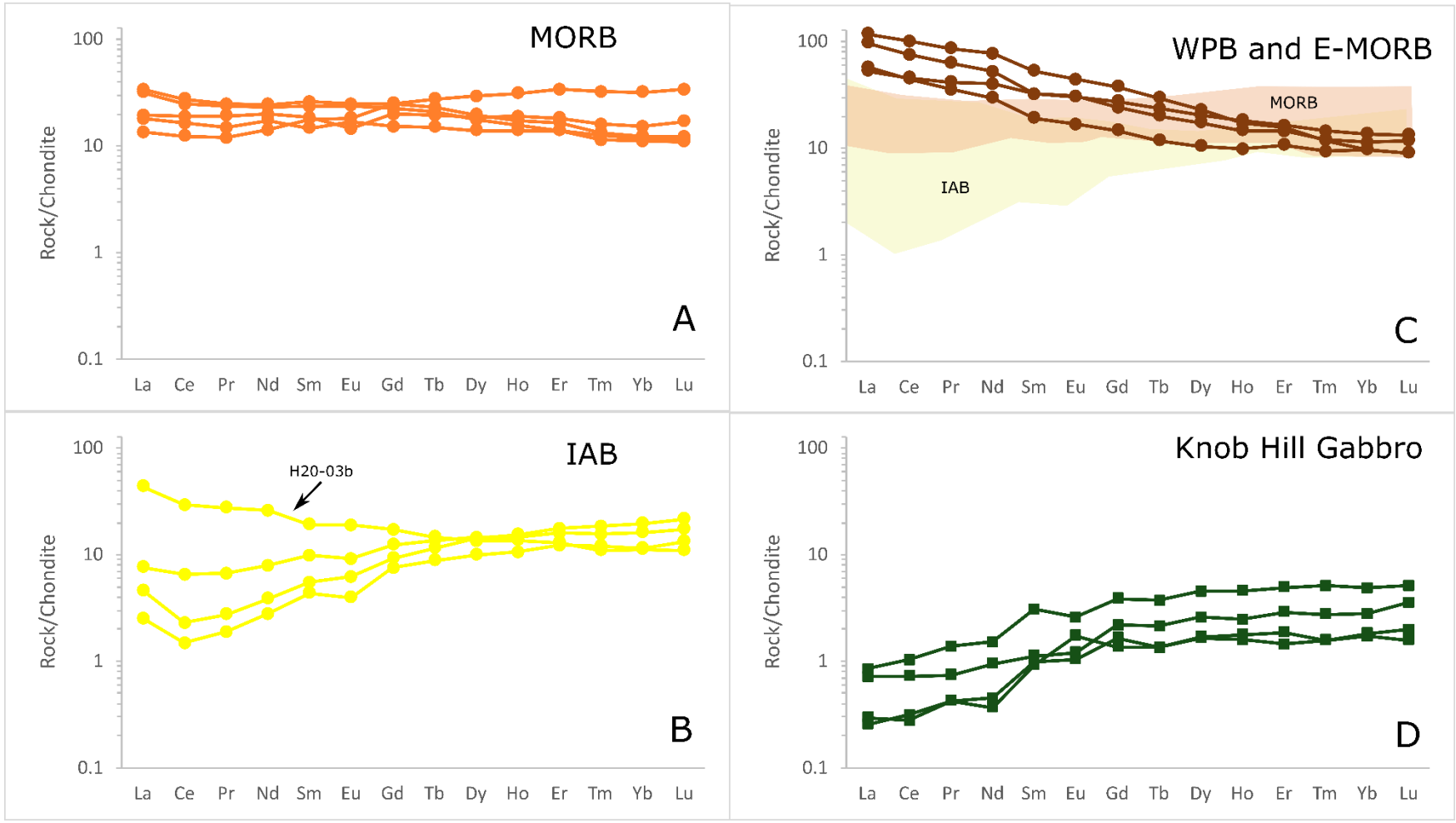

Figure 31. Chondrite-normalized REE diagrams (Sun and McDonough 1989) of mafic metavolcanic rocks collected from the Okanagan-Similkameen region for this study and segregated based on tectonic affinity obtained from Ti/V plots in Figure 26. A) MORB lavas of the Okanagan subterrane demonstrate flat REE patterns with enrichments up to 30 x chondrite values. B) IAB lavas generally show a positive REE slope and much lower total REE, between 2 and 10 x chondrite values. Lavas demonstrate a progressive depletion in REE, especially LREE during the evolution of the forearc from MORB to IAB signatures. C) Diabase dikes exhibiting within-plate (WPB) and enriched MORB (E-MORB) signatures demonstrate a negative slope with LREE values up to 100 x chondrite values. The orange and yellow shaded regions indicate the relative position of zones occupied by the MORB and IAB lavas shown in A & B, respectively. D) Gabbros from the Knob Hill Complex (data from Dostal et al. 2001) demonstrate considerable depletion to less than 5x chondrite values suggesting derivation from a previously depleted mantle.

2.4.2.1.2. Within Plate Basalts and Enriched-MORB

Within plate basalts and E-MORB lavas from the Okanagan subterrane are transitional to calc-alkaline. These samples have a negative slope on a chondrite-normalized REE diagram (Figure 31 C), enriched in LREE relative to the MORB-like and IAB-like lavas of the Okanagan subterrane with total REE values 10-100 times that of chondrites. Enriched lavas, at least locally, appear to be younger than IAB-like lavas. A WPB sample, Ola20-22, from the Old Tom assemblage 15 km NW of Keremeos, is from a red-weathering diabase dike that contains enclaves of green chert and intrudes through white to light grey chert, lithologies which yield Mississippian and younger fossil ages in this region. At a second locality 10 km to the NE, a steeply-dipping diabase dike with WPB geochemistry intrudes through black shale and red and white chert. A second diabase dike, less than 200 m to the east, intrudes through greenstone with MORB-like geochemistry. This latter dike was not geochemically analyzed but its proximity to the aforementioned WPB diabase dike suggests the two may be coeval.

2.6.2.2. Gabbro

Samples from a gabbro sill which intrudes greenstone of the Old Tom assemblage indicate within-plate geochemistry (Figure 26 A) with enriched REE and negative slopes on REE plots by Mortensen et al. (2017). Gabbros from the Knob Hill Complex near Greenwood have an island arc affinity with strong depletions in HFSE (Figures 26 and 30). A chondrite-normalized REE diagram of these Knob Hill gabbros have REE concentrations less than 5x chondritic values and a positive slope with LREEs depleted relative to HREEs (Figure 31 D).

2.6.2.3. Chert

Eighteen chert samples were collected during this study: three from the Knob Hill Complex, four from the Old Tom assemblage, and the remainder from the Shoemaker assemblage. The geochemical data are

shown in Appendix C. SiO_2 concentrations range between 74% and 97% with lower values where impurities from fine-grained siliciclastic sediments or significant mottling were present. La_n/Ce_n ratios normalized against North American Shale Composite (NASC; Gromet et al. 1984) range from 0.75 to 1.36 with an average of 1.05 ± 0.15. Binary plots (Figure 32 A&B; Murray 1994) show all samples fall within or near the overlapping 'pelagic' and 'continental margin' fields. NASC-normalized REE diagrams demonstrate flat REE patterns with total REE values up to 40 times lower than NASC values. Where metavolcanic rocks and chert were found together in outcrop, both were geochemically analyzed to assess correlations between the inferred tectonic environment of the lava and depositional environment of the chert. In these cases, chert samples that skewed toward the 'pelagic' field, i.e., relatively depleted in aluminum, were found associated with lavas of MORB-like geochemistry whereas cherts relatively enriched in aluminum and plotting firmly within the 'continental margin' field were associated with IAB-like lavas. A comparison plot of the Ti/V ratios of lavas and the $Al_2O_3/(Al_2O_3+Fe_2O_3)$ ratio of cherts demonstrates the increase in aluminum with decreasing age as an inverse relationship to the Ti/V ratio of lavas (Figure 28).

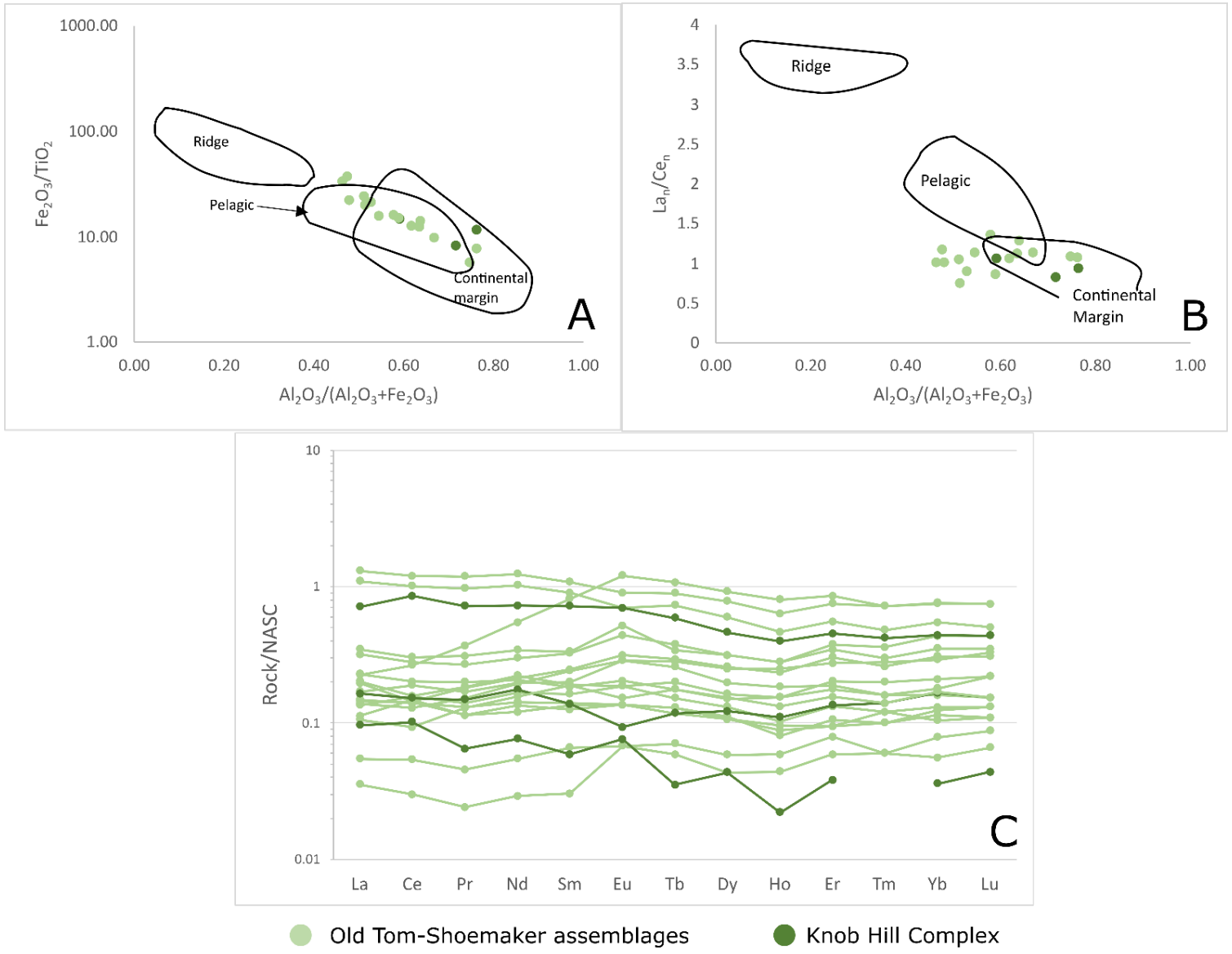

Figure 32. A&B) Chert discrimination diagrams as in Murray (1994). Cherts collected for this study (n = 18) appear in or near the continental margin field suggesting deposition near a source of terrigenous input. La_n/Ce_n ratio represents values normalized to average North American Shale Composite (NASC). C) Rare earth element diagram for chert rocks normalized against NASC demonstrating flat REE patterns with REE values up to 40 times lower than NASC values.

Chapter Three: Discussion

3.1. The Okanagan subterrane as an Ophiolite

Through a combination of field observations, whole rock geochemistry, structural analyses, and data compilation this study provides two main lines of evidence supporting an ophiolitic origin, and probably a subduction initiation rule ophiolite, for the Okanagan subterrane: 1) the subterrane is characterized by a suite of lithologies commonly associated with ophiolites, and 2) it has a magmatic evolution from older MORB-like to younger IAB-like magmatism.

Lithologies of the Okanagan subterrane include an oceanic assemblage of chert, carbonates, fine to coarse siliciclastic rocks, metabasalt, gabbro, serpentinized harzburgite and dunite, and podiform chromitite consistent with previous interpretations of the Okanagan subterrane as a supra-subduction zone ophiolite (Fyles 1990, Dostal et al. 2001, Massey 2006a, Massey et al. 2013).

Contrary to back-arc SSZ ophiolites which are comprised almost entirely of MORB-like lavas, data from the Okanagan subterrane suggests three distinct suites of mafic metavolcanic rocks. In order of decreasing stratigraphic age, these suites include: 1) MORB-like; 2) IAB-like; and 3) WPB and E-MORB lavas. A predominance of IAB-like lavas is consistent with forearc SSZ ophiolites (Shervais 1982, 2022). Volcanic rocks with MORB-like and IAB-like geochemistry plot in the respective domains typical of lower and upper lavas of subduction initiation rule ophiolites as defined by Whattam and Stern (2011). Intact sections where relative age can be inferred demonstrate a chemostratigraphic magmatic evolution consistent with a forearc SSZ ophiolite formed in response to subduction initiation. Relative to MORB-like lavas, IAB-like lavas are spatially associated with younger strata and follow a

continuum toward increased depletion in HFSE such as zirconium and yttrium (Figure 30), and chondrite-normalized REE patterns (Figure 31) consistent with derivation from a melt source which is becoming increasingly depleted. These characteristics align with expectations from increasing flux of subduction-related fluids into a common, evolving melt source which in a subduction initiation model reflects the mantle melt zone beneath the proto-forearc gap (Pearce et al. 1984, Whattam and Stern 2011). Following this interpretation, the Late Devonian to earliest Mississippian MORB-like lavas record the onset of upper plate spreading and decompressive melting of lherzolitic mantle flooding the proto-forearc gap during subduction initiation. The transition from MORB-like to IAB-like lavas by the early middle Mississippian occurs as the mantle source beneath the proto-forearc becomes depleted to a harzburgitic composition (Shervais 2001, Whattam and Stern 2011). The apparent corresponding increase in aluminum content of cherts may reflect the inclusion of volcanic ash or clays formed from the submarine alteration of volcanic ash and glass (O'Dowd 2017) rather than terrigenous clastic input. The NASC-normalized La_n/Ce_n ratios for all cherts analyzed are consistent with that of marginal cherts (Figure 32 B; Murray 1994) and show little variability with age. The stability in the La_n/Ce_n ratio supports an interpretation of volcanic ash as the aluminum source given that all cherts analyzed are being deposited during continuous volcanic activity.

The oldest units of the Okanagan subterrane, which are Middle Devonian in age, may represent rift fragments of pre-existing oceanic lithosphere retained following proto-forearc spreading. The intercalation of black and green pyritiferous chert and argillite with limestone and minor sandstone and chert pebble conglomerate suggest an organic-rich, anoxic or euxinic marine depositional environment receiving periodic incursions of coarser clastic detritus. The subsequent predominance of middle to late Famennian red chert indicates a transition to a deeper basin into which an influx of oxygen allowed for the crystallization of hematite in the sediments. The deposition of these cherts is coeval with or shortly

preceded emplacement of MORB-like lavas. In a subduction initiation model, the apparent deepening of the depositional basin may signify subsidence of the upper plate caused by downward flow of the proto-subducting plate prior to its collapse in the earliest stages (Matsumoto and Tomoda 1983, Stern and Gerya 2018). By the early Mississippian, deposition of crinoidal limestone and brachiopod-bearing argillite which accompanied emplacement of the IAB-like lavas signifies a shallowing of the basin to back above the carbonate compensation depth consistent with upper plate rebound following lower plate collapse and subsequent build-up of the proto-forearc in a subduction initiation model (Figure 33).

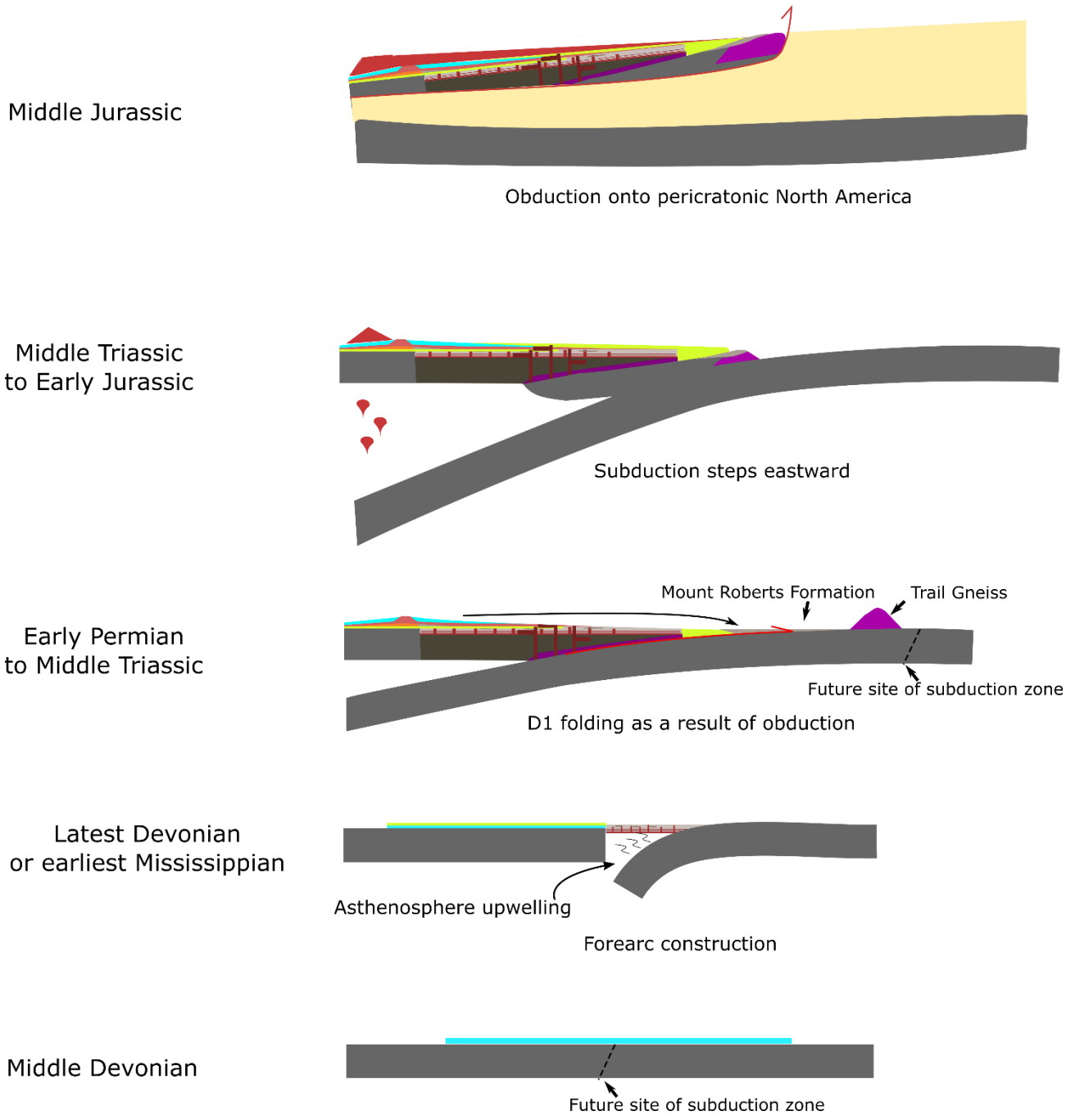

Figure 33. Proposed lifecycle of the Okanagan subterrane as a 'subduction initiation rule' ophiolite. Lithospheric weakness in a Middle Devonian oceanic floor provides a locus for future subduction initiation. Late Devonian or earliest Mississippian collapse of denser lithosphere to the east allows for upwelling of asthenospheric mantle. Extension initiates in the upper plate resulting in the initial eruption of MORB-like forearc basalts and subsequent eruption of forearc lavas with a volcanic arc (IAB-like) signature. Late Mississippian establishment of a localized magmatic arc. In the earliest Permian, uplifting, folding, and eroding of the Okanagan subterrane occurred with re-depositing of the reworked sediments as part of the Mount Roberts Formation (MRF) as the Okanagan subterrane accretes to the western margin of the Trail Gneiss as an extinct island arc within the lower plate. Eastward stepping of the subduction zone allows arc volcanism to return in the Middle Triassic and continue until final obduction. Middle Jurassic obduction of the Okanagan subterrane and overlying Triassic arc occurred because of its collision with pericratonic terranes to the east.

3.2. Tectonic History of the Okanagan subterrane

The Okanagan subterrane as a subduction initiation rule ophiolite has implications for tectonic models of Quesnellia. A potential tectonic model which places the subduction initiation recorded in the Okanagan subterrane within a Cordilleran context is presented here. The main stages of this model include: 1) Late Devonian subduction initiation in western Panthalassa to form the Okanagan subterrane as a marginal or intraoceanic forearc; 2) Late Mississippian to Early Permian uplift of the forearc followed by; 3) Early Permian to Middle Triassic accretion of an island arc resulting in 4) step-back of the subduction zone to build the Triassic arc and final obduction of the complex to pericratonic Laurentia in the Middle Jurassic (Figure 33).

3.2.1. Subduction initiation

The Okanagan subterrane is interpreted here as a forearc to a volcanic arc born in or near the Tethyan domain. Probability density plots of pre-Devonian detrital zircons within Late Devonian strata of the Okanagan subterrane correlate with the typical age ranges for northwestern Laurentia (Mortensen et al. 2017) apart from prominent peaks between 500 Ma and 1500 Ma which fall outside the typical western Laurentian age ranges. These outliers align with detrital zircon populations common in East Asia, Siberia, and Australia (Condie et al. 2009). Siberia and South China host fossil genera similar to those found within the enigmatic Ordovician limestone of the Okanagan-Similkameen Shoemaker assemblage (Pohler et al. 1989). With an eastern Panthalassa or Tethyan origin for the Okanagan subterrane, these cratons may represent potential sources for the limestone block and pre-Devonian detrital zircons. A non-Laurentian intraoceanic arc interpretation has been proposed for the Late Devonian Trail Gneiss Complex (Simony et al. 2006), the Silurian to Mississippian Eastern Klamath terrane (e.g. Lindsley-Griffin et al. 2008, Grove et al. 2008), and a portion of the Late Devonian to Permian Yukon-Tanana

terrane (e.g. van Staal et al. 2018). The Eastern Klamath and Yukon-Tanana terranes are southern and northern equivalents of Quesnellia, respectively. Early Paleozoic strata of the Eastern Klamath terrane contain detrital zircon and fossil populations exotic to southwestern Laurentia and researchers propose a western Panthalassa origin proximal to Baltica or Australia (Lindsley-Griffin et al. 2008, Grove et al. 2008). Small detrital zircon population peaks within the Eastern Klamath strata fall in the 700 Ma and 1000-1500 Ma age ranges represented in Okanagan subterrane clastic samples and may suggest a common source of detritus during subduction initiation in the Late Devonian.

3.2.2. Temporary uplift of the forearc

Several observations are consistent with the subduction of buoyant lithosphere resulting in temporary uplift of the Okanagan subterrane upper plate, including: 1) Late Mississippian- to Permian-aged units dominated by sedimentary strata including conglomerates, sandstones, argillite, chert, and shallow water carbonates; 2) latest Mississippian or Pennsylvanian limestone cobble conglomerate in the Harper Ranch Group; 3) an angular unconformity between the Chapperon and Harper Ranch groups in the Thompson-Nicola region; and 4) the general rarity of Pennsylvanian-aged strata within the Okanagan subterrane are all consistent with uplift and erosion of the forearc. Dark red shales intercalated with Old Tom assemblage greenstones northwest of Keremeos (Figure 12) may be interflow red bole horizons produced by aerial or sub-aerial exposure and weathering of basalt flows (Duraiswami et al. 2020).

The uplift and erosion of the forearc lithosphere are most readily explained as products of shallowing and flattening of the subducting slab either due to subduction of thickened lithosphere (seamounts or plateau) or due to the arrival of a spreading ridge or mantle plume swell. Seamounts and plateaus with crustal thicknesses less than 15 km and oceanic lithosphere less than 10 million years old are subductable but buoyant enough to cause temporary isostatic uplift of the leading edge of the upper plate

(Cloos 1993). For a half-spreading rate of 50 mm/year, oceanic lithosphere is adequately buoyant to begin uplifting a forearc as much as 1000 km before the arrival of the spreading center at the trench (Shervais 2001).

In some SSZ forearc ophiolites, the eruption of MORB-like and enriched lavas through the forearc has been interpreted as evidence for the subduction of a spreading ridge beneath the forearc (e.g. Shervais 2001, 2022, Snow and Shervais 2015). Following ridge subduction, MORB or WPB lavas leak through the resultant slab window to intrude the ophiolite (Dickinson and Snyder 1979, Thorkelson and Taylor 1989). The late-stage diabase dikes within the Okanagan-Similkameen region provide evidence supporting magmatic emplacement. Additionally, MORB-like lavas in the Kootenay-Boundary region stratigraphically overlie volcanic rocks with IAB-like geochemistry near Rock Creek (Massey and Dostal 2013). Both observations support a model of ridge subduction however the alternative scenarios of seamount, plateau, or mantle plume swell subduction cannot be ruled out with the data available.

3.2.3. Accretion of an Island Arc

The Permo-Triassic is dominated by tight to isoclinal folding, uplift, and erosion. Isoclinal folding is common in forearc supra-subduction zone ophiolites (e.g. Pindos Ophiolite Complex (Ross and Zimmerman 1996), Mirdita Ophiolite (Tremblay et al. 2015) Tsiknias Ophiolite (Lamont et al. 2020)) where they have been interpreted as fold nappes formed during shallow thrusting over a subducting plate. Ross (1981) interpreted D1 as a product of the east-directed obduction of nappes onto a west-dipping continental margin. The polarity was inferred, in part, due to the easterly vergence in some D1 folds. Accretionary orogenesis may be responsible for D1 however subsequent deformation events obscure the original orientation of D1 structures and inhibit interpretations as to the true polarity of nappe emplacement. Supporting evidence for east-directed obduction can be found from observations of

units outside the study regions. Folded strata eroded from the Okanagan subterrane are re-deposited as clastic strata of the Mount Roberts Formation while carbonate deposition continues into the Middle Permian at the Harper Ranch Group type section north of Kamloops. Relative to the subterrane's current configuration, these observations suggest that obduction and uplift were occurring along the active margin to the southeast while carbonate deposition was continuing in the northwest distal to the plate margin perhaps defining a back-arc region.

The Okanagan subterrane adjoins the Devonian Trail Gneiss Complex by way of the overlapping Mount Roberts Formation. The absence of D1 folds in the Mount Roberts Formation and the west-dipping mylonitic contact between the Mount Roberts Formation and the Trail Gneiss Complex suggests the two were tectonically adjoined as a result of east-directed thrusting possibly in the final stages of D1. The Castlegar Gneiss and Valhalla Gneiss Dome are considered younger facies of the Trail Gneiss Complex (Simony 1979) which has been interpreted as a Devonian intra-oceanic island arc (Simony et al. 2006). Thus, the D1 event may represent the east- to southeast-directed obduction of the Okanagan subterrane onto the Trail Gneiss Complex as part of an extinct island arc that lay within the subducting lower plate. The model proposed thus far is similar to one put forth by van Staal et al. (2018) for the Yukon-Tanana terrane as a composite terrane where the Permo-Triassic event results in accretion of a juvenile island arc to an intraoceanic rift fragment from the Laurentian margin. In other Cordilleran models, the Permo-Triassic has been invoked as the time period for closure of the Slide Mountain back-arc basin and repatriation of the Paleozoic arc to the North American margin (e.g. Nelson et al. 2006). Early to middle Permian Tethyan fauna in carbonates (Smith 1979, Ross 1981, Orchard and Forster 1988, Crasquin-Soleau and Orchard 1994, Beatty et al. 2006) suggest a significant ocean basin continued to separate the Okanagan subterrane from pericratonic crust of Laurentian affinity. The composite terrane model allows for a continued position in western Panthalassa for the Paleozoic arc.

3.2.4. Triassic volcanism and Obduction to Pericratonic North America

E1 extension initiated in the Kootenay-Boundary region and propagated toward the Okanagan-Similkameen region consistent with expectations for asymmetrical extension due to post-accretion gravitational collapse (e.g. Ranero and Pérez-Gussinyé 2010). Continued erosion of the uplifted Okanagan subterrane was the likely source of the basal sedimentary facies of the Nicola Group and Brooklyn Formation within the rift basin. Calc-alkaline volcanic and volcaniclastic rocks are as old as Ladinian age in both the Nicola Group and Brooklyn Formation (Dostal et al. 2001, Friedman et al. 2020) and commonly modelled as facies of a west-facing volcanic arc (e.g. Mortimer 1987, Monger and Price 2002). The opposite configuration is depicted for this model to close the Slide Mountain Ocean consistent with the van Staal et al. (2018) model where accretion of the rift fragment resulted in eastward step-back of the subduction zone to initiate Triassic arc volcanism. A west-facing Triassic arc is equally viable in models where west- and east-dipping plates are co-occuring (e.g. Monger and Price 2002). A detailed study of the Mesozoic arc to test these hypotheses is outside the scope of this work.

The timing of D2 is in-line with some Cordilleran models for the accretion of the Paleozoic composite terrane and its overlying Mesozoic arc, together forming Quesnellia, to pericratonic terranes of the Laurentian margin (e.g. Monger and Price 2002, Colpron et al. 2007, Johnston and Borel 2007). North- to northeast-dipping thrust faults in the Okanagan subterrane's Kootenay-Boundary region and the southwest vergence of most D2 folds in the study areas are consistent with the southwest transport of an imbricate thrust system (Poblet and Lisle 2011). The southeast-directed duplex thrust faults near Hedley in the Okanagan-Similkameen region would, therefore, represent back-thrusts within the D2 fold and thrust belt. This transport direction suggests west-directed obduction over a northeast-dipping plate. The axial planes of D2 folds in units outside the study area, the Mount Roberts Formation and Trail Gneiss Complex, are moderately- to shallowly-, west- to northwest-dipping, paralleling a pre-Middle

Jurassic thrust fault which juxtaposes the Trail Gneiss Complex with the Early Jurassic Rossland Group (Simony 1979). These observations are consistent with an eastward transport direction. Palinspastically restoring post-Jurassic deformation of the D2 fold and thrust belt is necessary to understand the true orientation of D2 at the end of the Middle Jurassic and properly constrain the final obduction direction.

Chapter Four: Further Work

4.1. Testing the Model

The polarity of the plate subducting beneath the Okanagan subterrane in the Late Devonian and Carboniferous cannot be conclusively determined without knowledge of the relative location of a volcanic arc and unravelling the polyphase deformation. Although some calc-alkaline greenstones were identified, the available datasets consulted in this study were insufficient to constrain the location of the arc. Geochemical patterns as well as fossil and detrital zircon ages, suggest that the units of the Okanagan-Similkameen region and the Anarchist Group may need to be further subdivided. A downplunge projection of the Okanagan-Similkameen region oriented based on the attitude of D2 folds in the OSR-S yields a potential new map pattern which requires field testing (Figure 34).

Detailed mapping and structural data from the Anarchist Group west of Rock Creek are lacking and as such, it is shown as one homogenous unit from Rock Creek to the Kobau Group. Parts of the Anarchist Group studied for their serpentinite-hosted podiform chromitite deposits and reported in MINFILE (1985) are described as folded and faulted and locally consisting of combinations of lithologies such as gabbro, quartzite, marble, meta-volcanic rocks, chert, and amphibolite. Detailed mapping is required to better define the structural and stratigraphic relationships within the group. Strategic sampling throughout the regions to create a more robust suite of geochemical and detrital zircon and fossil age data combined with detailed mapping and stratigraphic analysis especially along proposed map contacts is required to provide the necessary data to test the model and broaden our understanding of the tectonic history of the Okanagan subterrane.

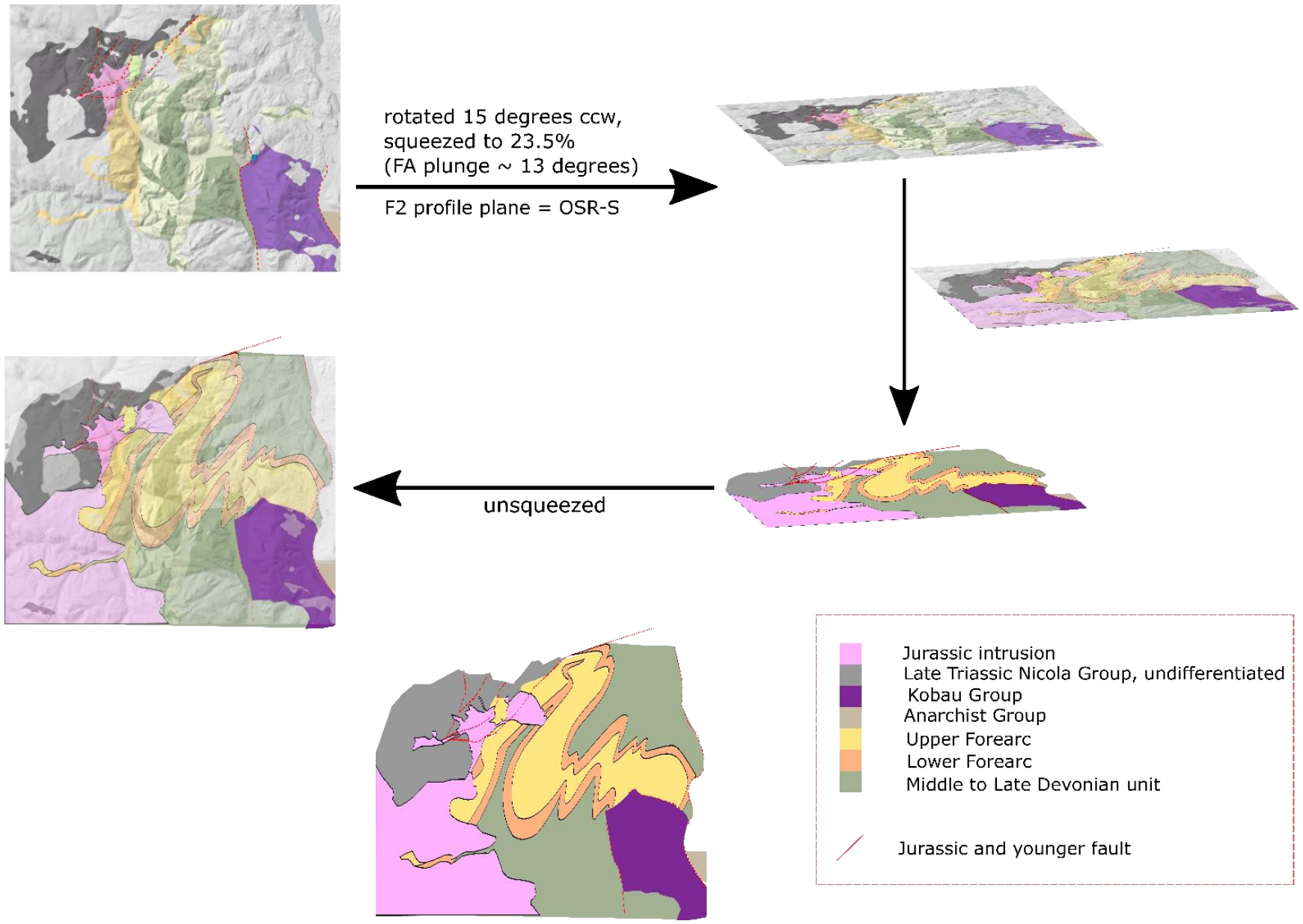

Figure 34. Downplunge projection of the Okanagan Similkameen region based on geochemical, detrital zircon age, and fossil age distribution. The un-squeezed result predicts a new map pattern for the Okanagan-Similkameen region. Additional Middle Jurassic plutons in the southwest have been added to demonstrate the connection to the Cahill Creek pluton.

4.2. Knob Hill Gabbros

Knob Hill gabbros demonstrate Low-Ti IAB geochemistry and are reported to exhibit a variety of characteristics including foliation and isotropy; and gradational and intrusive contacts (Fyles 1990, Massey et al. 2013, Höy 2018). Forearc gabbros associated with the earliest phase of subduction initiation are primarily layered but can be isotropic (Shervais 2001). They are foliated, often boudinaged, and are genetically related to sheeted dykes and MORB-like lavas (Shervais 2001). Gabbros associated with the eruption of IAB-like forearc lavas lack foliation and intrude as sills and dikes through older strata (Shervais 2001). The Knob Hill gabbros can potentially be divided into two or more sub-groups based on geochemistry, fabric, relative age, and stratigraphic relationships: those which represent feeders to the proto-forearc and those which may belong to older oceanic lithosphere. Further work is required to determine if this is the case and if so, segregate this unit accordingly. Documentation of foliation within gabbros as well as the trend of gabbroic and sheeted dikes could yield vital information as to the spreading direction of the proto-forearc.

4.3. Mantle Rocks

Most serpentinites in the Okanagan subterrane are sheared and foliated with a NW-SE orientation. Two primary differences seem to exist between serpentinites in the eastern exposures of the Kootenay-Boundary region and those within the Chapperon and Anarchist groups suggesting there may be two or more distinct suites: 1) podiform chromitite deposits are restricted to serpentinites in the Chapperon and Anarchist groups; and 2) a spatial association with Middle Jurassic regional thrust faults and/or Middle to Late Devonian gabbros exists only east of Rock Creek. Detailed mapping, particularly within the Anarchist Group as suggested above, will be instrumental in helping to determine the stratigraphic and

structural relationships of serpentinites to the adjacent lithologies and their place in the tectonic history of the region.

Geochemical analyses may also help elucidate distinct suites within the Okanagan subterrane serpentinites. Forearc serpentinites are formed when dehydration fluids from subducted sediments flux into the mantle wedge (Hyndman and Peacock 2003, Kodolányi et al. 2012). As a result, forearc serpentinites exhibit enrichments in Cs, Rb, Sr, and Li, orders of magnitude higher than that found in ocean floor serpentinites (Kodolányi et al. 2012). As well, overall trace element concentrations in forearc serpentinites are typically very low, 0.001-0.1 ppm, a reflection of derivation from harzburgitic mantle (Kodolányi et al. 2012). Ross (1981) reports that the stress profile and geochemical signatures of ultramafic rocks within the western exposures of the Anarchist Group are consistent with upper mantle material that was subjected to partial melting and metasomatism consistent with the subduction of slab material. Ultramafic rocks were not examined geochemically in this study and so, apart from Ross's (1981) interpretation, little existing data are available.

Conclusions

Distinct geochemical, lithologic, and structural characteristics allow for interpretation of the Okanagan subterrane as a forearc ophiolite formed over a long-lived west-dipping subduction zone initiating in western Panthalassa. Based on the data, subduction initiation occurred in the Latest Devonian or Mississippian. Subduction was punctuated by a period of uplift and erosion in the Late Mississippian or Pennsylvanian. Paleozoic strata were folded, uplifted, and eroded during a Permo-Triassic deformation event that likely records obduction of the forearc onto an extinct island arc within the lower plate. A stepping back or polarity reversal of the subducting plate resulted in the construction of an overlying Mesozoic arc. A Middle Jurassic folding and faulting event is interpreted as a result of final accretion of the composite arc terrane to pericratonic terranes of the western Laurentian margin. The Okanagan subterrane is commonly referred to as the basement to Quesnellia, therefore the forearc ophiolite model has significant impacts on existing Cordilleran models which focus on a North American origin for this terrane. An origin in western Panthalassa helps explain the protracted history of the Okanagan subterrane as well as Tethyan fauna and paleogeographic reconstructions which are difficult to reconcile with a Laurentian-proximal location. Data from the Okanagan subterrane are still relatively sparse; therefore, extensive mapping plus more detailed geochemical, stratigraphic, and structural analyses are required to test correlations and further constrain the model.

References

Acton, S.L., Paradis, S., and Johnston, S.T. 2000. Geologic Setting of Paleozoic Strata and Mineral Occurrences in the Mount Tod Region, South-Central British Columbia. In Geological Fieldwork 2000, Paper 2001-1, British Columbia Geological Survey

Agrawal, S., Guevara, M., and Verma, S.P. 2008. New Tectonic Discrimination of Basic and Ultrabasic Volcanic Rocks through Log-Transformed Ratios of Immobile Trace Elements. International Geology Review, **50**: 1057–1079. doi:10.2747/0020-6814.50.12.1057.

Allmendinger, R.W., Cardozo, N., and Fisher, D.M. 2012. Structural Geology Algorithms: Vectors and Tensors. Cambridge University Press.

Barnes, W.C., and Ross, J.V. 1975. The Blind Creek Limestone, Keremeos, British Columbia: Structure and Regional Tectonic Significance. Canadian Journal of Earth Sciences, **12**: 1929–1933. doi:10.1139/e75-170.

Beatty, Orchard, M., and Mustard, P.S. 2006. Geology and tectonic history of the Quesnel terrane in the area of Kamloops, British Columbia. Geological Association of Canada - Special Paper, **45**: 483–504.

Belasky, P., Stevens, C.H., and Hanger, R.A. 2002. Early Permian location of western North American terranes based on brachiopod, fusulinid, and coral biogeography. Palaeogeography, Palaeoclimatology, Palaeoecology, **179**: 245–266. doi:10.1016/S0031-0182(01)00437-0.

Brown, S.R., Gibson, H.D., Andrews, G.D., Thorkelson, D.J., Marshall, D.D., Vervoort, J.D., and Rayner, N. 2012. New constraints on Eocene extension within the Canadian Cordillera and identification of Phanerozoic protoliths for footwall gneisses of the Okanagan Valley shear zone. Lithosphere, **4**: 354–377. Geological Society of America.

Church, B.N. 1986. Geological Setting and Mineralization in the Mount Attwood - Phoenix Area of the Greenwood Mining Camp. BC Ministry of Energy Mines and Petroleum Resources.

Colpron, M., Nelson, J.A.L., and Murphy, D.C. 2007. Northern Cordilleran terranes and their interactions through time. GSA Today, **17**: 4–10. doi:10.1130/GSAT01704-5A.1.

Condie, K.C., Belousova, E., Griffin, W.L., and Sircombe, K.N. 2009. Granitoid events in space and time: Constraints from igneous and detrital zircon age spectra. Gondwana Research, **15**: 228–242. doi:10.1016/j.gr.2008.06.001.

Crasquin-Soleau, S., and Orchard, M.J. 1994. Upper Paleozoic Ostracodes of the Harper Ranch Beds (South-Central British Columbia, Canada). Micropaleontology, **40**: 242–254. The Micropaleontology Project, Inc. doi:10.2307/1485818.

Cui, Y., Miller, D., Schiarizza, P., and Diakow, L.J. 2017. British Columbia digital geology. British Columbia Ministry of Energy, Mines and Petroleum Resources, British Columbia Geological Survey Open File, **8**.

Daughtry, K.L., Thompson, R.I., and Erdmer, P. 2000. New field studies of the Chapperon Group , Vernon southwest map area , British Columbia. Natural Resources Canada, Geological Survey of Canada.

Delong, S.E., and Fox, P.J. 1977. Geological Consequences of Ridge Subduction. *In* Island Arcs, Deep Sea Trenches and Back-Arc Basins. American Geophysical Union (AGU). pp. 221–228. doi:10.1029/ME001p0221.

Dickinson, W.R., and Snyder, W.S. 1979. Geometry of Subducted Slabs Related to San Andreas Transform. The Journal of Geology, **87**: 609–627. The University of Chicago Press. doi:10.1086/628456.

Dostal, J., Church, B.N., and Hoy, T. 2001. Geological and geochemical evidence for variable magmatism and tectonics in the southern Canadian Cordillera: Paleozoic to Jurassic suites, Greenwood, southern British Columbia. Canadian Journal of Earth Sciences, **38**: 75–90. doi:10.1139/e00-078.

Duraiswami, R.A., Sheth, H., Gadpallu, P., Youbi, N., and Chellai, E.H. 2020. A simple recipe for red bole formation in continental flood basalt provinces: weathering of flow-top and flow-bottom breccias. Arabian Journal of Geosciences, **13**: 953. doi:10.1007/s12517-020-05973-9.

Friedman, R.M., Mihalynuk, M.G., and Diakow, L.J. 2020. Geochronologic data from samples collected near Pothole Lake and Pennask Mountain (NTS 92H/15, 16) as part of the Southern Nicola Arc Project. British Columbia Ministry of Energy, Mines and Low Carbon Innovation, British Columbia Geological Survey GeoFile, **2020–12**: 1–6.

Fyles, J.T. 1990. Geology of the Greenwood-Grand Forks area, British Columbia. British Columbia Ministry of Energy, Mines, and Petroleum Resources, Open File: 1–19.

Google Earth V 7.3.6.9345. (n.d.). Landsat / Copernicus, Southern British Columbia, Canada. 10U 709354.75 m E, 5503133.63 m N, Eye alt 5168 km. Available from http://www.earth.google.com [accessed 15 December 2023].

Gromet, P., Dymek, R.F., Haskin, L.A., and Korotev, R.L. 1984. The "North American shale composite": Its compilation, major and trace element characteristics. Geochimica et cosmochimica acta, **48**: 2469–2482.

Grove, M., Gehrels, G.E., Cotkin, S.J., Wright, J.E., and Zou, H. 2008. Non-Laurentian cratonal provenance of Late Ordovician eastern Klamath blueschists and a link to the Alexander terrane. doi:10.1130/2008.2438(08).

Höy, T. 2018. Geology of the Greenwood Map Area (NTS 082E / 02), Boundary District, Southern British Columbia.

Huppert, K.L., Perron, J.T., and Royden, L.H. 2020. Hotspot swells and the lifespan of volcanic ocean islands. Science Advances, **6**: eaaw6906. American Association for the Advancement of Science. doi:10.1126/sciadv.aaw6906.

Hyndman, R.D., and Peacock, S.M. 2003. Serpentinization of the forearc mantle. Earth and Planetary Science Letters, **212**: 417–432. doi:10.1016/S0012-821X(03)00263-2.

Johnston, S.T., and Borel, G.D. 2007. The odyssey of the Cache Creek terrane, Canadian Cordillera: Implications for accretionary orogens, tectonic setting of Panthalassa, the Pacific superwell, and break-up of Pangea. Earth and Planetary Science Letters, **253**: 415–428. Elsevier B.V. doi:10.1016/j.epsl.2006.11.002.

Jones, A.J. 1959. Vernon map-area, British Columbia. Memoir, Geological Survey of Canada.

Kodolányi, J., Pettke, T., Spandler, C., Kamber, B.S., and Ling, K.G. 2012. Geochemistry of ocean floor and fore-arc serpentinites: Constraints on the ultramafic input to subduction zones. Journal of Petrology, **53**: 235–270. Oxford Academic. doi:10.1093/petrology/egr058.

Lamont, T.N., Roberts, N.M.W., Searle, M.P., Gopon, P., Waters, D.J., and Millar, I. 2020. The Age, Origin, and Emplacement of the Tsiknias Ophiolite, Tinos, Greece. Tectonics, **39**: e2019TC005677. doi:10.1029/2019TC005677.

Le Bas, M., Le Maitre, R., Streckeisen, A., Zanettin, B., and Rocks, I.S. on the S. of I. 1986. A chemical classification of volcanic rocks based on the total alkali-silica diagram. Journal of petrology, **27**: 745–750. Oxford University Press.

Lindsley-Griffin, N., Griffin, J.R., and Farmer, J. 2008. Paleogeographic significance of ediacaran cyclomedusoids within the Antelope Mountain Quartzite, Yreka subterrane, eastern Klamath Mountains, California. Special Paper of the Geological Society of America, **442**: 1–37. doi:10.1130/2008.442(01).

Mäder, U., Lewis, P., and Russell, J.K. 1988. Geology and Structure of the Kobau Group Between Oliver and Cawston, British Columbia: With Notes on Some Auriferous Quartz Veins (82E/4E).

In Geological Fieldwork 1988, British Columbia Ministry of Energy, Mines, and Petroleum Resources Geological Survey Paper

Massey, N.W.D. 2006a. Boundary Project : Reassessment of Paleozoic Rock Units of the Greenwood Area (NTS 82E / 02), Southern British Columbia. *In* Geological Fieldwork 2006, British Columbia Ministry of Energy, Mines, and Petroleum Resources Geological Survey Paper.

Massey, N.W.D. 2006b. Boundary Project: Rock Creek Area (NTS 082E/02W, 03E), Southern British Columbia. *In* Geological Fieldwork 2006, British Columbia Ministry of Energy, Mines, and Petroleum Resources Geological Survey Paper.

Massey, N.W.D. 2011. Southern Nicola Project: Geochemistry of Volcanic Rocks of the Nicola Group West of the Boundary Fault (Parts of NTS 092H/02, 07, and 10). *In* Geological Fieldwork 2010, British Columbia Ministry of Energy, Mines, and Petroleum Resources Geological Survey Paper.

Massey, N.W.D., and Dostal, J. 2013. Geochemistry of metabasalts from the Knob Hill complex and Anarchist Group in the Paleozoic basement to southern Quesnellia. *In* Geological Fieldwork 2012, British Columbia Ministry of Energy, Mines and Natural Gas, British Columbia Geological Survey Paper.

Massey, N.W.D., Gabites, J.E., and Mortensen, J.K. 2013. LA-ICP-MS geochronology of the Greenwood gabbro, Knob Hill complex, southern Okanagan, British Columbia. *In* Geological Fieldwork 2012, British Columbia Ministry of Energy, Mines and Natural Gas, British Columbia Geological Survey Paper.

Massey, N.W.D., Gabites, J.E., Mortensen, J.K., and Ullrich, T.D. 2010. Boundary Project: Geochronology and Geochemistry of Jurassic and Eocene Intrusions, Southern British Columbia (NTS 082E). : 17.

Matsumoto, T., and Tomoda, Y. 1983. Numerical Simulation of the Initiation of Subduction at the Fracture Zone. Journal of Physics of the Earth, **31**: 183–194. doi:10.4294/jpe1952.31.183.

Milford, J.C. 1984. Geology of the Apex Mountain Group, north and east of the Similkameen River, south-central British Columbia (MSc Thesis, University of British Columbia).

MINFILE. 1985. Podiform Chromite Occurrences: Okanagan, Harper Ranch, and Quesnel terranes. Report. Available from https://minfile.gov.bc.ca/report.aspx?r=Summary_Inventory.rpt&f=PDF [accessed 30 June 2022].

Miyashiro, A. 1975. Classification, Characteristics, and Origin of Ophiolites. The Journal of Geology, **83**: 249–281. The University of Chicago Press. doi:10.1086/628085.

Monger, J.W.H. 1977. Upper Paleozoic rocks of the western Canadian Cordillera and their bearing on Cordilleran evolution. Canadian Journal of Earth Sciences, **14**: 1832–1859. NRC Research Press, Ottawa, Canada. doi:10.1139/e77-156.

Monger, J. and Price, R. 2002. The Canadian Cordillera: Geology and Tectonic Evolution. CSEG Recorder: 17–36.

Monger, J.W.H., Price, R.A., and Tempelman-Kluit, D.J. 1982. Tectonic accretion and the origin of the two major metamorphic and plutonic welts in the Canadian Cordillera. Geology, **10**: 70. doi:10.1130/0091-7613(1982)10<70:TAATOO>2.0.CO;2.

Mortensen, J., Lucas, K., Monger, J., and Cordey, F. 2017. Synthesis of U-Pb and fossil age, lithogeochemical and Pb-isotopic studies of the Paleozoic Basement of the Quesnel Terrane in south-central British Columbia and northern Washington State. *In* Geoscience BC, Report.

Mortensen, J.K., Lucas, K., Monger, J.W.H., and Cordey, J.W.H. 2011. Geological Investigations of the Basement of the Quesnel Terrane in Southern British Columbia (NTS 082E, F, L, 092H, I): Progress Report.

Mortimer, N. 1987. The Nicola Group: Late Triassic and Early Jurassic subduction-related volcanism in British Columbia. Canadian Journal of Earth Sciences, **24**: 2521–2536. NRC Research Press. doi:10.1139/e87-236.

Murray, R.W. 1994. Chemical criteria to identify the depositional environment of chert: general principles and applications. Sedimentary Geology, **90**: 213–232. doi:10.1016/0037-0738(94)90039-6.

Nelson, J., Colpron, M., Piercey, S., Murphy, D., Dusel-Bacon, C., and Roots, C.F. 2006. Paleozoic tectonic and metallogenetic evolution of pericratonic terranes in Yukon, northern British Columbia and eastern Alaska. pp. 323–360.

O'Dowd, C. 2017. Analysis of volcanic ash. Senior Honors Thesis, Eastern Michigan University.

Okulitch, A.V. 1973. Age and Correlation of the Kobau Group, Mount Kobau, British Columbia. Canadian Journal of Earth Sciences, **10**: 1508–1518. doi:10.1139/e73-143.

Okulitch, A.V. 1979. Geology and mineral occurences of the Thompson-Shuswap-Okanagan Region, south-central British Columbia. Geological Survey of Canada, Open File.

Orchard, M.J., and Forster, P.J.L. 1988. Permian conodont biostratigraphy of the Harper Ranch Beds, near Kamloops, south-central British Columbmia.

Pearce, J.A. 2003. Supra-subduction zone ophiolites: The search for modern analogues. *In* Geological Society of America Special Paper.

Pearce, J.A., Lippard, S.J., and Roberts, S. 1984. Characteristics and tectonic significance of supra-subduction zone ophiolites. Geological Society, London, Special Publications, **16**: 77–94. Geological Society of London. doi:10.1144/GSL.SP.1984.016.01.06.

Pearce, J.A., and Norry, M.J. 1979. Petrogenetic implications of Ti, Zr, Y, and Nb variations in volcanic rocks. Contributions to Mineralogy and Petrology, **69**: 33–47. doi:10.1007/BF00375192.

Piercey, S.J., Murphy, D.C., and Creaser, R.A. 2012. Lithosphere-asthenosphere mixing in a transform-dominated late Paleozoic backarc basin: Implications for northern Cordilleran crustal growth and assembly. Geosphere, **8**: 716–739. doi:10.1130/GES00757.1.

Poblet, J., and Lisle, R.J. 2011. Kinematic evolution and structural styles of fold-and-thrust belts. Geological Society, London, Special Publications, **349**: 1–24. doi:10.1144/SP349.1.

Pohler, S.M.L., Orchard, M.J., and Tempelman-Kluit, D.J. 1989. Ordovician conodonts identify the oldest sediments in the Intermontane Belt, Olalla, south-central British Columbia. Current Research, Part E, Geological Survey of Canada, Paper 89-1E: 61–67.

Ranero, C.R., and Pérez-Gussinyé, M. 2010. Sequential faulting explains the asymmetry and extension discrepancy of conjugate margins. Nature, **468**: 294–299. Nature Publishing Group. doi:10.1038/nature09520.

Ray, G.E., and Dawson, G.L. 1994. The geology and mineral deposits of the Hedley gold skarn district, southern British Columbia. Province of British Columbia, Ministry of Energy, Mines and Petroleum Resources.

Ray, G.E., Dawson, G.L., and Webster, I.C.L. 1996. The stratigraphy of the Nicola Group in the Hedley district, British Columbia, and the chemistry of its intrusions and Au skarns. Canadian Journal of Earth Sciences, **33**: 1105–1126. doi:10.1139/e96-084.

Ray, G.E., Webster, I.C.L., Dawson, B.C., and Ettlinger, A.D. 1992. A geological overview of the Hedley gold skarn district southern British Columbia (92H).

Read, P.B., and Okulitch, A.V. 1977. The Triassic unconformity of south-central British Columbia. Canadian Journal of Earth Sciences, **15**: 323–324. doi:10.1139/e78-034.

Roback, R.C., Sevigny, J.H., and Walker, N.W. 1994. Tectonic setting of the Slide Mountain terrane, southern British Columbia. Tectonics, **13**: 1242–1258. doi:10.1029/94TC01032.

Roback, R.C., and Walker, N.W. 1995. Provenance, detrital zircon U-Pb geochronometry, and tectonic significance of Permian to Lower Triassic sandstone in southeastern Quesnellia, British Columbia and Washington. Geological Society of America Bulletin, **107**: 665–675.

Ross, J.V. 1981. A geodynamic model for some structures within and adjacent to the Okanagan Valley, southern British Columbia. Can. J. Earth Sci, **18**: 1581–1598.

Ross, J.V., and Zimmerman, J. 1996. Comparison of evolution and tectonic significance of the Pindos and Vourinos ophiolite suites, northern Greece. Tectonophysics, **256**: 1–15. doi:10.1016/0040-1951(95)00160-3.

Ross, P.-S., and Bédard, J.H. 2009. Magmatic affinity of modern and ancient subalkaline volcanic rocks determined from trace-element discriminant diagrams. Canadian Journal of Earth Sciences, **46**: 823–839.

Ruks, T.W., Piercey, S.J., Ryan, J.J., Villeneuve, M.E., and Creaser, R.A. 2006. Mid- to late Paleozoic K-feldspar augen granitoids of the Yukon-Tanana terrane, Yukon, Canada: Implications for crustal growth and tectonic evolution of the northern Cordillera. GSA Bulletin, **118**: 1212–1231. doi:10.1130/B25854.1.

Shervais, J.W. 1982. TiV plots and the petrogenesis of modern and ophiolitic lavas. Earth and Planetary Science Letters, **59**: 101–118. doi:10.1016/0012-821X(82)90120-0.

Shervais, J.W. 2001. Birth, death, and resurrection: The life cycle of suprasubduction zone ophiolites. Geochemistry, Geophysics, Geosystems, **2**. doi:10.1029/2000GC000080.

Shervais, J.W. 2022. The petrogenesis of modern and ophiolitic lavas reconsidered: Ti-V and Nb-Th. Geoscience Frontiers, **13**: 101319. doi:10.1016/j.gsf.2021.101319.

Simony, P.S. 1979. Pre-Carboniferous basement near Trail, British Columbia. Canadian Journal of Earth Sciences, **16**: 1–11. NRC Research Press. doi:10.1139/e79-001.

Simony, P.S., Sevigny, J.H., Mortensen, J.K., and Roback, R.C. 2006. Age and origin of the Trail Gneiss complex: basement to Quesnel terrane near Trail, southeastern British Columbia. Paleozoic Evolution and Metallogeny of Pericratonic Terranes at the Ancient Pacific Margin of North America, Canadian and Alaskan Cordillera: Geological Association of Canada, Special Paper, **45**: 505–515.

Smith, R.B. 1979. Geology of the Harper Ranch Group (Carboniferous-Permian) and Nicola Group (upper Triassic) northeast of Kamloops, British Columbia. University of British Columbia. doi:10.14288/1.0052516.

Snow, C.A., and Shervais, J.W. 2015. Cuesta Ridge ophiolite, San Luis Obispo, California: implications for the origin of the Coast Range ophiolite. Anderson, TH; Didenko, AN; Johnson, AN; Khanchuk, CL,: 285–298.

van Staal, C.R., Zagorevski, A., McClelland, W.C., Escayola, M.P., Ryan, J.J., Parsons, A.J., and Proenza, J. 2018. Age and setting of Permian Slide Mountain terrane ophiolitic ultramafic-mafic complexes in the Yukon: Implications for late Paleozoic-early Mesozoic tectonic models in the northern Canadian Cordillera. Tectonophysics, **744**: 458–483. Elsevier B.V. doi:10.1016/j.tecto.2018.07.008.

Stern, R.J. 2004. Subduction initiation: Spontaneous and induced. Earth and Planetary Science Letters, **226**: 275–292. doi:10.1016/j.epsl.2004.08.007.

Stern, R.J., and Bloomer, S.H. 1992. Subduction zone infancy: Examples from the Eocene Izu-Bonin-Mariana and Jurassic California arcs. Geological Society of America Bulletin, **104**: 1621–1636. doi:10.1130/0016-7606(1992)104<1621:SZIEFT>2.3.CO;2.

Stern, R.J., and Gerya, T. 2018. Subduction initiation in nature and models: A review. Tectonophysics, **746**: 173–198. doi:10.1016/j.tecto.2017.10.014.

Sun, S.S., and McDonough, W.F. 1989. Chemical and isotopic systematics of oceanic basalts: Implications for mantle composition and processes. Geological Society Special Publication, **42**: 313–345. Geological Society of London. doi:10.1144/GSL.SP.1989.042.01.19.

Tempelman-Kluit, D., and Parkinson, D. 1986. Extension across the Eocene Okanagan crystal shear in southern British Columbia. Geology, **14**: 318–321. Geological Society of America.

Thorkelson, D.J., and Taylor, R.P. 1989. Cordilleran slab windows. Geology, **17**: 833–836. doi:10.1130/0091-7613(1989)017<0833:CSW>2.3.CO;2.

Tremblay, A., Meshi, A., Deschamps, T., Goulet, F., and Goulet, N. 2015. The Vardar zone as a suture for the Mirdita ophiolites, Albania: Constraints from the structural analysis of the Korabi-Pelagonia zone. Tectonics, **34**: 352–375. doi:10.1002/2014TC003807.

Unterschutz, J.L.E., Creaser, R.A., Erdmer, P., Thompson, R.I., and Daughtry, K.L. 2002. North American margin origin of Quesnel terrane strata in the southern Canadian Cordillera: Inferences from geochemical and Nd isotopic characteristics of Triassic metasedimentary rocks. Bulletin of the Geological Society of America, **114**: 462–475. GeoScienceWorld. doi:10.1130/0016-7606(2002)114<0462:namooq>2.0.co;2.

Verma, S.P., and Agrawal, S. 2011. New tectonic discrimination diagrams for basic and ultrabasic volcanic rocks through log-transformed ratios of high field strength elements and implications for petrogenetic processes. Revista Mexicana de Ciencias Geológicas, **28**: 24–44.

Verma, S.P., and Verma, S.K. 2013. First 15 probability-based multidimensional tectonic discrimination diagrams for intermediate magmas and their robustness against postemplacement compositional changes and petrogenetic processes. Turkish Journal of Earth Sciences, **22**: 931–995. The Scientific and Technological Research Council of Turkey.

Whattam, S.A., and Stern, R.J. 2011. The "subduction initiation rule": A key for linking ophiolites, intra-oceanic forearcs, and subduction initiation. Contributions to Mineralogy and Petrology, **162**: 1031–1045. Springer. doi:10.1007/s00410-011-0638-z.

Appendices

Appendix A: Sedimentary Overlap assemblages

Nicola Group

Nicola Group sedimentary rocks include limestone, calcareous siltstone, lithic arkose and conglomerate. Pyritiferous, thinly bedded, turbiditic dark calcareous siltstone is interbedded with white and dark grey limestone and light brown-weathering fine- to medium-grained lithic arkose. Conglomerates are polymict and matrix-supported with a fine-grained light grey-weathering arkose matrix. The Nicola Group in the Hedley region has been divided into four lithologically distinct, coeval, fault-bounded formations interpreted as facies of an arc-related volcaniclastic sequence (Ray et al. 1996). Paleocurrent indicators indicate derivation from an eastern source and transportation of sediment westward into a deepening, tectonically active basin (Ray et al 1996). The predominance of clasts from Okanagan subterrane units within coarse-grained Nicola Group sediments is consistent with such an interpretation.

Brooklyn Group

Sedimentary units of the Brooklyn Group consist of fine- to medium-grained sandstone interbedded with dark grey siltstone, marl, light grey-brown weathering marble, and micrite. Pyrite is abundant and concentrated along sandstone layers. Beds are 10-25cm thick and exhibit parallel internal laminations and occasional flame structures. Underlying the sandstone/siltstone beds are poorly-sorted, granule to cobble conglomerates containing subrounded angular clasts of varicolored chert, quartzite, limestone, and minor amygdaloidal greenstone. Conglomerates weather burgundy, sage-green or

grey, are matrix-supported by coarse sand of the same composition and are locally interbedded with discontinuous layers of siltstone or micrite. At an outcrop 8km east of Greenwood, chert pebble conglomerate overlies coarse limestone breccia along a steeply west-dipping contact (Figure 15).

Appendix B: Whole Rock Geochemistry of metavolcanic rocks from this study

Raw data from lithogeochemical analyses of volcanic rock samples from the Okanagan subterrane. Major element values in weight percent, trace element values in ppm. Major oxides and minor elements were determined by lithium borate fusion followed by laser ablation Inductively Coupled Plasma Emission Spectroscopy (ICP-ES). Trace elements were measured by Inductively Coupled Plasma Mass Spectrometry (ICP-MS). The standards analyzed recorded concentrations of major elements to within 3% and LILE and HFSE to within 5% of expected values. Analyses were completed using the LF200 method at Bureau Veritas Commodities Canada Laboratory, Vancouver, British Columbia.

Sample		H20-03	Ash20-03	Ash20-06	Ash20-07	Ola20-07	Ola20-08	Ola20-10	Ola20-12	Ola20-21	Ola20-22	Ker20-07	RC20-02	Gre20-03	Gre20-20
UTM Zone		10U	10U	11U	11U	11U	11U	11U	11U	11U	11U	11U	11U	11U	11U
UTM		716214 E, 5470595 N	718303 E, 5452234 N	281547 E, 5453340 N	281954 E, 5456138 N	291332 E, 5463151 N	291168 E, 5463353 N	290463 E, 5463534 N	288533 E, 5463323 N	286153 E, 5459463 N	285796 E, 5459271 N	290588 E, 5454335 N	360551 E, 5441983 N	385633 E, 5439527 N	381930 E, 5440177 N
MDL[d]															
%															
SiO_2	0.01	47.42	45.30	45.87	57.34	51.36	50.17	44.93	51.68	44.58	46.99	47.19	48.52	48.23	44.64
Al_2O_3	0.01	14.40	16.04	12.8	17.49	12.79	12.74	16.11	17.24	15.84	15.10	15.80	13.51	12.30	13.17
Fe_2O_3[a]	0.04	11.50	15.03	10.38	7.12	15.94	15.96	11.94	8.63	11.29	11.85	9.38	14.42	11.87	11.32
MgO	0.01	5.17	7.32	6.93	3.78	5.34	5.79	9.87	2.74	11.51	5.73	7.82	6.72	5.47	6.24
CaO	0.01	16.14	4.56	8.44	2.87	2.72	4.30	6.47	9.47	7.24	8.77	9.61	9.76	7.71	10.17
Na_2O	0.01	1.69	3.37	2.54	2.41	0.84	1.97	2.45	3.53	1.83	3.80	3.75	3.21	2.29	3.95
K_2O	0.01	0.95	0.44	1.62	2.48	4.13	0.69	1.24	0.84	1.17	0.72	0.72	0.26	0.47	0.59
TiO_2	0.01	0.87	1.80	1.36	0.64	2.06	1.05	0.86	1.52	0.40	2.31	1.11	0.48	1.99	1.86
P_2O_5	0.01	0.24	0.17	0.12	0.14	0.11	0.18	0.06	0.48	0.05	0.29	0.09	0.04	0.21	0.54
MnO	0.01	0.22	0.31	0.25	0.06	0.09	0.23	0.22	0.16	0.23	0.15	0.15	0.30	0.17	0.14
Cr_2O_3	0.002	0.009	0.058	0.018	0.011	0.022	<0.002	0.034	0.017	0.055	0.021	0.043	0.013	0.003	0.036
LOI[b]	-5.1	1.1	5.3	9.1	5.4	4.4	6.6	5.5	3.5	5.6	4.0	4.1	2.5	9.0	7.1
Sum	0.01	99.75	99.76	99.77	99.82	99.83	99.88	99.74	99.81	99.89	99.84	99.78	99.78	99.78	99.75
ppm															
Ba	1	325	61	3472	749	329	1418	697	420	442	666	220	83	220	112
Ni	20	27	277	53	29	76	<20	132	44	238	41	86	82	53	118
Sc	1	31	29	37	19	37	32	57	21	42	34	35	62	24	19
Be	1	<1	<1	1	<1	<1	<1	<1	2	<1	<1	<1	<1	<1	1
Co	0.2	27.0	61.9	41.4	18.1	29.4	35.8	53.1	22.2	60.0	38.1	39.5	52.4	38.3	33.2
Cs	0.1	1.2	1.7	6.8	2.8	5.5	1.8	0.7	0.4	0.5	0.2	0.8	1.7	1.8	1.7
Ga	0.5	15.5	22.4	12.9	14.7	18.7	14.6	12.5	19.0	11.3	20.2	10.6	10.0	17.5	18.3
Hf	0.1	1.3	2.5	2.4	2.5	3.3	2.3	1.2	3.2	0.7	3.9	1.8	0.7	2.5	5.9
Nb	0.1	1.8	10.8	4.3	6.0	6.7	3.9	2.6	28.1	1.0	15.4	3.5	0.3	6.9	17.3
Rb	0.1	22.2	14.2	50.4	71.1	73.6	13.6	17.3	10.5	22.2	11.0	11.1	7.8	14.0	9.8
Sn	1	1	<1	<1	<1	1	<1	<1	<1	<1	1	<1	<1	<1	1
Sr	0.5	556.3	176.2	137.6	371.8	36.2	84.0	50.0	488.9	33.9	185.6	174.8	163.4	321.9	285.9
Ta	0.1	<0.1	0.6	0.2	0.3	0.5	0.3	0.1	1.7	<0.1	0.9	0.3	<0.1	0.5	0.7

Th	0.2	1.0	0.6	0.3	3.4	0.5	0.4	0.2	2.5	<0.2	1.0	0.2	<0.2	0.8	1.8
U	0.1	0.6	1.1	0.1	1.3	0.1	<0.1	<0.1	0.6	<0.1	0.4	<0.1	<0.1	0.2	0.5
V	8	334	289	294	158	175	166	330	184	219	272	221	347	251	161
W	0.5	0.6	1.0	1.9	0.9	<0.5	<0.5	1.4	<0.5	<0.5	<0.5	<0.5	<0.5	0.7	1.8
Zr	0.1	40.5	77.5	80.8	89.7	115.4	71.3	38.4	127.0	18.1	148.1	65.0	16.9	88.1	249.7
Y	0.1	19.1	22.4	26.8	14.5	28.3	48.4	20.7	22.8	16.2	26.6	20.0	22.3	25.3	25.0
La	0.1	10.4	7.6	4.6	13.7	7.0	3.2	1.8	23.2	0.6	12.6	4.3	1.1	8.0	28.0
Ce	0.1	17.9	15.1	11.6	27.4	17.7	7.6	4.0	46.2	0.9	28.0	10.0	1.4	17.0	62.0
Pr	0.02	2.62	2.26	1.82	3.37	2.91	1.14	0.63	6.00	0.18	3.95	1.42	0.26	2.35	8.22
Nd	0.3	12.2	10.9	9.3	13.8	15.0	6.6	3.7	24.6	1.3	18.7	8.1	1.8	11.4	36.3
Sm	0.05	2.93	3.63	2.83	2.93	4.56	2.74	1.51	4.95	0.67	4.97	2.25	0.84	3.97	8.12
Eu	0.02	1.10	1.39	0.84	0.97	1.42	1.06	0.53	1.79	0.23	1.76	0.98	0.36	1.44	2.56
Gd	0.05	3.54	4.62	4.09	3.03	5.42	5.07	2.54	4.94	1.55	5.71	3.12	1.91	5.15	7.78
Tb	0.01	0.55	0.78	0.73	0.44	0.91	1.03	0.51	0.75	0.33	0.88	0.56	0.43	0.86	1.11
Dy	0.05	3.43	4.50	4.77	2.66	5.51	7.48	3.68	4.40	2.54	5.15	3.54	3.58	5.01	5.86
Ho	0.02	0.77	0.88	1.07	0.56	1.09	1.77	0.83	0.83	0.60	1.04	0.79	0.87	0.99	0.97
Er	0.03	2.15	2.31	3.01	1.77	2.90	5.64	2.65	2.41	2.03	2.72	2.32	2.90	2.74	2.60
Tm	0.01	0.28	0.29	0.41	0.24	0.36	0.82	0.40	0.31	0.31	0.37	0.32	0.47	0.34	0.30
Yb	0.05	1.91	1.88	2.59	1.66	2.32	5.42	2.74	1.93	1.96	2.33	2.00	3.35	2.10	1.66
Lu	0.01	0.28	0.28	0.43	0.23	0.34	0.86	0.44	0.30	0.34	0.34	0.30	0.55	0.31	0.23
TotREE[c]		60.06	56.42	48.09	72.76	67.44	50.43	25.96	122.61	13.54	88.52	40.00	19.82	61.66	165.71

[a] Total iron expressed as Fe_2O_3

[b] Loss on ignition

[c] Total concentration of rare earth elements

[d] Method detection limit

Appendix C: Whole Rock Geochemistry of chert rocks from this study

Raw data from geochemical analyses of chert rock samples from the Okanagan subterrane. Major element values in weight percent, trace element values in ppm. Major oxides and minor elements were determined by lithium borate fusion followed by laser ablation Inductively Coupled Plasma Emission Spectroscopy (ICP-ES). Trace elements were measured by Inductively Coupled Plasma Mass Spectrometry (ICP-MS). The standards analyzed recorded concentrations of major elements to within 3% and LILE and HFSE to within 5% of expected values. Analyses were completed using the LF200 method at Bureau Veritas Commodities Canada Laboratory, Vancouver, British Columbia.

Sample		Ash20-01	Ash20-05	Ash20-06	Ola20-01	Ola20-01b	Ola20-03	Ola20-06	Ola20-07	Ola20-09	Ola20-14	Ola20-21	Ola20-24	Ker20-03	Ker20-04	Ker20-07	RC20-01	Gre20-03	Gre20-18
UTM Zone		11U	11U	11U	11U	11U	11U	11U	11U	11U	11U	11U	11U	11U	11U	11U	11U	11U	11U
Easting		283262	281513	281546	295629	295629	294826	291691	291446	291305	287713	286490	295179	295870	295486	290588	360051	385633	384854
Northing		5455786	5453208	5453340	5466994	5466994	5475547	5463057	5463129	5463581	5463104	5459803	5465265	5456613	5456276	5454335	5441051	5439527	5439457
	MDL[d]	SM	OT	OT	SM	SM	SM	SM	SM	SM	OT	OT	SM	SM	SM	SM	KH	KH	KH
%																			
SiO_2	0.01	95.63	86.93	94.76	91.35	93.17	89.08	73.68	94.55	96.71	95.53	91.88	93.32	77.28	62.11	90.22	92.99	74.85	96.3
Al_2O_3	0.01	1.28	3.98	1.20	3.32	1.59	2.50	0.68	1.76	0.89	1.34	2.68	2.05	10.30	15.33	3.28	2.59	11.11	1.52
Fe_2O_3[a]	0.04	1.21	2.47	1.07	1.91	0.79	2.71	0.75	1.23	1.03	1.12	1.96	1.95	3.22	5.18	1.86	1.79	4.41	0.47
MgO	0.01	0.43	0.97	0.32	0.72	0.21	0.67	0.55	0.46	0.15	0.53	0.69	0.66	1.38	3.49	0.79	0.43	1.54	0.13
CaO	0.01	0.36	1.72	0.84	0.13	1.92	0.21	13.05	0.35	0.22	0.28	0.48	0.21	2.37	5.59	0.94	0.07	0.66	0.33
Na_2O	0.01	0.16	0.78	0.05	0.36	0.51	0.38	0.17	0.02	0.01	0.07	0.54	0.05	1.22	1.25	0.66	0.04	4.13	0.73
K_2O	0.01	0.21	0.54	0.32	0.95	0.31	0.64	0.03	0.48	0.35	0.36	0.31	0.62	1.94	4.57	0.63	0.69	1.02	0.07
TiO_2	0.01	0.06	0.19	0.05	0.15	0.08	0.12	0.02	0.08	0.03	0.07	0.12	0.08	0.41	0.89	0.13	0.12	0.53	0.04
P_2O_5	0.01	0.03	0.03	0.13	0.06	1.20	0.04	<0.01	0.03	0.02	0.03	0.10	0.02	0.13	0.15	0.05	0.05	0.04	<0.01
MnO	0.01	0.03	0.13	0.03	0.03	0.02	0.16	0.17	0.13	0.10	0.02	0.24	0.02	0.03	0.05	0.04	0.01	0.07	<0.01
Cr_2O_3	0.002	<0.002	0.002	<0.002	0.003	0.002	0.004	<0.002	<0.002	<0.002	<0.002	<0.002	0.002	0.006	0.013	0.002	0.002	0.008	<0.002
LOI[b]	-5.1	0.6	2.0	1.2	0.9	0.2	3.5	10.8	0.9	0.5	0.5	0.8	0.9	1.6	1.1	1.4	1.0	1.5	0.4
Sum	0.01	100	99.94	99.99	99.98	99.99	99.98	99.98	99.99	100.00	99.99	99.97	99.99	99.92	99.82	99.97	99.99	99.89	100.01
ppm																			
Ba	1	164	1892	554	331	120	154	545	103	71	978	1210	744	390	1122	69	1997	278	19
Ni	20	<20	<20	<20	<20	<20	<20	<20	<20	<20	<20	65	<20	24	45	<20	<20	31	<20
Sc	1	3	7	2	4	3	3	<1	3	2	4	6	2	9	15	3	2	17	1
Be	1	<1	<1	<1	<1	<1	<1	<1	<1	<1	<1	<1	<1	3	3	<1	<1	3	<1
Co	0.2	4.5	7.2	2.8	2.0	0.8	5.2	1.5	6.1	1.9	1.9	8.3	2.2	5.8	16	2.9	1.7	13.3	0.5
Cs	0.1	0.2	0.2	0.2	1.9	0.3	1.2	<0.1	0.5	0.2	<0.1	0.1	0.7	2.2	3.1	0.7	0.6	0.4	<0.1
Ga	0.5	2.9	6.4	1.1	3.5	<0.5	2.9	<0.5	2.9	<0.5	0.5	3.5	2.2	10.6	18	3.4	2.5	11.4	<0.5
Hf	0.1	0.5	1.0	0.3	0.9	0.5	0.8	<0.1	0.5	0.2	0.4	0.7	0.5	2.0	4.5	0.7	0.6	2.4	0.2
Nb	0.1	1.3	1.2	1.6	3.1	1.7	2.0	0.2	1.4	0.4	1.3	0.9	1.2	10.0	13.7	2.0	2.0	8.5	0.6
Rb	0.1	6.6	10.3	9.7	40.9	7.2	24.2	0.6	18.2	13.4	6.8	10.3	21.1	64.9	111.0	14.4	18.5	19.6	1.0
Sn	1	<1	<1	<1	<1	<1	<1	<1	<1	<1	<1	<1	<1	<1	<1	<1	<1	2	<1
Sr	0.5	22.0	50.0	33.4	8.8	36.9	23.9	112.8	7.2	2.6	7.5	60.9	9.8	167.1	233.3	19.7	12.1	208.5	13.2
Ta	0.1	<0.1	0.1	0.1	0.2	0.2	0.2	<0.1	0.1	<0.1	0.1	0.1	<0.1	0.6	0.8	0.2	0.2	0.7	<0.1
Th	0.2	1.0	0.8	0.8	2.1	1.3	1.5	<0.2	1.2	0.4	0.8	0.7	1.3	11.0	13.5	2.0	1.5	10.7	0.8

U	0.1	0.4	0.3	2.1	0.3	3.7	0.5	<0.1	0.3	<0.1	2.0	0.3	0.4	1.5	2.7	0.4	0.3	1.6	<0.1
V	8	<8	69	9	17	17	43	<8	10	<8	39	18	12	57	106	28	27	111	<8
W	0.5	<0.5	0.6	<0.5	0.6	<0.5	1.6	<0.5	<0.5	<0.5	<0.5	0.8	<0.5	0.7	1.4	<0.5	0.9	0.7	<0.5
Zr	0.1	18.0	35.5	13.1	33.2	19.5	26.2	4.2	18.0	9.9	17.2	30.8	18.3	75.7	162.5	26.7	24.2	80.7	7.8
Y	0.1	2.8	7.7	6.6	5.1	12.3	2.9	2.0	3.5	1.8	4.0	8.0	2.9	18.0	22.8	6.0	4.2	14.2	1.2
La	0.1	3.5	4.3	5.3	7.1	9.9	4.5	1.1	4.2	1.7	3.3	6.1	4.6	34.0	40.6	6.3	5.1	22.1	3.0
Ce	0.1	9.9	8.6	12.6	13.4	18.5	9.5	2.0	10.4	3.6	6.2	9.6	9.3	67.3	79.9	10.5	10.2	56.8	6.8
Pr	0.02	0.9	1.2	1.34	1.58	2.13	0.9	0.19	1.11	0.36	1.02	1.43	1.04	7.66	9.36	1.46	1.17	5.69	0.51
Nd	0.3	3.3	5.3	5.4	5.7	8.2	3.7	0.8	4.6	1.5	4.3	5.8	3.9	28.1	33.9	6.1	4.8	19.9	2.1
Sm	0.05	0.75	1.35	1.12	1.02	1.82	0.70	0.17	0.91	0.37	1.05	1.38	0.78	5.03	6.04	1.07	0.77	4.04	0.33
Eu	0.02	0.16	0.34	0.34	0.24	0.52	0.16	0.08	0.22	0.08	0.18	0.37	0.16	0.82	1.06	0.22	0.11	0.82	0.09
Gd	0.05	0.74	1.53	1.29	0.99	1.98	0.64	0.29	0.90	0.42	1.01	1.61	0.73	4.40	5.04	1.13	0.67	3.34	0.34
Tb	0.01	0.11	0.24	0.22	0.15	0.32	0.10	0.05	0.13	0.06	0.15	0.25	0.11	0.62	0.76	0.17	0.10	0.50	0.03
Dy	0.05	0.64	1.50	1.18	0.90	1.88	0.64	0.26	0.79	0.35	0.92	1.55	0.67	3.57	4.69	0.98	0.73	2.77	0.26
Ho	0.02	0.13	0.34	0.25	0.21	0.38	0.12	0.06	0.14	0.08	0.18	0.32	0.11	0.63	0.86	0.21	0.15	0.54	0.03
Er	0.03	0.32	0.93	0.64	0.60	1.17	0.32	0.20	0.45	0.27	0.53	1.03	0.36	1.88	2.55	0.69	0.46	1.54	0.13
Tm	0.01	0.06	0.14	0.08	0.08	0.15	0.05	0.03	0.06	0.03	0.07	0.13	0.05	0.24	0.36	0.10	0.07	0.21	<0.01
Yb	0.05	0.32	0.89	0.49	0.55	1.08	0.35	0.17	0.40	0.24	0.52	0.94	0.38	1.67	2.30	0.64	0.51	1.35	0.11
Lu	0.01	0.05	0.15	0.07	0.10	0.16	0.05	0.03	0.06	0.04	0.07	0.14	0.06	0.23	0.34	0.10	0.07	0.20	0.02
TotREE[c]		20.88	26.81	30.32	32.62	48.19	21.73	5.43	24.37	9.10	19.50	30.65	22.25	156.15	187.76	29.67	24.91	119.80	13.75

[a] Total iron expressed as Fe_2O_3

[b] Loss on ignition

[c] Total concentration of rare earth elements

[d] Method detection limit

Appendix D: Compiled Geochemistry Data of metavolcanic rocks from External Sources

*note: blank fields represent data not available; bdl = below detection limits

Oregon Claims Formation, Old Tom Assemblage, and Kobau Group

Rock unit		Oregon Claims		Old Tom										Kobau	
Source		Ray et al. (1996)		Milford (1984)										Massey and Dostal (2013)	
Sample		HD313	HD346	6191	6203	7211	7215	7237	8102	31912	31913	32014	32015	05NMA20-02	05NMA27-03
Ti-V Classification*			IAB											IAB	IAB
LDA Classification†			IAB												
UTM Zone														11	11
Easting														5450392	5451317
Northing														372191	381743
%															
	MDL														
SiO2	0.01	50.07	51.60											48.78	49.63
Al2O3	0.01	16.96	14.47											14.65	14.45
Fe2O3	0.04	1.49	1.51											13.22	11.27
MgO	0.01	5.53	5.85											8.30	8.82
CaO	0.01	7.69	11.54											11.66	11.59
Na2O	0.01	5.71	2.16											1.38	2.17
K2O	0.01	1.04	1.31											0.51	0.59
TiO2	0.01	0.75	0.79											0.45	0.74
P2O5	0.01	0.24	0.28											0.04	0.06
MnO	0.01	0.18	0.22											0.20	0.25
Cr2O3	0.002														
LOI	-5.1	1.36	0.72											4.96	0.79
Sum	0.01	99.19	99.51											104.15	100.36
ppm															
Cr		50	78											202	369
Ba	1	900	985											232	232
Ni	20	19	25											5	4
Sc	1		32												
Be	1														
Co	0.2	22	30											65	54
Cs	0.1	na	8												
Ga	0.5													6	9
Hf	0.1														
Nb	0.1	2	2	16	4	6	10	9	28	9	6	8	12		
Rb	0.1	16	23												
Sn	1														
Sr	0.5		573												

Ta	0.1	bdl	bdl												
Th	0.2	10	8												
U	0.1														
V	8		362											282	265
W	0.5														
Zr	0.1	58	57	204	32	54	75	73	216	81	46	57	118	28	42
Y	0.1	17	23	28	12	19	14	17	28	26	19	19	37		
La	0.1		26											17	15
Ce	0.1		31												
Pr	0.02														
Nd	0.3													67	108
Sm	0.05														
Eu	0.02														
Gd	0.05														
Tb	0.01														
Dy	0.05														
Ho	0.02														
Er	0.03														
Tm	0.01														
Yb	0.05														
Lu	0.01														

* Shervais (1982)

† Verma and Agrawal (2011)

Anarchist Group

Rock unit		Anarchist																					
Source		Massey and Dostal (2013)																					
Sample		06NMA02-06	06NMA03-04B	06NMA05-03	06NMA06-03	06NMA07-01-04	06NMA09-22Ave	06NMA12-16	06NMA12-19	06NMA23-14	06NMA25-07	07NMA01-19	07NMA05-01	07NMA05-08B	07NMA05-12	07NMA07-04	07NMA07-07B	07NMA07-09	07NMA07-13	07NMA08-11	07NMA13-10	07NMA15-01	07NMA15-02
Ti-V Classification*		MORB	IAB	MORB	OIB	OIB	MORB	OIB	OIB	IAB	IAB	LowTi-IAB	IAB	MORB	OIB	IAB	IAB	MORB	IAB	OIB	LowTi-IAB	OIB	MORB
LDA Classification†											IAB												
UTM Zone		11	11	11	11	11	11	11	11	11	11	11	11	11	11	11	11	11	11	11	11	11	11
Easting		5431599	5432519	5430363	5429726	5430487	5433053	5432871	5433044	5444351	5446026	5450092	5444220	5444751	5446337	5444921	5444659	5443924	5443315	5442046	5439193	5441048	5440948
Northing		355973	354934	352395	352113	352279	354666	346399	346714	353310	349738	338119	343373	341994	341735	340739	340836	341615	340005	344124	344306	345873	345985
MDL																							
%																							
SiO2	0.01	48.62	47.47	47.91	49.58	45.05	48.99	46.55	43.73	59.02	48.72	46.80	49.51	47.48	42.39	49.07	46.80	48.49	49.43	42.26	54.87	50.53	50.11
Al2O3	0.01	13.10	13.20	15.08	14.71	12.16	14.28	14.99	14.01	14.06	13.38	18.87	13.85	15.23	11.80	15.04	15.66	14.13	11.36	13.63	16.47	15.64	15.13
Fe2O3	0.04	13.20	14.88	11.82	10.57	12.35	11.87	15.86	14.38	8.77	14.38	7.17	11.52	12.44	13.05	14.19	14.92	15.14	10.85	14.58	8.33	10.78	11.36
MgO	0.01	6.35	7.64	7.05	6.61	13.95	6.88	4.14	6.23	4.39	6.72	9.73	9.89	7.74	11.92	7.29	7.46	6.40	12.28	8.69	7.26	6.25	5.40
CaO	0.01	10.02	9.18	9.22	8.56	6.14	9.55	4.48	6.87	8.12	8.37	14.85	9.55	7.89	9.62	7.80	6.72	8.31	8.09	6.47	4.56	6.89	6.85
Na2O	0.01	3.19	3.03	3.44	3.28	2.22	3.41	5.19	3.50	2.75	2.33	0.53	2.39	2.63	1.63	3.77	2.66	2.69	2.14	2.09	5.16	3.98	3.02
K2O	0.01	0.45	0.36	0.43	1.56	0.68	0.77	1.04	0.51	0.14	0.06	0.11	0.58	2.19	1.78	0.61	2.30	0.43	2.16	0.37	0.37	1.59	2.11
TiO2	0.01	1.65	1.29	2.16	2.46	1.81	2.06	3.27	3.35	0.58	0.57	0.16	0.42	1.88	2.55	1.06	1.34	2.47	0.50	2.68	0.24	1.55	1.82
P2O5	0.01	0.18	0.18	0.25	0.31	0.27	0.27	0.62	0.52	0.05	0.11	0.02	0.03	0.31	0.44	0.12	0.17	0.23	0.24	0.39	0.02	0.25	0.30
MnO	0.01	0.22	0.32	0.16	0.18	0.16	0.16	0.21	0.20	0.15	0.18	0.13	0.21	0.18	0.17	0.20	0.19	0.26	0.18	0.29	0.16	0.15	0.17
Cr2O3	0.002																						
LOI	-5.1	2.18	1.68	1.53	1.14	4.48	1.24	3.07	5.98	1.46	4.74	0.84	1.84	1.40	4.44	0.73	1.52	1.20	2.57	8.52	2.55	2.27	3.64
Sum	0.01	99.16	99.23	99.05	98.96	99.27	99.47	99.42	99.28	99.50	99.61	99.21	99.79	99.37	99.79	99.88	99.74	99.75	99.80	99.97	99.99	99.88	99.91
ppm																							
Cr		30	bdl	280	325	778	367	bdl	bdl	bdl	12	300	852	308	689	55	40	94	699	275	112	32	27
Ba	1	94	398	242	748	144	123	250	287	85	466	82	204	2653	1119	99	797	99	1883	33	212	731	562
Ni	20	10	11	12	41	24	16	24	13	8	64	bdl	19	95	55	8	90	bdl	36	12	8	23	37
Sc	1																						
Be	1																						
Co	0.2											48	52	43	57	52	48	54	46	57	35	47	46
Cs	0.1																						
Ga	0.5	3	4	12	14	14	17	36	29			7	4	29	48	11	11	13	6	26	4	23	25
Hf	0.1																						
Nb	0.1									3	4												
Rb	0.1									3	5												
Sn	1																						
Sr	0.5									131	171												
Ta	0.1																						
Th	0.2																						
U	0.1																						
V	8	398	461	270	283	254	292	351	359	346	372	237	272	269	285	338	415	463	260	256	223	163	192
W	0.5																						

Zr	0.1	103	77	113	126	104	142	247	208	41	36	10	27	140	193	67	86	156	43	179	21	160	177
Y	0.1									25	31												
La	0.1	bdl	bdl	bdl	bdl	bdl	bdl	bdl	bdl	bdl	bdl	bdl	10	10	25	23	11	bdl	24	18	13	20	24
Ce	0.1																						
Pr	0.02																						
Nd	0.3	57	68	113	134	527	165	17	22			80	311	106	256	50	61	57	160	164	64	66	62
Sm	0.05																						
Eu	0.02																						
Gd	0.05																						
Tb	0.01																						
Dy	0.05																						
Ho	0.02																						
Er	0.03																						
Tm	0.01																						
Yb	0.05																						
Lu	0.01																						

* Shervais (1982)
† Verma and Agrawal (2011)

Attwood Formation

Rock unit		Attwood															
Source		Massey and Dostal (2013)			Dostal et al. (2001)												
Sample		05NMA03-05A	05NMA03-06A	05NMA01-06	G-571	G-48	L-302	L-306	L-329	232	304	24--1	G-622	L-185	L-199	L-342	S-95
Ti-V Classification*		IAB	MORB	IAB	LowTi-IAB	IAB	IAB	IAB	IAB	BON	BON	BON	MORB	MORB	MORB	E-MORB	BON
LDA Classification†						IAB		IAB	IAB	MORB	IAB	MORB	MORB	MORB	MORB	OIB	IAB
UTM Zone		11	11	11	na	na	na	na	na	na	na	na	na	na	na	na	na
Easting		5435728	5435626	5438448													
Northing		383640	383526	385729													
MDL																	
%																	
SiO2	0.01	53.88	52.83	57.33	52.73	51.96	52.75	48.49	46.27	46.01	48.40	46.91	50.11	48.41	47.63	48.24	50.03
Al2O3	0.01	15.49	16.26	14.52	13.79	16.97	15.00	14.93	17.76	17.08	17.89	13.51	12.40	14.57	14.04	15.10	16.09
Fe2O3	0.04	10.96	6.74	10.86	7.64	10.00	8.33	11.11	13.93	6.06	6.57	11.05	16.36	16.06	12.84	11.76	6.65
MgO	0.01	5.10	2.15	4.05	10.33	4.53	7.80	5.48	8.08	10.50	10.56	13.18	5.53	8.21	6.11	7.96	11.52
CaO	0.01	7.11	7.01	3.57	10.71	5.30	9.79	9.38	5.29	14.37	10.90	9.37	8.43	4.74	10.36	8.00	9.54
Na2O	0.01	4.10	3.91	5.17	2.15	4.79	3.31	3.30	3.76	1.56	2.33	0.95	2.57	1.02	2.20	3.17	2.27
K2O	0.01	0.86	3.43	0.16	0.28	0.91	0.14	1.82	0.15	0.36	0.57	1.06	0.54	0.05	0.17	0.40	0.66
TiO2	0.01	0.73	0.72	0.67	0.22	1.03	0.96	0.88	0.95	0.10	0.11	0.24	2.22	2.04	1.54	2.30	0.14
P2O5	0.01	0.07	0.33	0.05	0.01	0.20	0.08	0.34	0.09	0.01	0.01	0.01	0.21	0.12	0.17	0.28	0.01
MnO	0.01	0.16	0.15	0.17	0.29	0.26	0.11	0.18	0.17	0.13	0.14	0.16	0.26	0.24	0.18	0.16	0.13
Cr2O3	0.002																
LOI	-5.1	2.10	2.11	3.02													
Sum	0.01	100.56	95.64	99.56													
ppm																	
Cr		105	bdl	60	691	21	209	60	301	382	254	1047	110	147	255	387	459
Ba	1	252	1236	bdl	99	1607	40	488	56	45	71	55	256	21	48	79	225
Ni	20	27	bdl	6	114	16	72	18	117	97	80	267	56	53	79	114	123
Sc	1																
Be	1																
Co	0.2	54	24	58													
Cs	0.1																
Ga	0.5	19	18	16	9	17	16	21	17	10	11	15	16	21	19	22	8
Hf	0.1				0.25	2.6	1.51	2.24	1.32	0.05	0.01	0.31	4.13	3.47	2.78	4.52	0.3
Nb	0.1	9	1	9	0.2	6.7	1.5	4.8	1.4	0.3	0.2	0.5	6.2	5.3	6	31.1	0.3
Rb	0.1	24	82	20	0.01	18	0.01	63	0.01	14	22	50	14	0.01	3	9	17
Sn	1																
Sr	0.5	176	836	50	87	235	174	644	101	178	247	59	160	233	288	214	90
Ta	0.1				0	0.14	0.02	0.07	0.02	0.01	0.01	0	0.19	0.32	0.18	1.02	0.01
Th	0.2	6	bdl	23	0.04	1.63	0.3	3	0.3	0.01	0.01	0.04	0.26	0.32	0.24	1.38	0.02
U	0.1	2	2	4													
V	8	260	179	297	266	239	285	288	482	130	137	211	446	528	330	284	164

W	0.5																
Zr	0.1	49	125	36	5	102	58	88	47	2	2	11	157	142	121	203	5
Y	0.1	12	30	16	6	21	19	18	18	2	3	7	55	39	31	25	4
La	0.1	22	26	33	0.19	8.72	2.3	11.67	2.92	0.07	0.06	0.2	4.21	5.32	4.99	15.2	0.17
Ce	0.1				0.45	18.8	6.35	25.52	6.56	0.17	0.19	0.63	13.45	15.01	14.03	35.8	0.44
Pr	0.02				0.06	2.52	1.01	3.46	1.12	0.04	0.04	0.13	2.4	2.4	2.13	4.78	0.07
Nd	0.3	33	24	46	0.33	11.14	5.67	15.65	5.68	0.17	0.21	0.71	13.97	12.9	10.87	21.48	0.44
Sm	0.05				0.32	3.02	1.89	3.98	2.16	0.14	0.15	0.47	5.3	4.26	3.68	5.21	0.17
Eu	0.02				0.14	0.99	0.71	1.24	0.7	0.1	0.06	0.15	1.65	1.74	1.36	1.82	0.07
Gd	0.05				0.6	3.44	2.67	3.89	2.88	0.28	0.34	0.79	7.93	5.85	4.91	5.75	0.45
Tb	0.01				0.12	0.56	0.47	0.54	0.5	0.05	0.05	0.14	1.41	1.03	0.87	0.88	0.08
Dy	0.05				1.02	3.67	3.23	3.33	3.37	0.42	0.43	1.15	9.73	7.15	5.45	5.04	0.66
Ho	0.02				0.23	0.78	0.71	0.68	0.71	0.09	0.1	0.26	2.09	1.52	1.19	0.98	0.14
Er	0.03				0.84	2.25	2.19	1.99	2.09	0.24	0.31	0.81	6.41	4.42	3.58	2.66	0.48
Tm	0.01				0.13	0.33	0.28	0.27	0.3	0.04	0.04	0.13	0.96	0.67	0.5	0.36	0.07
Yb	0.05				0.92	2.33	1.93	1.85	1.88	0.29	0.31	0.83	6.18	4.4	3.33	2.23	0.47
Lu	0.01				0.17	0.34	0.3	0.29	0.26	0.04	0.05	0.13	0.97	0.66	0.47	0.32	0.09

* Shervais (1982)

† Verma and Agrawal (2011)

Knob Hill Complex

Rock unit		Knob Hill																	
Source		Massey and Dostal (2013)																	
Sample		05NMA01-07	05NMA15-03	05NMA15-07	05NMA15-08	05NMA16-01	05NMA16-03	05NMA16-06	05NMA16-15	05NMA17-03	05NMA17-05	05NMA17-08A	05NMA17-09	05NMA21-04	05NMA21-05	05NMA21-08	05NMA21-14	05NMA22-08A	05NMA22-08B
Ti-V Classification*		IAB	MORB	MORB	OIB	IAB	OIB	IAB	IAB	IAB	IAB	OIB	IAB	IAB	BON	Below OIB	IAB	IAB	MORB
LDA Classification†			MORB	MORB	OIB	IAB	OIB			MORB	IAB	OIB	IAB						MORB
UTM Zone		11	11	11	11	11	11	11	11	11	11	11	11	11	11	11	11	11	11
Easting		5437968	5438598	5439785	5439608	5442788	5442948	5443273	5442491	5442075	5441706	5442677	5442736	5438928	5439016	5438486	5438720	5442775	5442775
Northing		385395	361106	361451	361524	363426	363116	363694	362507	360492	360603	361648	361704	354555	354806	355551	355103	355158	355158
MDL																			
%																			
SiO2	0.01	51.48	45.29	47.89	44.27	48.89	44.55	50.72	49.42	49.86	48.48	47.74	48.05	57.35	54.92	53.26	54.83	52.08	49.25
Al2O3	0.01	14.70	13.18	13.12	18.73	14.93	13.93	11.75	13.71	13.36	13.61	13.38	13.14	14.94	12.86	13.51	16.41	11.50	12.53
Fe2O3	0.04	9.38	8.53	10.04	16.44	12.28	15.64	16.88	13.39	13.03	13.48	15.14	13.02	11.39	7.88	14.31	8.66	14.26	14.48
MgO	0.01	7.25	5.97	10.91	3.97	8.01	3.63	5.60	8.44	7.82	6.92	5.00	6.77	4.96	9.97	5.97	5.36	5.83	7.14
CaO	0.01	5.23	7.85	5.61	1.60	6.67	8.50	8.34	8.01	8.43	12.11	7.19	10.02	1.92	6.42	1.77	4.78	9.52	7.49
Na2O	0.01	3.81	3.47	1.47	3.31	3.74	3.12	1.78	3.16	3.39	2.11	3.29	3.73	3.94	3.89	0.21	5.52	0.14	0.78
K2O	0.01	0.25	0.97	0.09	2.73	0.43	1.11	0.29	0.42	0.17	0.11	1.78	0.77	0.11	0.29	2.89	0.19	0.19	0.49
TiO2	0.01	0.50	1.06	1.12	3.29	0.69	2.93	1.43	0.67	0.39	0.52	2.81	0.87	0.53	0.23	2.63	0.44	1.17	1.20
P2O5	0.01	0.04	0.19	0.19	0.57	0.06	0.35	0.11	0.05	0.03	0.05	0.38	0.07	0.04	0.02	0.23	0.03	0.12	0.02
MnO	0.01	0.18	0.12	0.17	0.21	0.22	0.18	0.23	0.29	0.24	0.20	0.20	0.18	0.15	0.10	0.18	0.13	0.23	0.21
Cr2O3	0.002																		
LOI	-5.1	6.69	6.79	9.79	4.60	3.73	6.46	2.85	3.19	2.94	3.58	3.30	4.88	5.00	3.62	5.38	3.29	5.05	6.55
Sum	0.01	99.51	93.43	100.39	99.71	99.65	100.40	99.99	100.75	99.66	101.17	100.22	101.50	100.33	100.20	100.34	99.64	100.10	100.14
ppm																			
Cr		154	242	306	116	212	61	52	110	78	159	42	131	bdl	542	216	45	35	64
Ba	1	26	102	41	1696	422	1001	232	663	95	95	542	128	bdl	73	764	bdl	421	3410
Ni	20	44	34	56	56	89	61	55	74	78	67	42	76	bdl	166	179	27	43	54
Sc	1																		
Be	1																		
Co	0.2	56	48	62	85	71	70			83	82	69	69	71	55	84	54	73	74
Cs	0.1																		
Ga	0.5	15	bdl	16	25	18	25	23	19	17	19	24	19	17	13	22	15	21	20
Hf	0.1																		
Nb	0.1	bdl	2	8	52	2	19	3	5	2	17	21	16	3	3	48	1	2	1
Rb	0.1	22	28	16	42	20	22			13	bdl	31	5	27	18	53	21	4	11
Sn	1																		
Sr	0.5	87	381	204	193	207	281	64	193	92	81	228	81	71	226	57	170	223	239
Ta	0.1																		

Th	0.2	20	6	18	27	16	12			14	5	11	6	32	11	23	18	10	13
U	0.1	4	2	3		3	1			2	1	1	1	4	3	2	4	1	2
V	8	245	146	167	240	280	353	466	335	269	305	317	339	315	205	51	256	403	244
W	0.5																		
Zr	0.1	21	81	68	239	42	179	75	38	20	40	182	55	24	17	185	23	65	64
Y	0.1	17	21	18	13	17	18			16	13	18	13	11	17	13	19	17	16
La	0.1	29	30	46	100	34	62			29	24	54	28	37	16	72	21	33	40
Ce	0.1																		
Pr	0.02																		
Nd	0.3	39	34	48	87	45	57			43	36	53	38	52	26	65	34	43	48
Sm	0.05																		
Eu	0.02																		
Gd	0.05																		
Tb	0.01																		
Dy	0.05																		
Ho	0.02																		
Er	0.03																		
Tm	0.01																		
Yb	0.05																		
Lu	0.01																		

* Shervais (1982)

† Verma and Agrawal (2011)

Knob Hill Complex continued…

Rock unit		Knob Hill																	
Source		Massey and Dostal (2013)																	
Sample		05NMA22-09Ave	05NMA22-10	05NMA23-07B	05NMA23-09	06NMA18-13A	06NMA18-13B	06NMA18-14A	06NMA18-18	06NMA18-20B	06NMA19-01-02	06NMA19-07	06NMA19-12	06NMA19-15	06NMA20-06	06NMA20-07	06NMA22-09	06NMA24-02	06NMA24-06
Ti-V Classification*		IAB	IAB	IAB	MORB	IAB	BON	IAB	IAB	IAB	IAB	IAB	MORB	MORB	IAB	IAB	MORB	IAB	IAB
LDA Classification†		IAB		IAB	OIB	IAB						IAB	CRB	OIB	IAB		MORB	IAB	IAB
UTM Zone		11	11	11	11	11	11	11	11	11	11	11	11	11	11	11	11	11	11
Easting		5443015	5444052	5443330	5443533	5441737	5441737	5441617	5442007	5442503	5442989	5443933	5443469	5443706	5442430	5442782	5445038	5445293	5446036
Northing		355214	356180	357303	357420	351904	351904	352709	351894	351868	351219	351270	350725	350011	349248	349257	352846	350835	351174
MDL																			
%																			
SiO2	0.01	48.59	45.92	48.45	48.40	47.10	51.14	47.87	48.60	49.25	48.51	47.53	49.16	47.65	50.09	50.65	48.55	49.48	49.44
Al2O3	0.01	14.21	13.94	12.92	13.43	13.21	10.52	13.17	14.05	13.78	15.52	13.21	14.68	15.30	12.61	13.99	13.20	15.68	17.49
Fe2O3	0.04	11.60	13.26	16.07	12.61	11.58	7.45	13.72	12.08	11.80	13.81	15.85	9.04	8.97	14.76	12.62	19.51	9.00	9.36
MgO	0.01	8.36	8.18	5.95	6.72	7.57	5.41	8.57	8.25	8.29	8.29	5.58	6.62	6.46	7.56	7.51	4.26	6.39	6.60
CaO	0.01	9.90	7.51	7.71	10.87	6.95	16.07	7.32	6.78	9.52	2.60	6.88	9.11	9.54	7.30	4.28	6.15	6.50	9.71
Na2O	0.01	1.11	2.98	2.84	3.03	1.76	0.20	3.02	2.60	2.86	3.20	2.24	3.59	3.94	2.59	4.10	4.39	4.84	3.17
K2O	0.01	1.02	0.66	0.45	0.10	0.45	0.78	0.26	1.35	0.20	0.33	0.38	0.25	0.41	0.17	0.11	0.37	0.92	0.69
TiO2	0.01	0.45	0.83	0.67	1.45	0.41	0.22	0.67	0.65	0.40	0.86	1.68	1.62	2.17	0.80	0.92	1.41	0.74	0.37
P2O5	0.01	0.04	0.06	0.06	0.14	0.04	0.07	0.07	0.06	0.09	0.07	0.20	0.27	0.28	0.13	0.15	0.16	0.12	0.04
MnO	0.01	0.19	0.22	0.20	0.20	0.17	0.23	0.20	0.19	0.18	0.19	0.20	0.13	0.18	0.19	0.15	0.21	0.27	0.18
Cr2O3	0.002																		
LOI	-5.1	4.56	5.80	4.96	3.53	10.10	7.15	4.36	4.45	2.93	5.93	5.21	5.02	4.37	3.01	5.06	0.96	5.60	2.79
Sum	0.01	100.06	99.35	100.27	100.48	99.38	99.26	99.26	99.17	99.31	99.36	99.02	99.52	99.30	99.23	99.56	99.18	99.65	99.86
ppm																			
Cr		243	159	47	234	96	215	19	bdl	49	165	bdl	252	164	bdl	bdl	bdl	214	74
Ba	1	591	317	391	148	448	243	302	1128	139	486	624	321	315	215	247	87	1145	217
Ni	20	84	95	62	90	73	68	68	82	82	107	30	104	86	58	40	48	133	53
Sc	1																		
Be	1																		
Co	0.2	64	75	92	63														
Cs	0.1																		
Ga	0.5	18	17	19	20														
Hf	0.1																		
Nb	0.1	8	bdl	4	8	3	3	bdl	bdl	bdl	bdl	9	25	23	3	bdl	3	4	3
Rb	0.1	19	13	9	bdl	15	16	6	22	7	9	9	7	8	5	5	8	21	21
Sn	1																		
Sr	0.5	90	97	70	119	54	246	108	55	125	51	77	252	254	168	77	115	312	325
Ta	0.1																		
Th	0.2	6	15	19	3														

U	0.1	1	2	2	1														
V	8	251	328	387	325	301	170	320	316	264	378	471	247	285	400	379	478	235	205
W	0.5																		
Zr	0.1	29	31	32	74	31	26	44	44	31	53	109	131	150	50	61	63	53	27
Y	0.1	16	13	12	15	22	16	22	29	17	24	37	24	18	29	30	44	16	17
La	0.1	22	34	39	31	bdl	bdl	bdl	bdl	bdl	bdl	bdl	7	bdl	bdl	7	bdl	4	bdl
Ce	0.1																		
Pr	0.02																		
Nd	0.3	33	46	52	36														
Sm	0.05																		
Eu	0.02																		
Gd	0.05																		
Tb	0.01																		
Dy	0.05																		
Ho	0.02																		
Er	0.03																		
Tm	0.01																		
Yb	0.05																		
Lu	0.01																		

* Shervais (1982)

† Verma and Agrawal (2011)

Appendix E: Geochemical Sample Locations

Okanagan Similkameen Region

Kootenay-Boundary Region